UNIVERSITY OF OKLAHOMA

GRADUATE COLLEGE

BIOLOCIAL EVALUATION OF MITOCHONDRIA-TARGETING PHOTOSENSTIZERS AND SITE-SPECIFIC PRODRUGS

A DISSERTATION

SUBMITTED TO THE GRADUATE FACULTY

in partial fulfillment of the requirement for the

Degree of

DOCTOR OF PHILOSOPHY

By

PALLAVI RAJAPUTRA
Norman, Oklahoma
2013

BIOLOCIAL EVALUATION OF MITOCHONDRIA-TARGETING PHOTOSENSTIZERS AND SITE-SPECIFIC PRODRUGS

A DISSERTATION APPROVED FOR THE
DEPARTMENT OF CHEMISTRY AND BIOCHEMISTRY

BY

_____
Dr. Ann West, Chair

_____
Dr. Youngjae You

_____
Dr. George Richter-Addo

_____
Dr. Lester Reinke

_____
Dr. John Moore-Furneaux

Dedicated

To my mother, father and sister

Acknowledgments

I would like to express sincere gratitude to my advisor, Dr. Youngjae You, for his direction, criticism and encouragement, which has seen me through the project. I will be forever thankful to him for imparting his knowledge and providing me with excellent training. I try to keep his emphasis of perfection in my work.

I would like to thank the chair of my graduate committee Dr. Ann West, for her extraordinary direction and advice, my committee members; Dr. George Richter-Addo, Dr. Lester Reinke, and Dr. John Moore-Furneaux, for their understanding and encouragement throughout the program.

I would also like to thank the members of the medicinal chemistry laboratory both past and present especially Dr. Ethel Ngen who synthesized TPP-cations, Mr. Gregory Nkepang who synthesized CMP-cations, and Dr. Moses Bio who synthesized the prodrugs. I would like to thank Dr. Bibbin Paul for teaching *in vivo* techniques and for helpful discussion during his stay. I would like to thank Dr. Samuel Awuah, Ryan Watley and Vidya Biradar for encouragement, scientific and friendly discussions.

The journals entitled “Synthesis and in vitro biological evaluation of lipophilic cation conjugated photosensitizers for targeting mitochondria” (reference # 173) "Evaluation of delocalized lipophilic cationic dyes as delivery vehicles

for photosensitizers to mitochondria" (reference # 206) were reproduced in this dissertation with permission from Elsevier. The journals entitled "Site-Specific and Far-Red-Light-Activatable Prodrug of Combretastatin A-4 Using Photo- Unclick Chemistry" (reference #243) were reproduced in this dissertation with permission from American Chemical Society.

I would like thank my friends and family especially my cousin Dr. Suresh Rajaputra for his advice and guidance.

Table of contents

List of Abbreviations

$^1O_2$	Singlet oxygen
^1PS	Singlet state photosensitizer
$^3O_2$	Molecular oxygen or triplet oxygen
^3PS	Triplet state photosensitizer
CA4	Combretastatin A-4
CMPLCA4	dithiaporphyrin-linker- Combretastatin A-4
CMP	Core-modified porphyrin (Dithiaporphyrin)
DLC	Delocalized lipophilic cation
DMSO	Dimethyl sulfoxide
DNA	Deoxyribonucleic acid
ER	Endoplasmic reticulum
ET	Energy transfer
Fc	Fragment crystallizable
FRET	Fluorescence resonance energy transfer
IP	Intraperitoneal
ISC	Inter-system crossing
MCF-7	Michigan cancer foundation-7 (human breast adenocarcinoma cell line)
MTT	3-(4,5-Dimethylthiazol-2-yl)-2,5-diphenyltetrazolium bromide
NMR	Nuclear magnetic resonance
PCI	Photochemical internalization

PAMAM	Polyamidoamine
PBS	Phosphate buffered saline
PTPC	Permeability transition pore complex
PDT:	Photodynamic therapy
PEG	Polyethylene glycol
PGA	Polylactide-co-glycolide
PLA	Polylactic acid
PLGA	Polylactide-co-glycolide
PS	Photosensitizer
PCD	Programmed cell death
Rh-123	Rhodamine-123
Rh B	Rhodamine B
ROS	Reactive oxygen species
SO	Singlet oxygen
THF	Tetra hydro furan
tPP	Triphenyl phosphine
TPP-OH	5,10,15-Triphenyl-20-(4-hydroxyphenyl)-21*H*,23*H*-porphyrin

List of Tables

Page

List of Figures

Page

List of equations

Abstract

This dissertation focuses on two different delivery mechanisms utilizing the principle of PDT with a goal to enhance the availability of the cytotoxic agent at the tumor site.

In one approach, which utilizes the higher mitochondrial membrane potential of cancerous cell mitochondria over the normal cell, compounds containing cations will be delivered to cancer cell mitochondria specifically. Delocalized lipophilic cationic dyes conjugated with porphyrin were used to improve the delivery of photosensitizer to mitochondria. Tetranitrogenic porphyrin, which absorbs around 650 nm, and either rhodamine B or acridine orange were used as porphyrin and cations. Due to their fluorescence properties, most of these dyes were visualized using fluorescence microscopy to confirm the mitochondrial localization. Uptake, photo and dark toxicity were then explored.

In a continuing project, core modified porphyrin photosensitizers with near IR absorption (690nm), high singlet oxygen quantum yield and known mitochondrial localizing cationic dyes like rhodamine B and triphenyl phosphene were explored. The photophysical properties of the conjugates like UV absorption, fluorescence, lipophilicity, singlet oxygen generation, and FRET efficiency were studied. Once it was confirmed that conjugation with cations did not alter the photophysical and singlet oxygen (SO) generation capacity of the dyes, biological evaluation was performed. All of these dyes,

due to their fluorescence properties, were visualized using fluorescence microscopy to confirm mitochondrial localization. Uptake and photo and dark toxicity were explored. In vivo biodistribution studies show that the cation conjugated compound accumulated more in the tumor when compared to the photosensitizer itself.

In a different approach (of delivery), the site-specific delivery of porphyrin-anti-cancer prodrug conjugate to deliver and activate anti-cancer drug only at the tumor site was explored. Biological evaluation of these compounds was carried out to see that the concept works under in vitro conditions by exposing only a region of cells. Upon successful PDT the anti cancer drug was released to cause cell destruction. Once the concept was proved in vitro, in vivo studies were performed to see the anti tumor efficacy of the drugs. Additionally, the mechanism of cell death was also studied.

Overall, with this dissertation, the goal of delivering the cytotoxic agent to the tumor site and limiting its non-specific effect was achieved.

Chapter 1. Introduction

The objective of cancer research these days is to develop treatment methods to reduce side effects in treatment. Cancer is a group of cells that divide without control[1]; whereas normal cells divide and die at a regular fashion. Several approaches are implemented for cancer treatment like surgery, irradiation, immunotherapy, hormone therapy, and chemotherapy. Though widely used, chemotherapy is limited due to its non-specific action on both normal and diseased cells. Current research is focused on developing targeted therapies that are more specific to cancer cells and leave normal cells to be unharmed. Photodynamic therapy (PDT) is one such modality where specificity could be achieved by both preferential accumulation of photosensitizers and precise activation with light only at the tumor site.

1.2. Photodynamic therapy-mechanism of action

PDT is a minimally (or non-)invasive technique that involves a pharmacologically inert agent called a photosensitizer (PS), light, and oxygen.[2, 3] Initially a PS is administered either intravenously, intraperitonially or topically. After the PS gets cleared from unaffected tissue, a light made either with light emitting diode (LED) or some kind of laser, which can emit light of near IR wavelength, is shined upon the affected region. Upon irradiation with light, the PS absorbs a photon and goes from ground state to

a singlet excited state (^{1}PS). Then via intersystem crossing (ISC) the ^{1}PS attains a triplet state (^{3}PS). At the triplet state the PS is not stable and follows one of three fates – type I, type II or emitting phosphorescence[1]. In the Type I mechanism, either a hydrogen-atom abstraction or electron-transfer between the PS and a substrate occurs, yielding highly reactive free radicals and radical ions which generate superoxide anions or hydroxyl radicals. In the Type II mechanism, an energy transfer step converts the ground state triplet oxygen to singlet oxygen.[4, 5] Both Type I and Type II products are highly toxic and react with the nearby biological molecules to carry out cytotoxicity.[2, 6]

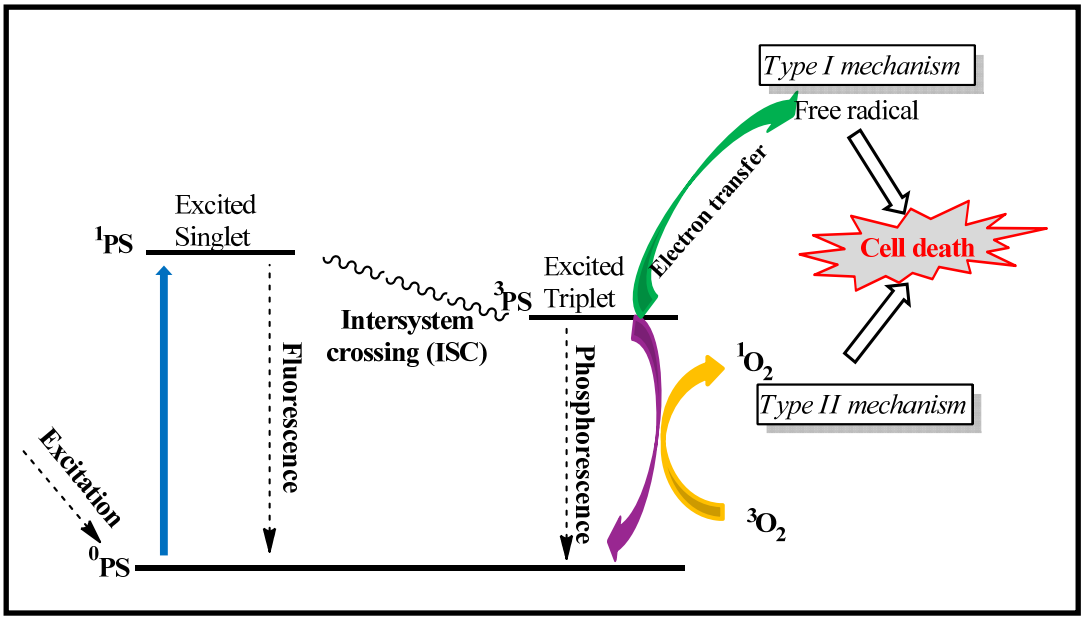

Figure 1. Schematic illustration of simplified model of PDT mechanism.[7, 8]

1.3. Important components of PDT

Three photochemical reactants form the heart of PDT: 1) light, 2) singlet oxygen and 3) photosensitizer.

1.3.1. Light

Light sources used in PDT are primarily categorized as laser and non-laser light sources.[9] Broadband light sources like xenon arch lamps or light sources equipped with filters were used to eliminate light of short wavelength. Their relative low cost, reliability and simplicity made lamps a good choice in PDT.[10] However, due to low light intensity and poor coupling efficiency into mono fibers, lamps are not the best choice to be used as optical fibers. High intensity power output (to avoid tissue attenuation), monochromatic character, no thermal effect, and flexibility to couple with fiber optics for endoscopic light delivery make lasers commonly used light sources.

Light interaction and penetration into tissue depends on the wavelength and the intended treatment volume. Not all wavelengths of light are advantageous in PDT. Most of the incident light is absorbed by components of blood at in vivo conditions. Hemoglobin can absorb light around 425, 544, and 577 nm hence the need for light > 600 nm to ensure significant amounts of light.[11] Photon energy at wavelengths < 850-900 nm light may not be high

enough to activate triplet oxygen ($^3O_2$). For wavelengths > 1200 nm, light absorption by water molecules are significantly high. Hence wavelengths between 600-800 nm are designated as the "therapeutic window" in clinical PDT.[12]

1.3.2. Singlet oxygen

At ground state, oxygen is in the triplet configuration ($^3O_2$). The excited state configuration, singlet oxygen ($^1O_2$) is the main cytotoxic agent involved in biochemical reactions. Generation of singlet oxygen occurs due to the interaction of an excited PS in triplet state and ground state molecular oxygen. The quantum yield of singlet oxygen depends on three factors. 1) the triplet state quantum yield of the PS (0.2-0.9),[13] 2) quenchers, and 3) yield of singlet oxygen per collision (0.2 to 0.7).[14, 15]

The lifespan of singlet oxygen (SO) is thought to be 10-40 ns in cells (ranges between 10-100 μs in organic solvents[16]), and its diffusion distance is 10-20 nm[17](no larger in diameter than the cell membrane). Due to its short lifespan and diffusion distance the site of PDT damage is the site where there is higher concentration of PS.[18-20] The tissue lifetime of triplet state of PS (10 μs)[21, 22] is sufficient enough to convert molecular oxygen to singlet oxygen.[23, 24] Further, oxygen concentration is most critical in PDT. Normal tissue contains about 5% oxygen where as the hypoxic region of the tumor

contains < 1% oxygen.[25] Hence it can be easily understood that PDT is not efficient at hypoxic conditions .

1.3.3. Photosensitizers

A non-toxic compound which gets activated by absorbing light of particular wavelength is called a PS. Upon absorbing light, it reaches an excited singlet state (^{1}S). Later via a intersystem crossing (ISC) PS reaches a triplet state (^{3}PS) and further transfers energy to molecular oxygen, and converts it to a cytotoxic reactive oxygen species (ROS)[3]. Most PSs possess tetrapyrollic macrocycles similar to heme or chlorophyll molecules.

Though not yet clearly known, why certain PSs accumulate preferentially in the tumor the following physiological properties of tumor could be an explanation. Tumor specific properties such as large abundance of lipids to allow retention of lipophilic dyes,[26], presence of leaky vasculature, large interstitial stromal space to allow easy flow of large molecules, compromised lymphatic system to allow the retention of lipophilic compounds,[27] low pH levels that allow protonation of anionic PS imparting lipophilicity for their easy uptake,[3] availability of tumor associated macrophages to swallow lipophilic PSs,[28] presence of newly formed collagen that bind to porphyrins[29] are some properties implicated for the preferential accumulation of PSs into the tumor.

PSs are broadly categorized into three groups based on their chemical structure:[28] 1) Porphyrin based, (for example famous Photofrin. Most of the current clinically approved PS fall under this category), 2) Chlorophyll based (such as chlorins and bacterochlorins), and 3) Dye based (such as phthalocynanins)..

1.3.3.1. First generation PSs

Porfimer sodium (HpD, a hematoporphyrin derivative) is a first-generation PS. The dawn of modern day PDT began with the development of HpD by Lipson and Schwartz in 1960.[29] HpD was further purified in the 1970 through 80's and was called the drug Photofrin®. HpD shows some notable physical limitations such as it is not a pure compound but is a mixture of compounds made of variable composition, absorbs at lower wavelength (630 nm) and molar extinction coefficient of 3,000 M^{-1} cm^{-1} on electronic spectrum hence requires higher dose and high light intensity for treatment. Although clinically approved against several types of cancers, HpD shows some clinical draw backs such as long term skin phototoxicity (up to 6 weeks) post treatment, poor selectivity in tumor cells and non-specific binding to normal cells can cause damage.[30, 31] As a result of the above physical and clinical shortcomings, a list of properties have been proposed to describe an ideal PS.

An ideal PS[32] should have the following physical properties such as; 1) be pure, characterized to be a single compound, 2) be an efficient producer of SO, 3) absorb at wavelengths > 650 nm, 4) have high extinction coefficient, 5) possess longer triplet state life time. It should have the following biological properties such as; 1) show minimum or no toxicity without light, 2) should preferentially accumulate and retain in area of interest, and 3) exhibit low systemic toxicity by being rapidly excreted from the body..

A few other compounds obtained from natural sources like chlorins, bacterochlorins and porphyrins also fall under first generation PS[33] (Figure 2). However, they face some drawbacks. 5-Aminolevulinic acid (ALA) gets metabolized to protoprophyrin IX. But not all tissues produce protoporphyrin IX. Protoporphyrin IX absorbs at lower wavelength of 635 nm and has an extinction coefficient of 5,000 M^{-1} cm^{-1}.[2] Although, chlorins absorb at 660nm and bacteriochlorins absorb at 750-800 nm, they get re-aromatized,[34] which limits their in vivo availability.

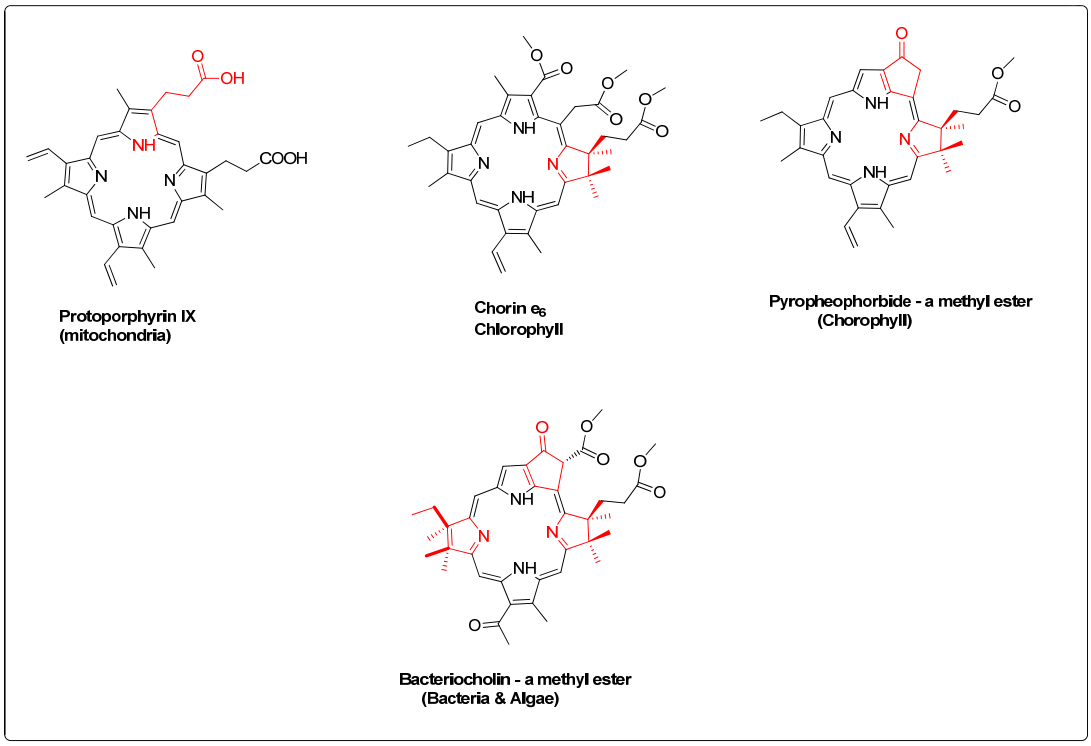

Figure 2. First generation photosensitizers

1.3.3.2. Second generation PS

While no PS is believed to have all the properties of an ideal PS, a number of second generation PSs with enhanced photophysical and photosensitizing properties have been developed. Several PSs such as benzoporphyris, chlorins, phthalocyanines, napthalocyanines, methylene blue, hypericins and hypocerillins were studied to overcome the drawbacks of Photofrin.[35] Examples of the second generation PSs are given below (Figure 3).

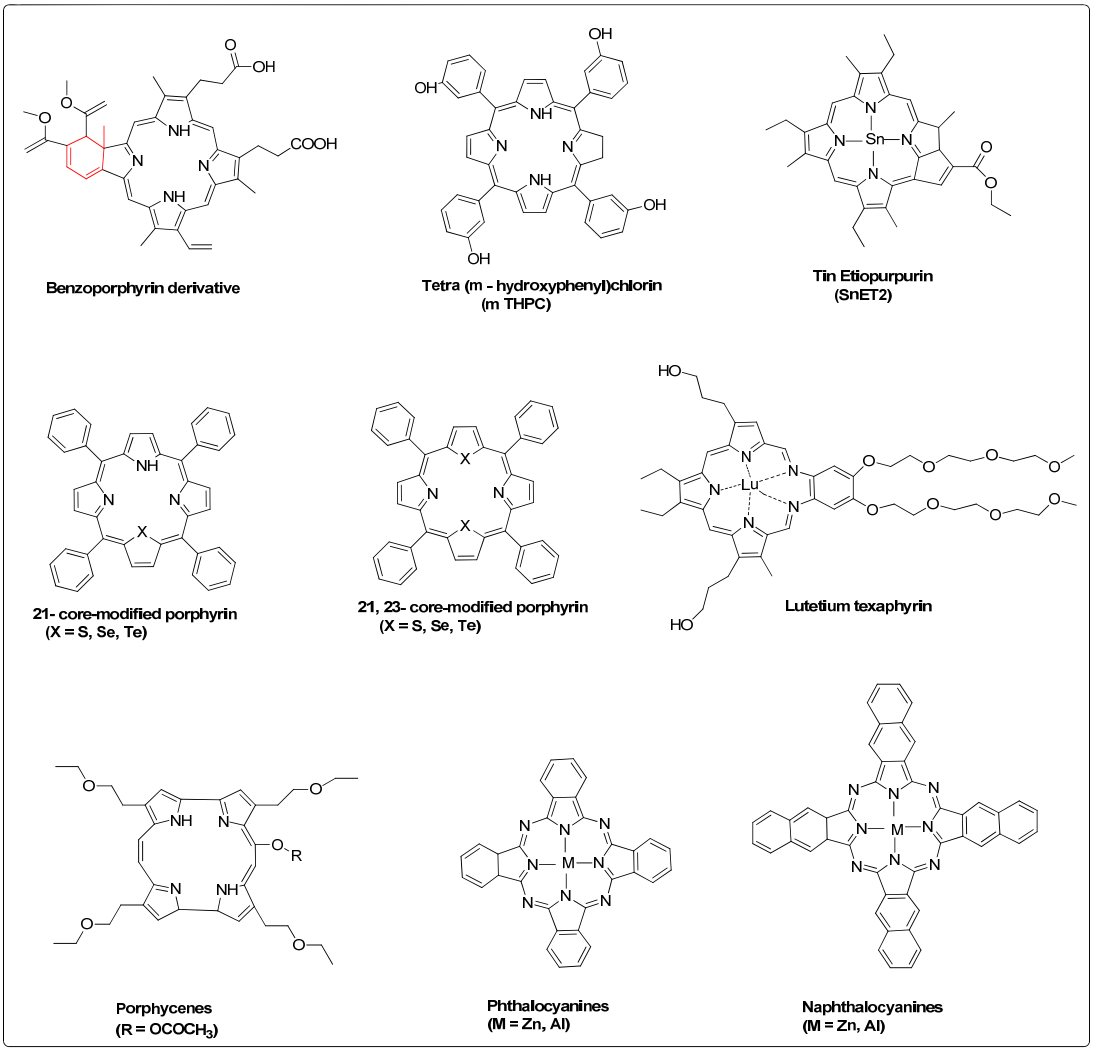

Figure 3. Second generation photosensitizers

1.3.3.3.Third generation PSs

Derived from the second generation PSs, third generation PSs were made by attaching them to targeting vectors to specifically deliver PSs to particular cells.[36] Non-specific storage of PSs in healthy cells has been a major reason

for drawbacks such as skin photosensitivity in PDT.[37-40] Some targeting vectors coupled with PS are amino acids, polymers, proteins, carbohydrates, antibodies against tumor specific antigens, and carrier inclusion complexes.[36] New methodologies to exclusively deliver PSs to tumor cells have been explored. These methodologies generally utilize differences in both molecular and physiological properties between cancerous (tumor) and normal cells (tissue). Some of these properties are high vascularization of tumor tissue, over expressed cell surface receptors, high metabolic rate of cancerous cells, and involvement of enzymes in the activation of PS prodrugs.

Vascular targeting has gained considerable interest recently.[41, 42] Tumor tissue displays physiological variations compared to those of normal tissue, due to the complex vasculature, imbalance in pro and anti-angiogenic factors, and high interstitial pressure. These variations include rapid proliferation rate, enhanced permeability, asymmetric branching, lack of pericytes and basement membrane coverage.[39] Compared to traditional approaches for targeting tumor cells, targeting tumor vasculature is much easier, more efficient, and has a lower probability of developing drug resistance.[40] Vascular targeting in PDT could be either passive or active.[40] In passive targeting, rapid proliferative blood vessels help retain PS. Active targeting facilitates covalent coupling of PS to molecules having higher affinity to cellular components like integrins, VEGFR and fibronectins.[43, 44] Several PSs, like ethylethipurprin (SnET2), lutetium texaphyrin (Lutex) and

Tookad,[39] are known to passively target tumor vasculature.[39] Along with the supply of nutrients and removal of metabolic wastes, tumor vasculature helps maintain exchange of materials between blood plasma and interstitial fluids[45]. The main aim of vascular targeting is to incorporate vascular shutdown. Vascular sensitization in PDT causes loss of vascular barrier function, which is seen as one of the earliest events.[46, 47] Increased vascular permeability has been observed after PDT with several PSs[46] like Verteporfin.[48] Although targeting vasculature is very powerful in tumor ablation, the heterogeneity of central versus. peripheral vasculature brings varying results in tumor destruction. Also, cellular adaptation to hypoxic stress might result in tumor reoccurrence.[38]

Another strategy for tumor targeting is through photosensitizer immunoconjugates, which recognize cell surface antigen on tumor.[44, 49-51] This strategy provides dual advantages: firstly, activation of PS occurs only in presence of light; secondly, immunoconjugates interact with the specific antigens present only on tumor cells. Drawbacks associated with this strategy are: multiple PS molecules need to be attached to an antibody to produce the desired effect, extreme modification could render antibody unrecognizable by the antigen, and the immunoconjugate might be considered as non-self and destroyed.[52] Staneloudi *et al*. found single-chain monoclonal antibody (scFv) fragment more efficient in penetrating tumor

masses due to their small size and effective clearance from the circulation due to lack of an Fc (fragment crystallizable) domain.[51]

A number of delivery vehicles such as microspheres, low density lipoproteins (LDL), liposomes, and high molecular weight non-specific carriers such as albumin and polyethylene glycols (PEGs), have also been developed to transport and release PS to tumor cells.[49, 52] Some cancerous cells over express folate (KB cells) and LDL receptors. Folate and LDL conjugated PSs have been developed to target such receptor positive sites on the tumor cell surface.[49]

Zheng *et al.* developed photodynamic molecular beacons (PMBs). PMBs constitute a PS conjugated to a quencher via a disease-specific peptide linker. The PSs effect is suppressed untill it approaches the disease specific protease enzyme, for example, matrix metalloproteinase-7.[53]

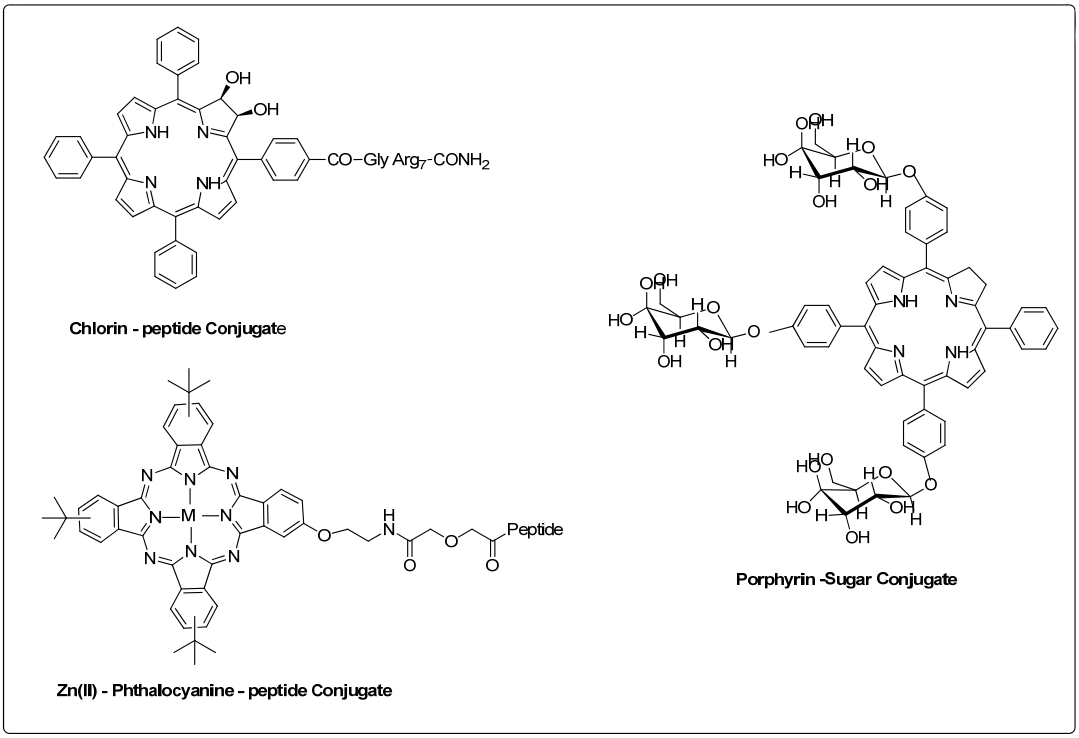

Figure 4. Third generation photosensitizers

1.4. Cell killing by PDT

In PDT, tumor or tissue damage is mediated through multiple pathways. Firstly, direct cellular damage, where photochemical interactions of PS, light and molecular oxygen generate reactive oxygen species (ROS) to induce cellular damage and consequent tumor ablation.[54] Generated ROS can elicit a cascade of events that result in direct cell death by apoptosis/necrosis.[55, 56] Secondly, indirect damage where ROS generated upon excitation of PS by light can cause vesicular shutdown and leads to a deficiency of oxygen and

nutrients[57-59] and/or up regulation of immune regulators of immune system such as cytokines and interleukins to elicit an immune response.[60-62]

The earliest studied cell death process was necrosis. Later, other forms of cell death have been recognized. Cells respond to various signals like injury and decide to die via a pathway called programmed cell death (PCD). In Type I PCD, cells shrink and chromatin condensation occurs. This method of cell death is also called apoptosis. In Type II PCD, enzymatic digestion (lysosomal enzymes) removes damaged cellular components in a process also called autophagy. In Type III PCD, cell swelling occurs, and the plasma membrane loses integrity in a process alternatively called as necrosis. All the above pathways allow the elimination of abnormal, unnecessary, and damaged cells. Defects in a PCD mechanisms can lead to diseases like cancer.

1.4.1. Apoptosis

Apoptosis is a highly regulated method of programmed cell death that occurs due to exposure of cells to heat, chemicals, radiation or stress.[63-66] Alternatively, depletion of nutrients required for the growth of the cell, cytokine, and ligands-receptor interactions could also induce apoptosis.[67] Morphological changes like blebbing, cell shrinkage, nuclear fragmentation,

chromatin condensation, and chromosomal DNA fragmentation are unique events occurring during apoptosis.[68]

The cellular power plant mitochondria are quite unique due to their involvement in the majority of apoptotic pathways.[69-75] In the intrinsic pathway, proapoptotic proteins lead to the loss of mitochondrial membrane potential causing the opening of permeability transition pore complex (PTPC) on the outer membrane, this releases proteins like cytochrome c, second mitochondrial activator of caspases (SMAC), and apoptosis inducing factor (AIF) into the cytoplasm. Later cytochrome c along with procaspases, form the apoptosome. At this stage, procaspases get activated. Caspase-3, also called as executioner caspase, further cleaves many cellular proteins, which results in chromatin condensation, DNA fragmentation, and conclusion of apoptosis. Alternatively, death receptors on the cell surface when triggered recruit additional cytoplasmic proteins to form death inducing signaling complex (DISC), which activate caspases-8 and 10 and further activates caspase-3.[76]

The mechanism of apoptosis gained importance in PDT after it was first studied by Agarwal *et al*.[77] in non-adherent cells. PDT induces apoptosis both in cultured cells and in vivo conditions.[55, 77] Compared to several other inhibiting agents, apoptosis in PDT may occur in any stage of the cell cycle[78, 79] and even after cell cycle arrest.[80] The distinctive aspect of apoptosis in PDT is its molecular target of PSs as the initial photodamage

occurs at the site of PS accumulation. PSs targeting mitochondria causes changes in PTP complex, Bcl-2, bcl-xl, and cardiolipins.[81]. Mitochondria localizing PS such as Verteporfin induces rapid apoptosis.[82] Endoplasmic reticulum (ER) targeting PSs damage calcium pumps to release stored calcium into cytosol and then into mitochondria[81]. Lysosomal PSs damage the lysosomal membrane releasing cathepsins and hydrolases that activate apoptotic mediators like Bid, and further promote mitochondrial apoptosis.[76]

1.4.2. Autophagy

Autophagy is a catabolic process to degrade dysfunctional cellular organelles or to recycle unnecessary cellular components during starvation to support cell survival[83]. Cells undergoing autophagy become isolated from rest of the cells and form double-membrane enclosed vacuoles called autophagosomes, which are then engulfed[84] by lysosomes and recycled.[85] At lower doses of PDT, autophagy promotes cell survival, but at higher doses cell death occurs.[86] Autophagy occurs as a common initial response following PDT whether or not apoptosis is blocked.[87, 88] Kessel *et al*. studied the role of apoptosis and autophagy following PDT and suggested there could be crosstalk between both the mechanisms.[89]

1.4.3. Necrosis

Necrosis occurs due to external factors like cytokins, heat, ischemia, heat, irradiation, and pathogens[90]. Necrosis is unregulated, and products of cell death are released into the immediate surroundings. The accumulation of PSs in plasma membrane at doses high enough to damage components of other pathways may cause necrosis.[91]

Several factors determine the mechanism of cell death in PDT treated cells. At higher concentration, PS induces necrosis, and at lower concentrations, it induces apoptosis[92-95] The site of localization of PS also plays a key role in determining the cell death mechanism. The localization of the PS varies based on the time of incubation.[96] The initial site of accumulation of few a PS may not be the actual damaged site.[97] Different reactive species formed at the same site may show different cellular responses.[98, 99]

1.5. Subcellular targets of PS

SO ($^1O_2$) is the cytotoxic agent in PDT. SO has very short lifetime (< 40 ns) and small radius of diffusion in biological systems (< 20 nm).[17] Hence the location of a PS is considered to be the site of photodamage. This section will elaborate the significance of different organelles (nuclei, plasma membrane, lysosomes, microtubules, endoplasmic reticulum, and mitochondria) in bringing out the desirable effect in PDT.

1.5.1 Nuclei

Due to their hydrophobic nature, most clinically approved PSs accumulate either in cytoplasmic membrane or in organelles but not in the nuclei. However, a few PSs that target nuclei have been developed and studied. Rosenkranz *et al*. designed peptide conjugates of PSs that showed improved cell-specificity, internalization, and possessed ability to escape from intracellular vesicles and target nucleus.[100] Nuclear targeting of these peptide PS conjugates improved the photodynamic activity to about 2500-fold higher than that of free PS. However, another study done by Gomer *et al.* showed that cell death due to DNA damage was not as effective when compared to damage caused to membranes in PDT.[101, 102]

1.5.2. Plasma membrane

The role of the plasma membrane in carrying out cell death in PDT is considered inconclusive. Both the plasma membrane targeting PSs (Photofrin) and mitochondria targeting PSs (ALA and Pc-4) have shown lack of response to growth factors and cytokines,[103, 104] This suggests that both photo activation of the plasma membrane and oxidative reactions or signaling mechanism initiated at the mitochondria can damage it. Lipophilic PSs, for example HpD, partition into the phospho lipid bilayer of the plasma membrane and hence show membrane damage.[105] Such damage is

observed only during the initial incubation period (1 h). However after prolonged incubation (18 h) with HpD, more intracellular damage to lysosomes (discussed in next section) and especially to mitochondria was observed.[106] Usually, photo damage to plasma membrane has been coupled with the necrotic mode of cell death.[106, 107].

1.5.3. Lysosomes

A few PSs are known to localize in lysosomes and induce apoptotic cell death. Other PSs like mTHPC[108] and ATX-S10[109] showed lysosomal damage. Few lysosomally bound PSs showed apoptosis due to their relocalization into mitochondria.[110, 111] Lysosomal damage in PDT was associated with cleavage of Bid, release of cytochrome c from mitochondria and activation of caspases 9 and 3. NPe6 treated murine hepatoma 1c1c7 cells showed delay in apoptotic cell death.[112] Whereas, Tao cells (derivatives of 1c1c7 cells), which are aryl hydrocarbon receptor (AhR) deficient lines, did not show any effect to NPe6 treatment.[113] When cells with varying AhR levels were compared to those with higher levels of AhR, they showed rapid cleavage of Bid, activation of caspases and higher rate of apoptosis. Hence, though considered to be a critical means for PDT, lysosomal damage was later demonstrated to elicit no direct response.

Lysosomally accumulated PSs undergo photochemical internalization (PCI), a mechanism well studied by Berg et al.[114-118] In PCI, PSs are uptaken and entrapped into lysosomal vesicles. Upon photoirradiation and disruptive action by SO, lysosomally trapped PSs are released and relocate to critical intracellular organelles like mitochondria via passive diffusion to cause cell death.[119]

1.5.4. Microtubules

Microtubules are a component of the cytoskeleton. They are important in maintaining the cell structure, motility, and cell signaling. Due to their involvement in separation of duplicate chromosomes during the mitotic cell division, microtubules have been a point of interest in cancer therapy.[120] Several PS, have been identified to disorganize microtubules, cause mitotic arrest and further leads to the induction of apoptotic cell death. Photofrin,[121, 122] sulphonated meso-tetraphenylporphyrines,[123] and Zinc(II)-phthalocyanine[124] were shown to cause cellular inhibition due to interuption of microtubule assembly by photoactivation.

1.5.5. Mitochondria

Generally, drugs interfering with mitochondrial function are known to be more effective in killing tumor cells.[81] This also holds true in the case of PDT agents.[81] Of all the intracellular organelles, mitochondria are thought to be the most attractive target in PDT.[69-71, 125] Mitochondria are called the power house of cells due to their involvement in energy production in the form of ATP, metabolism, calcium ion signaling, maintaining redox potential, etc.[126, 127] Following mitochondrial photo damage a series of events such as loss of mitochondrial membrane potential, and release of proapoptotic factors (Smac/Diablo, AIF and cytochorme c) into cytosol, which leads to activation of caspases in presence of energy. Following activation of caspases, cell death occurs via apoptosis.[55, 63] Several models have been suggested to explain the mechanism of PDT post mitochondrial damage. One model is the PTPC model. This model suggests release of apoptosis related mitochondrial factors, mitochondrial proteins located in the mitochondrial intermembrane space, and collapse of mitochondrial transmembrane potential occur due to opening of PTPC.[73, 125, 128-130] PSs targeting mitochondria are commonly more efficient than those that do not. Several PSs like Photofrin, protoporphyrin IX, zinc phthalocyanine and silicon phthalocyanine have been found to affect mitochondrion by chance.[131] There is a need for rational design of mitochondrial targeting PSs.[132]

1.6. Mitochondrial targeting in PDT

The idea of mitochondrial targeting has its foundations during late 1980's, when Chen et al. observed that an enhanced mitochondrial transmembrane potential ($\Delta\Psi_m$) is a prevalent tumor cell property.[133, 134] Over 200 cell lines, including tumorous and normal varieties, were studied, and the authors demonstrated that a typical 60 mV higher mitochondrial transmembrane potential was observed in tumor cells than in normal cells. Only 2% of cell types did not show this characteristic.[133, 135] It was also observed that a few cationic molecules accumulated preferentially in the cancer cell mitochondria.[136] This is possible due to the negative plasma transmembrane potential (inner side of the cell) and inner mitochondrial transmembrane potential on the matrix side of the organelle. Due to the charge, cationic compounds were drawn through membrane and accumulated preferentially in the mitochondria. Hence, the concept of specific targeting of cancer cells through mitochondrial targeting is based on the findings that a large amount of cationic compounds tend to preferentially localize and retain in cancerous cell mitochondria compared to normal cell mitochondria.[137, 138]

The selective localization of cationic compounds can be explained using the Nernst equation. According to the Nernst equation, the plasma transmembrane potential is normally -60 mV while the mitochondrial transmembrane potential is usually -120 mV for normal cells and -180 mV for cancerous cells.[133]

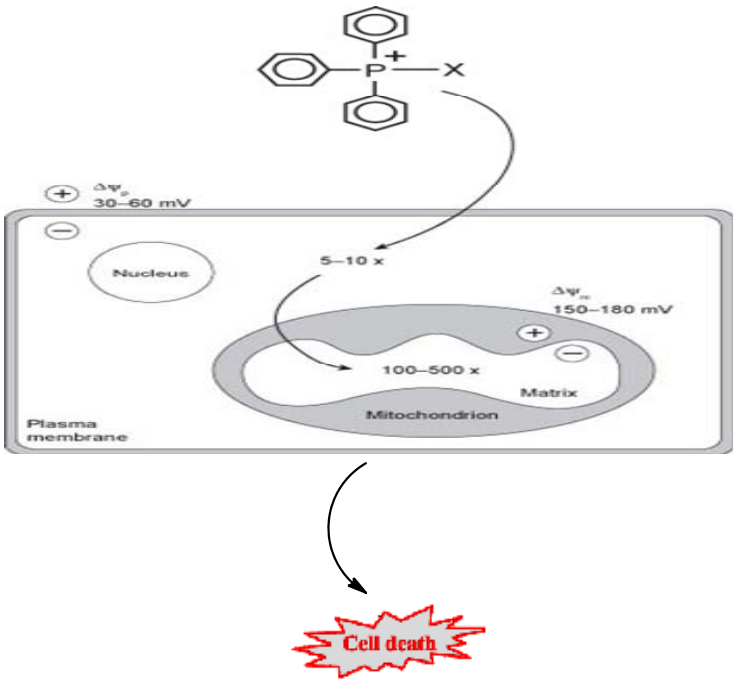

Figure 5. Schematics of mitochondrial targeting of DLCs (extracted and modified)[139].

Every -60 mV could lead to a 10 fold increase in the accumulation of positively charged molecules. Hence, upto a 1000-fold higher accumulation in the mitochondria compared to the cytoplasm can occur with molecules containing delocalized lipophilic cations (DLCs).[134]

Hence, a number of PSs have been developed by conjugating porphyrin based PSs (with good photosensitizing properties) to molecules that contain DLCs to achieve mitochondrial targeting.[140, 141]

1.7. Current Strategies for targeted drug delivery systems

1.7.1. Liposomal drug delivery

A liposome is an artificially synthesized encapsulated structure composed of an amphiphilic phospholipid bilayer with an aqueous interior.[142] Liposomes range in a size from 80-100 nm. Liposomes usually consist of phospholipids such as phosphatidylcholine and also contain mixed lipid chains with a blend of a surface active agent like phosphatidylethanolamine. A liposome consists of a lipophilic membrane that encapsulat a region of aqueous solution. This prevents the aqueous solution from escaping through the lipid envelope. Water insoluble compounds can be dissolved into the lipid membrane, and in this way, liposomes can carry both lipophilic molecules and hydrophilic molecules.

Thus using liposomes, compounds can be delivered to cell membranes where the liposome fuse with the cell membranes. Otherwise indiffusable lipophilic compounds such as DNA and drugs, can be delivered into the cells in the form of liposomes. Usually, all liposomes have a hydrophilic layer embedded. Although it is not a necessity. Various procedures have been followed for the encapsulation, such as a gradient method for vincristine[143] and ammonium sulfate method for doxorubicin.[144] Introduction of a hydrophilic polymer like polyethylene glycol (PEG) will lower detection by the reticuloendothelial system,[145] enhance circulation lifetime and prevent

interference between liposome and plasma proteins. Nevertheless, liposomes still suffer drawbacks suchas complexity in controlling the release of drugs from liposomes, extravasation from the blood and binding to cell surface receptors.[146]

1.7.2. Polymer drug delivery

Synthetic polymers are widely used for targeted drug delivery.[147] Most commonly used synthetic polymers are the aliphatic polyesters, specifically, hydrophobic polylactic acid (PLA), hydrophilic polyglycolic acid (PGA), and copolymers polylactide-co-glycolide (PLGA).

A distinctive characteristic of polymers in drug delivery is their controlled release profile spanning from days (PGA) to months (PLA), which can be accomplished by modification of the ratio of PLA to PGA.[148] Controlled release systems aim to improve efficacy by modifying pharmacokinetics and the pharmacodynamics of drug[149, 150] such as the release profile and capacity to cross biological carriers (which depends on the size of the particle), biodistribution, clearance, and stability (metabolism).

In sustained release, the active substance is steadily released with a kinetic profile of zero-order; thus the therapeutic effect is retained over a long period of time.[151]

Both the sustained and controlled drug release from internalized or localized PLGA nanoparticles can be very useful as they offer capability to control the rate, duration and amount of intracellular drug concentration. The rate and extent of duration of release are important factors in improving efficacy. Some polypeptides still have drawbacks in their drug delivery potential such as limited sites for conjugation with drug and ineffective sustained release.

1.7.3. Dendrimer drug delivery

Dendrimers are monodisperse macromolecules with recurring branching structures that originat from a central core.[152] Drug molecules can be entrapped in the labyrinthine core created by the branches.[153, 154] Poly(amidoamine) (PAMAM) is a well known dendrimer for drug delivery. The core of PAMAM is a diamine (also known as ethylene diamine). This reacts with methyl acrylate, one more diamine making a generation-0 PAMAM. Successive reactions can generate higher generation PAMAM with varying properties. The PAMAM core is used as a drug reservoir and has been used for delivery of small molecules.[153, 155] Upon conjugation with other chemical species onto the dendrimer, surface, they act as targeting molecules (for example folic acid for targeting tumors).[156] Dendrimers have served as multivalent systems due to their large number of functional groups. Along with use as drug delivery tools, dendrimers are also conjugated to prostate-

antigen-specific antibodies for targeting the prostate[157] and peptides for targeting vascular endothelium[158] and intestinal epithelium.[159]

Even though dendrimeric drug delivery improves selectivity and stability of therapeutic agents, there are still limitations such as uptake by the reticuloendothelial system, leakage of the drug, exert immunogenic response, hemolytic toxicity, and hydrophobicity.[160]

1.8 Aim and scope

Current research scientists are in search for new methods to better cure cancer. One such new therapeutic modality is photodynamic therapy. PDT is a localized therapy in which an administered photosensitizer generates reactive oxygen species (ROS) upon excitation with red light. Even though PDT has become an established treatment for a variety of diseases, its clinical application remains narrow because of drawbacks of the so far used PDT agents or drugs. In order to improve the acceptability of PDT, several strategies including the development of third-generation photosensitizers with more favorable properties and combination with anticancer drugs are being investigated. The goals of this dissertation project were to develop new or improve upon existing photosensitizers.

Overall, this dissertation investigates ways of improving the photodynamic response of photosensitizers. Two approaches to deliver photosensitizers

were investigated: 1) using DLC dyes to exploit membrane potential differences between the cytoplasm and the mitochondria in delivering photosensitizers specifically to the mitochondria. 2) using photosensitizer-anticancer drug prodrug system where the two are connected via a singlet oxygen cleavable bond to deliver and release anti-cancer drug only at the tumor region. (Figure 6)

This dissertation is divided into three distinct projects with each having their own objective. These include:

1) To evaluate the potential of tetranitrogenic porphyrin (TPP)-cation conjugates to serve as mitochondria delivery vehicles for photosensitizers.

2) To evaluate the potential of core-modified porphyrin (CMP)-cation conjugates to serve as mitochondria delivery vehicles for photosensitizers.

3) To evaluate the potential of prodrug system to provide site-specific release of anti-cancer drugs.

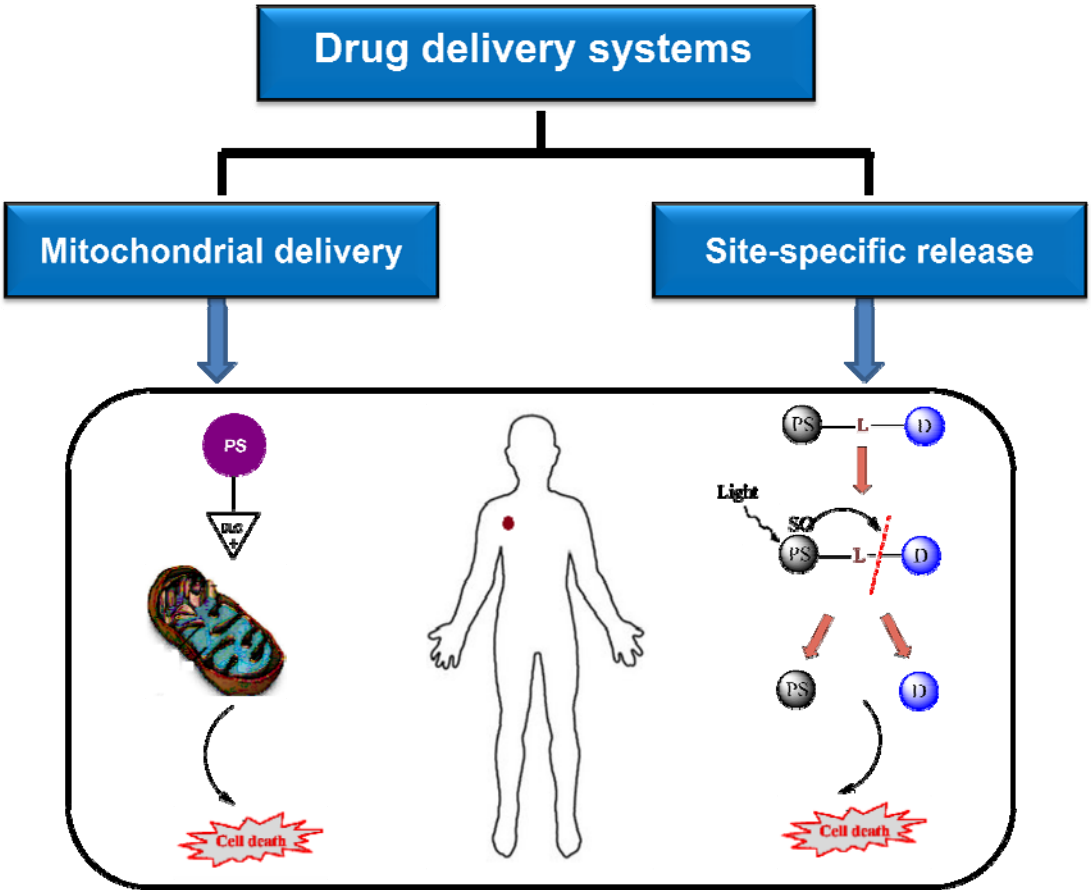

Figure 6. Schematics of scope of the dissertation showing the two approaches of drug delivery

Chapter 2. In vitro biological evaluation of tetra nitrogenic prophyrin based lipophilic cation conjugated photosensitizers for targeting mitochondria

2.1. Introduction

A functional mitochondrion has a membrane potential difference across the membrane.[133] Under in vitro conditions a maximum potential difference of ~180 mV has been recorded across the mitochondrial membrane.[135] Due to this potential difference, molecules with delocalized lipophilic cations navigate through the inner mitochondrial membrane and localize in the negative mitochondrial interior. The selective localization of cationic compounds can be explained using the Nernst equation. The plasma transmembrane potential is normally -60 mV while the mitochondrial transmembrane potential is usually -120 mV for normal cells and -180 mV for cancerous cells.[133]

The Nernst equation describes the ratio of cations accumulated in the mitochondria in response to those outside as follows.

$$\Delta\Psi_m = -\frac{RT}{ZF} \ln\left(\frac{A_{in}}{A_{out}}\right) \quad (1)$$

Where $\Delta\Psi_m$ is the membrane potential difference, R is the gas constant (8.314 JK^{-1} mol^{-1}), T is the absolute temperature, F is Faraday's constant

(96485.34 $Cmol^{-1}$), Z is the valence or charge, and A is the chemical activity of the ions inside and outside the mitochondria respectively.

A more simplified form of the above equation for monovalent cation at 37 °C, considering the chemical activity and concentration as follows:

$$\Delta\Psi_m = -61.5 \log_{10}\left(\frac{C_{in}}{C_{out}}\right) \quad (2)$$

Every -60 mV leads to a 10 fold increase in the accumulation of positively charged molecules. Hence, up to thousand fold higher accumulation into the mitochondria as compared to the cytoplasm can occur with molecules containing delocalized lipophilic cations.[134] However these maximum concentration are rarely achieved in most biological systems, they could be achieved with proper design of molecules.[161]

In order for maximum mitochondrial accumulation of these selected cationic dyes, the mechanism of mitochondrial targeting must be the predominant mode of subcellular distribution. One such process that might prohibit mitochondrial localization is lipophilic partitioning[136]. In order to achieve high tumor cell selectivity, the lipophilicity of the cationic dye must be low enough to prevent any contributions arising form lipophilic partitioning as this can compete with the transmembrane potential guided mitochondrial localization process[136]. In absence of which the accumulation of the cationic dye in tumor

cells *vs.* normal cell will decrease significantly;[136] consequently, loss of selectivity may occur. Accumulation of the dye into other organelles may occur with equal efficiency.[138, 162-164] Hence, the accumulation of lipophilic cationic compound into the mitochondria of tumor cells will be hypothetically possible only if the transmembrane potential-driven processes are greater than that of the process of lipophilic partitioning or any other competing subcellular distribution mechanism.[136]

Keeping the above criteria into consideration, several delocalized lipophilic cation containing PS as discussed below have been developed for mitochondrial targeting.

A number of cationic compounds are known to accumulate in the mitochondria of cells, yet, only a small sub-class of these compounds are recognized to induce the desired photochemical effect in cancerous cells with a high degree of specificity.[132] Crystal Violet (CV^+, Figure 7), belonging to the class of cationic triarylmethanes (TAM^+), is a relatively low toxicity compound.[165] It has been used in a variety of medicinal applications such as antihelmintics, antiseptics, and for treatment of umbilical cords of newborns,[166] as well as an antifungal to treat both topical and vaginal infections caused by *Candida*.[167] CV^+ localizes in the mitochondria and then kills the tumor cells (HT-29).[138]

Ethyl Violet (EV^+, Figure 7) is another cation which is a known cytotoxic agent. Indig and colleagues have demonstrated EV^+ accumulates both in mitochondria and lysosomes of both normal (CV-1) and cancerous cells (MES-SA)[138]. Furthermore, the cytotoxicity observed is due to a combination of mitochondrial damage and subcellular toxic events.[138] However, the studies involving both CV^+ and EV^+ were of high importance, as they disclose that only compounds localizing in mitochondria exclusively can induce the cytotoxicity of tumor cells with high level of selectivity. Further, these researchers identified that compounds processing a lipophilic/hydrophilic property similar to that of the mitochondrial specific probe Rhodamine-123 (Rh-123) are effectively up taken by cancer cells in huge amounts and demonstrate selectivity to cancer cells[168].

Rh-123 is an affiliate of a class of dyes (rhodamines) well-known to accumulate in mitochondria of cells. Due to its high fluorescence properties, Rh-123 is commonly used as a biological probe in fluorescence microscopy. This was the first compound to be identified as a mitochondrial probe by Chen and colleagues.[133, 134, 169] Rh-123 accumulates and is retained for a longer time in tumor cells vs. normal cells. The means of cellular uptake and sub cellular localization into mitochondria of Rh-123 is controlled chiefly by transmembrane potential.[133, 134] It was also noticed that the compound passes directly into mitochondria without staining any of the organelles like plasma membrane, nuclear envelope, lysosomes, endoplasmic reticulum or

Golgi apparatus.[170] Due to easy mitochondrial uptake and retention, low cellular toxicity and high fluorescing nature makes Rh-123 a great choice by a lot of researchers. However, it shows poor photosensitizing properties.[171]

Further, several other PSs have been evaluated for mitochondiral targeting. To list some cyanines, xanthenes, phenothiazinium, triarylmethanes, chalcogenapyryliums, oxazines, and thiopyrylium dyes[171]. Despite their specificity in localizing into mitochondria they suffer several drawback: instability in vivo, low absorbance's in the NIR region and poor quantum yields for singlet oxygen generation[172]. Hence, a number of photosensitizers have been developed by conjugating porphyrin-based photosensitizers with good photosensitizing properties to DLC containing molecules for mitochondrial targeting.[140, 141]

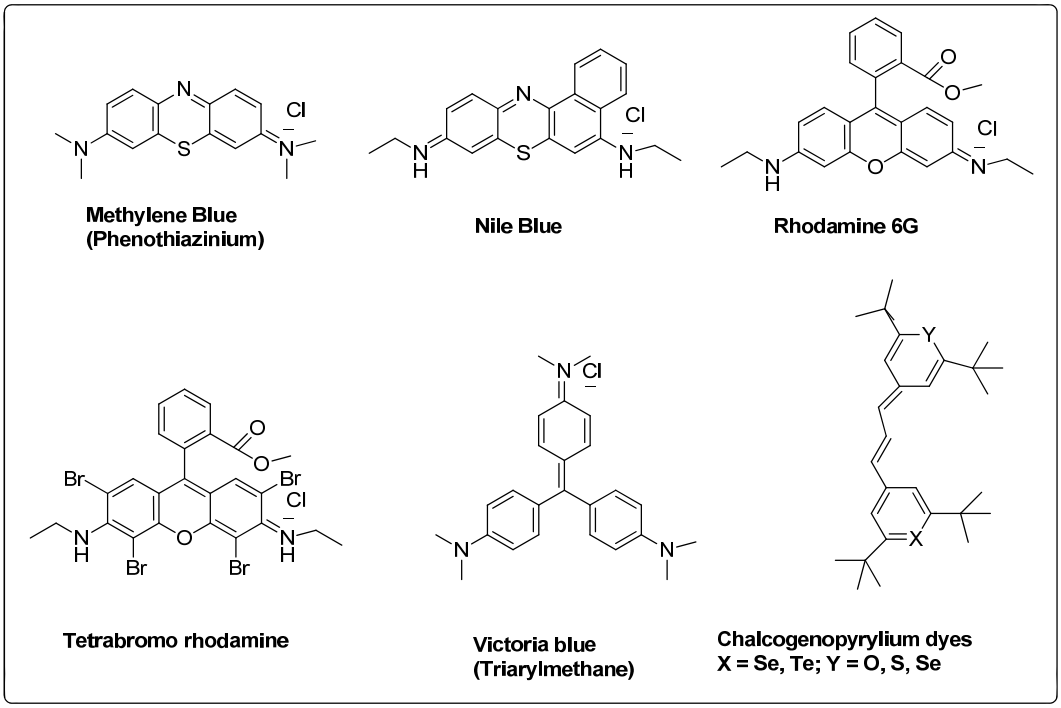

Figure 7. Examples of DLCs

2.2. Hypothesis

It can be hypothesized that a porphyrin-based photosensitizers tethered to a DLC containing dye via short aliphatic linker system would deliver the photosensitizer to the mitochondria by taking advantage of the mitochondrial membrane potential difference, finally improving the photodynamic effect.

Two DLC containing dyes were thus chosen: rhodamine B and acridine orange.

The choice of Rhodamine B was because it contains a DLC and could be easily conjugated to a porphyrin by esterification. Furthermore, derivatives of rhodamine, such as rhodamine 123, have been shown to specifically accumulate in the mitochondria by utilizing the property of mitochondrial membrane potential difference.[133]

The second dye, Acridine orange, was a choice due to its ease of conjugation to a porphyrin by alkylation to obtain a quaternary amine, similar to nonyl acridine orange[173]. Nonyl acridine orange, a known cardiolipin specific moiety, has been demonstrated to favor mitochondrial localization.[126] Hence, along with taking advantage of the mitochondrial membrane potential difference, acridine orange-porphyrin conjugates might also bind to cardiolipin, to further enhance mitochondrial uptake.

2.3. Experimental design

The synthesis and evaluation of the photophysical properties of the two conjugates was done by Dr. Ethel Ngen.[173] Briefly, a porphyrin–rhodamine B conjugate (TPP–Rh) and a porphyrin-acridine orange conjugate (TPP–AO), each possessing a single delocalized lipophilic cation, were synthesized. The conjugates were synthesized by conjugating a monohydroxy porphyrin (TPP-OH) to rhodamine B (Rh B) and acridine orange base (AO), respectively, via saturated hydrocarbon linkers.

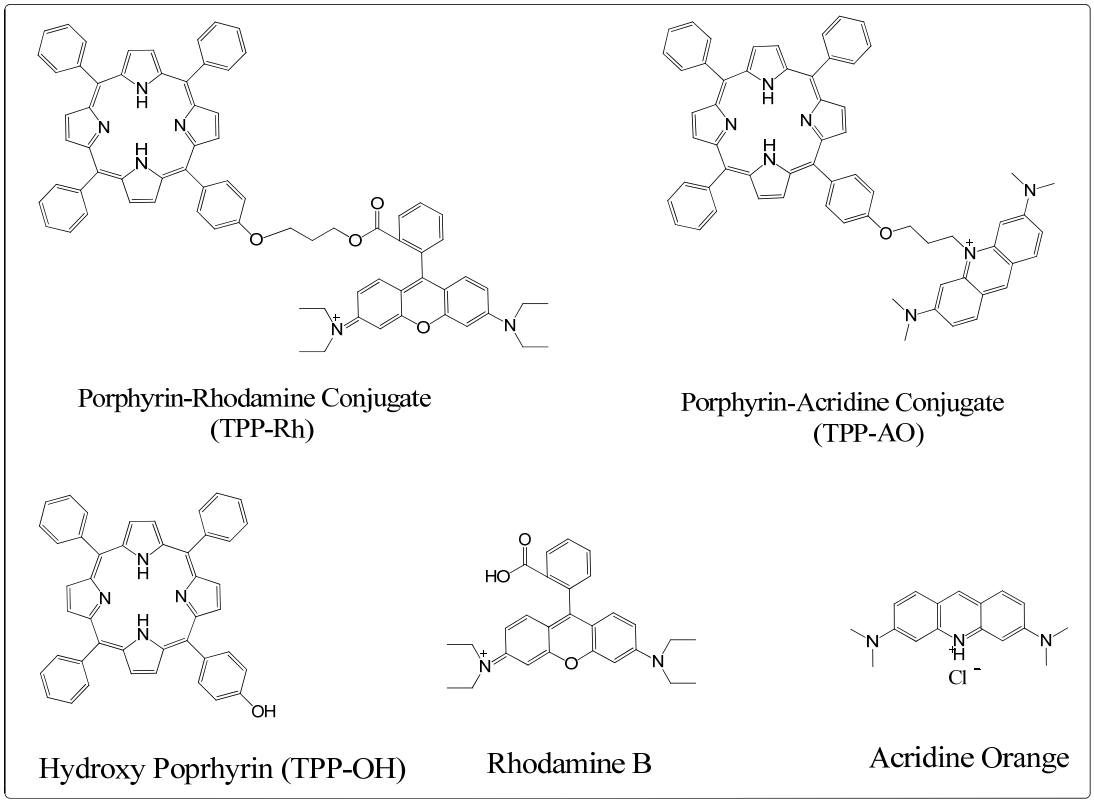

Figure 8. Structures of DLC-conjugated to TPP[173]

To evaluate the efficiency of the conjugates as photosensitizers, their photophysical properties and in vitro photodynamic activities were studied in comparison to those of TPP-OH, the parent porphyrin photosensitizer.

My contribution for this project was to perform the in vitro evaluation of the conjugates.

2.4. Experimental procedure

2.4.1. Cells and culture conditions

The rodent mammary adenocarcinoma cell line (R3230AC) was used for all biological experiments. All reagents and culture media were obtained from Invitrogen and Sigma-Aldrich. The cells were maintained in minimum essential medium (α-MEM) supplemented with 10% bovine growth serum, 50 units/mL penicillin G, 50 µg/mL streptomycin and 1.0 µg/mL Fungizone. The cells were incubated at 37 °C in 5% CO_2 using a Sanyo MCO-18AIC-UV incubator. The cells were sub-cultured biweekly to maintain the cells at approximately 80% confluency. The dyes in all studies except for in vivo studies were initially dissolved in DMSO to make a 2 mM stock solution. For in vivo studies samples were prepared in a mixture of 1% Tween 80 and 5% dextrose solution[174]. A Lab-line Barnstead International orbital shaker was used for all phototoxicity tests and a Molecular Devices SpectraMax M2 microplate reader was used to read UV/Vis absorbance's. Either an Edinburgh Instruments F900 spectrophotometer or a Molecular Devices SpectraMax M2 microplate reader was used to read the fluorescence.

2.4.2. Intracellular accumulation

Dye concentrations in cells were determined using the fluorescence intensities of the dyes at appropriate excitation and emission wavelengths,

following the procedures in our previous reports.[175, 176] Briefly, 2 mM porphyrins stock solutions were prepared by dissolving the appropriate amount of the respective dyes in DMSO. The stock solutions were diluted to the appropriate concentrations with complete media immediately before the addition to cells. 10 μL of the respective dilute solutions were then added to 190 μL of complete media in each well and the well plates incubated for 24 h. After incubation, the medium was removed and the R3230 cell monolayer was rinsed twice with a 0.9% NaCl solution. 50 μL of DMSO was then added to solubilize the cells and the fluorescence from the porphyrins was read using a fluorescence multi-well plate reader (Molecular Devices, SpectraMax M2 model) set at the appropriate excitation and emission wavelengths. The intracellular porphyrin concentrations were then determined from a standard fluorescence curve obtained by dissolving porphyrin standards in DMSO to obtain dilute solutions. Results were expressed in fmol/cell.

$$\text{Intracellular Accumilation} = \frac{\text{Amount of dye in cell (fmol)}}{\text{Number of cells}} \quad (3)$$

$$\text{Amount of dye (mol)} = \text{Concentration (M)} \times \text{Volume (L)} \quad (4)$$

2.4.3. Stability of the ester bond of TPP-Rh in culture media with cells

The cells were seeded at 2.0 - 3.0 $\times$ 10^4 cells/well complete media using 96 well plates and incubated for 24 h. The dye stock solutions were then diluted to the appropriate concentrations with complete media, and added to the

cells. The cells were incubated for 24 h, after which the medium was removed and the cell monolayer was rinsed twice with a 0.9% NaCl solution. DMSO (1900 µL) was then added to disrupt the cells and the fluorescence was read at λ_{ex} = 550 nm and λ_{em} = 650 nm. The fluorescence spectra of TPP-Rh in the cell lysate (DMSO digested) was compared to the spectra obtained for TPP-Rh in DMSO . The ratio of the 580 nm and 650 nm fluorescence peaks of TPP-Rh in the cell lysate was also compared to that of TPP-Rh in DMSO.

2.4.4. Dark toxicity

The cells were treated and cell viability was determined as described in our previous reports.[175, 176] Porphyrin stocks solutions (2 mM), prepared by dissolving the appropriate amounts of the respective dyes in 1.5 mL of DMSO, were then diluted to the appropriate concentrations in complete media immediately before addition to cells. 10 µL of the respective dilute solutions was then added to 190 µL of complete media in each well and the well plates incubated for 24 h. The medium was then removed and the cell monolayer rinsed twice with 190 µL of a 0.9 % NaCl solution. Clear medium, with neither phenol red nor bovine growth serum, was then added to the wells and the well plates kept in the dark for 1 h. After this the clear medium was removed and 190 µL of complete medium added. The cultures were

then incubated at 37 °C in 5 % CO2, for 24 h, after which the cell viability was determined by MTT assay MTT assay is a colorimetric assay which measures enzyme activity in living cells, thus is used in determining cell viability after treatment with cytotoxic agents. MTT (3- (4,5-Dimethylthiazol-2-yl)-2,5-diphenyltetrazolium bromide), is a yellow tetrazole which upon reduction by reductases present in the mitochondria of living cells, is converted to a purple formazan salt.

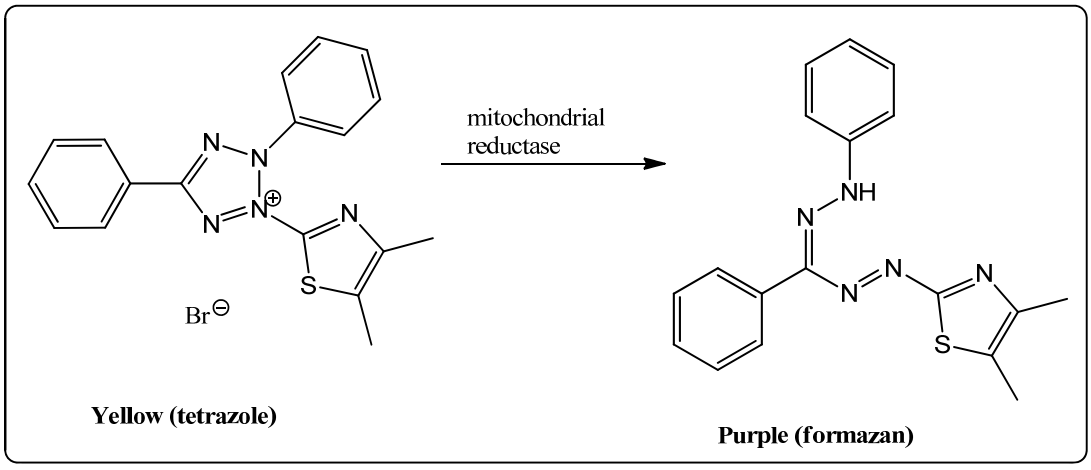

Figure 9. MTT reduction to formazan (MTT Assay)

On the day of assay a 10 uL of a 10 mg/mL solution of MTT prepared in PBS was added to 190 uL of complete media in the wells and the cells incubated for 4 h. The solutions were then removed and the cell pellets dissolved in 50 uL of DMSO and the absorbance measured at 570 nm with background substraction at 650 nm. The cell viability was then quantified by measuring the absorbances of the treated cells, compared to that of the untreated cells

(controls) and expressed as a percentage. The controls used in the dark toxicity tests were cells kept in the dark and not incubated with porphyrins.

$$\% \text{ Cell survival} = \frac{(A_{570\ nm} - A_{650\ nm})\ \text{Treated cells}}{(A_{570\ nm} - A_{650\ nm})\ \text{Control}} \times 100\% \quad (5)$$

2.4.5. Phototoxicity

The cells were seeded at 1.0 - 1.5 $\times$ 10^4 cells/well in complete media (section 2.4.1) using 96 well plates then incubated for 24 h. The stock solutions of the dyes were then diluted to the appropriate concentrations with complete media and added to the cells. The cells were incubated for 24 h. After this the medium was removed and the cell monolayer was rinsed twice with 190 µL of a 0.9% NaCl solution. Clear medium was then added to the wells and the well plate was placed on the well plate shaker. The well plate lids were removed and the wells were exposed to broadband visible light delivered at 3 $mWcm^{-2}$ from a 60 W halogen light source for an hour. The broadband light was filtered through a 3.5 cm water filter (400-850 nm) to prevent heating of the cells. Uniform irradiation of the entire well plate was achieved by gently orbiting the well plate on the shaker. After irradiation, the clear media was removed and 190 µL of complete media added to the wells. The cells were again incubated for 24 h, after which the cytotoxicity was determined by MTT

assay and expressed as a percent of the controls (cells exposed to light in the absence of the dyes).

2.4.6. Sub-cellular localization

Dual staining of each dye with Mitotracker Green (MG, M-7514 from Invitrogen Co.) was performed to determine their mitochondrial localization. Since both TPP-OH and the conjugates (TPP-Rh and TPP-AO) fluoresce in the red region of the optical spectrum, a green filter (Propidium Iodide filter, exciter: HQ535/50; emitter: HQ645/75; set: 41005 from Chroma Technology Co.) was used to acquire the images. For MG, which fluoresces in the green region of the optical spectrum, the images were obtained using a red filter (FTC/Bdipy/Fluo3/DiO filter, exciter: HQ480/40; emitter: HQ535/50; set: 41001 from Chroma Technology Co.). However, because some fluorescence from the photosensitizers could be captured with the FTC/Bdipy/Fluo3/DiO (green) filter and some of the fluorescence of Mitotracker Green with the Propidium Iodide filter (red), the exposure time was carefully monitored to avoid/minimize cross contamination from each other. To determine the appropriate exposure times, the minimum time required to take an image of cells singly stained with MG, TPP-OH, TPP-Rh, or TPP-AO were first obtained. The cells were then doubly stained with MG and either TPP-OH, TPP-Rh or TPP-AO and images obtained using both the green and red

filters. The green and red images were then superimposed, and the regions of colocalization appeared as yellow.

Cells were seeded at 2.0 - 3.0 $\times$ 10^4 cells/well in 24 well plates containing 12 mm diameter cover slips and then incubated for 24 h. The dyes diluted to the appropriate concentrations were then added to the well plates and incubated for 8 h. After 7 h, 1μM of Mitotracker Green was added to the cells and the cells incubated for 1 more hour. After 8 h, the media was removed and the cell monolayer was rinsed three times with 3 mL of complete media. The cover slide was then mounted on a slide and the images taken using a Leica DMI4000B fluorescence microscope fitted with a QImaging Fast 1394 camera and Qcapture processing software. The images were modified for better visualization with Adobe Photoshop Element 5.0.

2.4.7. Statistical analyses

All experiments were done in triplicates at least twice, and statistical analyses were performed using the Student's t-test for pairwise comparisons.

$$t = \frac{\overline{X}_1 - \overline{X}_2}{\sqrt{\frac{S_1^2}{N_1} + \frac{S_2^2}{N_2}}} \qquad (6)$$

$$S = \sqrt{\frac{\sum_{i=1}^{n} \left(X_i - \overline{X}\right)}{N}} \qquad (7)$$

Where $\overline{X}_1 - \overline{X}_2$ are the respective means of the different trials, N1 and N2 are the number of data points in each trial; S1 and S2 are the standard deviation within each trial. The calculated t-values were then compared to standard t-values obtained from a table at a 95 % confidence level (*P*-value = 0.05). Whereas, calculated t-values greater than the standard t-values indicated a significant difference between the means calculated t-values less than standard t-values indicated no significant difference between the means.

All data outliers were removed after performing a Q-test:

$$Q_N = \frac{(X_a - X_b)}{R} \qquad (8)$$

Where, Q_N is the calculated Q-value calculated from N data points; X_a is the suspected outlier, X_b is the data point closest to suspected outlier (X_a) and R is the data range. The calculated Q-values were then compared to standard Q-values obtained from a Q-table at a 95 % confidence level (*P*-value = 0.05). All calculated Q-values greater than the standard Q-value at the given degree of freedom, indicated the presence of an outlier and were discarded, while Q-values less than the standard Q-values at the given degree of freedom were retained. All error bars represent standard deviations from the mean.

The phototoxicity data was further fitted into the S-Plot software, which is based on the Hill (sigmoid E_{max}) equation, to determine the exact IC50 values.

$$\mathrm{Log}_{10}\left(\frac{\text{Response}}{E_{max} - \text{Response}}\right) = \mathrm{Log}_{10} C_R - \mathrm{Log}_{10} C_{R,\,50\%} \qquad (9)$$

Where Emax is the maximum PDT response, C_R is the concentration at a given PDT response, and $C_{R\ 50\%}$ is the concentration needed to induce 50 % of the maximum response.

2.5. Results and discussion

2.5.1. Intracellular accumulation

The conjugates accumulated more compared to the unconjugated dye (Figure 8). TPP-AO showed the highest uptake of about 12 times higher than TPP-OH with 68.2 vs. 5.6 fmol/cell. TPP-Rh showed an uptake of 8 times higher than that of TPP-OH with 44.0 vs. 5.6 fmol/cell. The uptake of TPP-OH and Rh B were < 10 fmol/cell. The higher uptake of the conjugates compared to the unconjugated dyes could be accredited to the lipophilic cation on the compounds and their increased flexibility by the aliphatic linker. The lipophilic cation on the compounds might aid in binding to negatively charged proteoglycan on cell membrane and diffusion into the cells and the mitochondria against the potential gradient.[177-180] The increased flexibility of

the conjugate may be the reason for the improved uptake partly by increasing the entropy of the conjugates.[181] Along with that, aggregation of the conjugates might also be effected by the flexibility for the higher cellular uptake.[182]

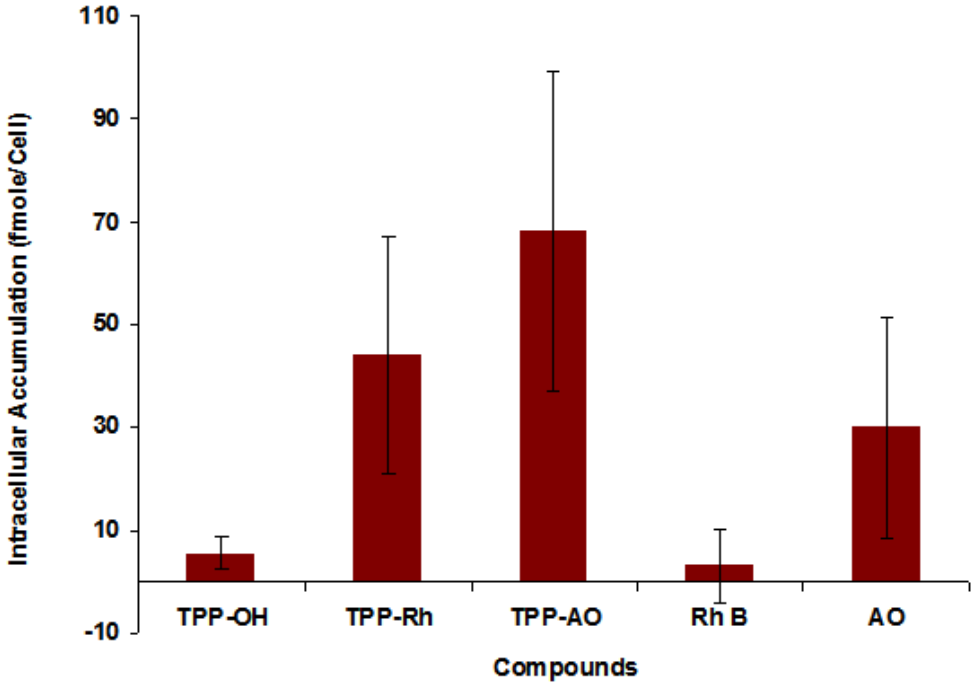

Figure 10. Intracellular accumulation of dyes in R3230AC cells. Cells were incubated with the respective dyes (10 μM) for 24 h and the intracellular uptake determined from a fluorescence calibration curve. Each data point represents the average from three separate experiments, error bars are the SEM.

2.5.2. Stability of the ester group of TPP-Rh in culture media with cells

Since ester bonds can be acted upon by esterases in the cells, the stability of the ester bond in TPP-Rh was determined. Signature of fluorescence peaks of TPP-Rh was used to study the changes. The fluorescence spectrum of TPP-Rh in the cell lysate was similar to that of TPP-Rh in DMSO and different from that of an equimolar mixture of TPP-OH and Rh B in DMSO (Figure 11). In addition, the ratio of the intensity of the fluorescence peak at 580 nm to that at 650 nm of TPP-Rh in the cell lysate was similar to that of TPP-Rh in DMSO. A ratio of 0.25 was obtained for TPP-Rh in the cell lysate and 0.21 for TPP-Rh in DMSO. This signifies that the ester bond might not be cleaved in cells unless both cleaved products, TPP and Rh B derivatives, are cleared from the cell immediately. This is probably due to steric hindrance in the conjugate. As a result, it can be inferred that TPP-Rh, acted as the conjugate once delivered to the cells.

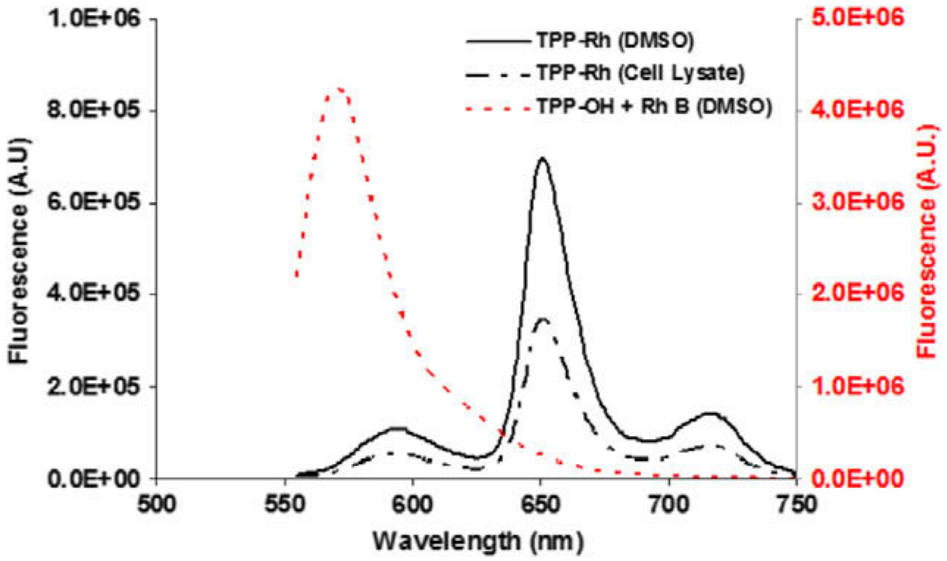

Figure 11. Stability of the ester group in TPP–Rh: fluorescence spectra of TPP–Rh and a mixture of TPP-OH and Rh B in DMSO (each 10 μM) and R3230AC cell lysate after incubated with TPP–Rh (10 μM) for 24 h. Samples were excited at 550 nm and the fluorescence read from 555 to 750 nm. Two Y-axis scales were used to take into account the differences in fluorescence intensities of TPP–Rh (Y1: black colored scale) and TPP-OH + Rh B (Y2: red colored scale).

2.5.3. Dark toxicity

No significant dark toxicity was observed in cells treated with up to 20 μM of either TPP-Rh, TPP-OH, or Rh B. This was most likely due to their inability to generate singlet oxygen in the dark. However minimal dark toxicity was observed in cells treated with more than 5 μM of either AO·HCl or TPP-AO

(Figure 12). Presumably, it was caused by inherent toxic mechanisms of AO such as DNA intercalation and inhibition of protein synthesis.[183-188]

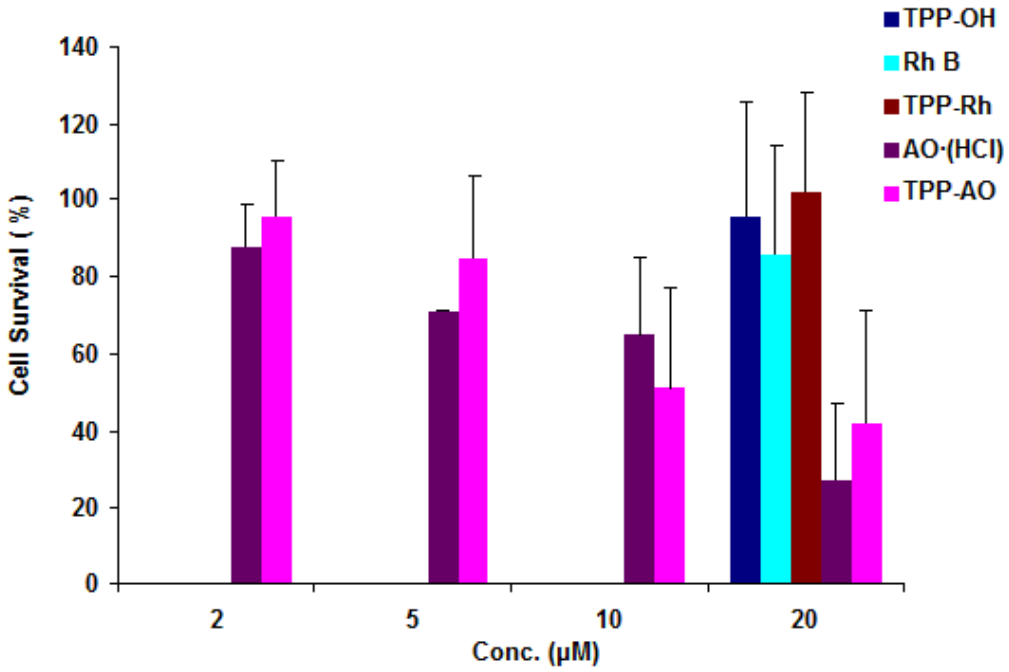

Figure 12. Dark toxicities of the respective dyes incubated in R3230AC cells for 24 h at different concentrations. Whereas TPP-OH, TPP–Rh, and Rh B were incubated at 20 μM, TPP–AO, and AO-HCl were incubated at 2 μM, 5 μM, 10 μM and 20 μM and kept in the dark. Each data point represents the average from three separate experiments, error bars are the SEM.

2.5.4. Phototoxicity:

No significant photo toxicity was observed in cells treated with up to 20 μM of either TPP-OH or Rh B and irradiated with a 60 W halogen lamp at 3 $mWcm^{-2}$ for an hour (Figures 13). On the other hand, cells treated with either TPP-Rh, TPP-AO or AO·HCl and irradiated under the same conditions showed significant phototoxicity. AO·HCl showed the highest phototoxicity under the above irradiation conditions with an IC_{50} of 2.29 μM, followed by TPP-AO with an IC_{50} of 3.28 μM and then TPP-Rh with an IC_{50} of 3.95 μM. The absence of phototoxicity observed in the cells treated with up to 20 μM of either TPP-OH or Rh B could be attributed to a number of reasons. In TPP-OH this might be due to its low intracellular accumulation and formation of aggregates in aqueous media. While in Rh B this might be due to low intracellular accumulation and low quantum yields for singlet oxygen generation. On the other hand, the greater phototoxicity observed with TPP–Rh and TPP–AO, despite their large size, high lipophilicity, and tendency to aggregate in aqueous media, could be attributed to their high intracellular accumulation and sub-cellular localization in singlet oxygen-sensitive organelles like mitochondria. Although there was no significant generation of singlet oxygen under our experimental condition, AO-HCl showed the most phototoxic effect. It might be due to the phototoxic effect via type I mechanism in addition to its dark toxicity.[189]

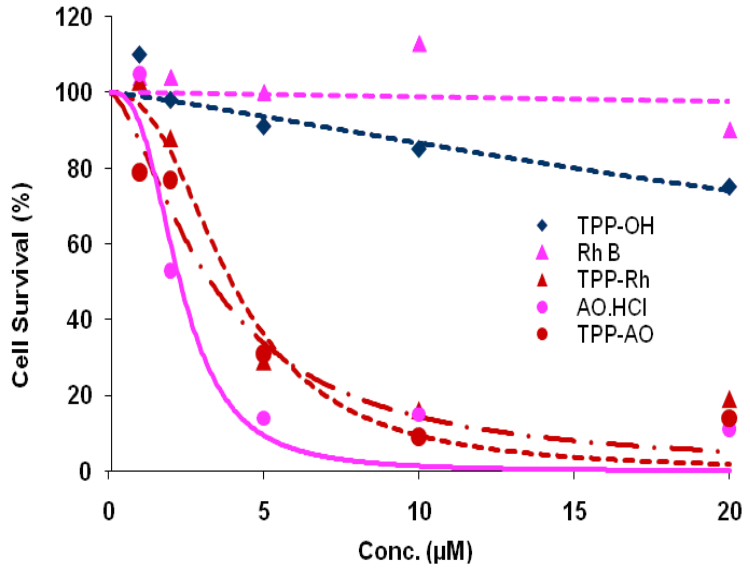

Figure 13. Phototoxicity of R3230AC cells treated with the respective dyes and irradiated with a 60W halogen lamp at 3 $mWcm^{-2}$ for 1 h. Cells were incubated with the respective dyes at 1, 2, 5, 10, and 20 μM, respectively, for 24 h prior to irradiation. Each data point represents the average from three separate experiments, error bars are the SEM.

2.5.5. Sub-cellular localization

Dual staining of each dye with MG (MitoTracker Green) was first performed to determine localization in mitochondria. The dual staining of TPP–Rh with MG was successful. However, TPP-OH and TPP–AO dual staining with MG was not possible due to the overlapping fluorescence of TPP-OH and TPP–AO with MG. Whereas, for cells stained with 1 μM MG, exposure times of 37 ms and 5 s were required for the green and red filter, respectively, the

following exposure times were required for the other dyes using the green and red filters, respectively: 2 μM TPP-OH (5 s and 5 s), 5 μM TPP–Rh (4.5 s and 330 ms), and 2 μM.

TPP–AO (40 ms and 2 s). In the dual staining of TPP–Rh with MG, the green and red filter could capture fluorescence from MG and TPP–Rh, respectively. Exposure times of 23 ms and 230 ms were needed for the green and red filter, respectively, which are close to the time scales for taking an image from individual staining with each filter. Since dual staining was not successful for TPP-OH and TPP–AO with MG, fluorescence images of individual staining were used to assess the sub-cellular localization. Both TPP–Rh and TPP–AO showed a different localization pattern from that of TPP-OH (Figure 14). Whereas TPP-OH seemed to have been accumulated in localized vesicles in the peri-nuclear area (Figure 14b), TPP–Rh was distributed throughout the cytoplasm like MG (Figure 14d–f). However, TPP–AO showed two differences in pattern compared to TPP–Rh and MG (not shown). Staining of TPP–AO was more homogeneous throughout cytosol and also stained the nucleus, presumably due to interactions with cytosolic RNAs and nuclear DNA. In contrast, TPP–Rh and MG showed punctuate staining patterns consistent with mitochondrial localization. TPP– Rh showed a very similar staining pattern to MG. This sub-cellular localization of TPP–Rh was further confirmed by the dual staining studies. From the image analysis of the superimposed MG (green filter) and TPP–Rh (red filter)

images, the yellow regions indicate regions of colocalization (Figure 14f). The TPP–Rh might be accumulated in mitochondria due to the presence of the delocalized lipophilic cation which permitted their accumulation in mitochondria.

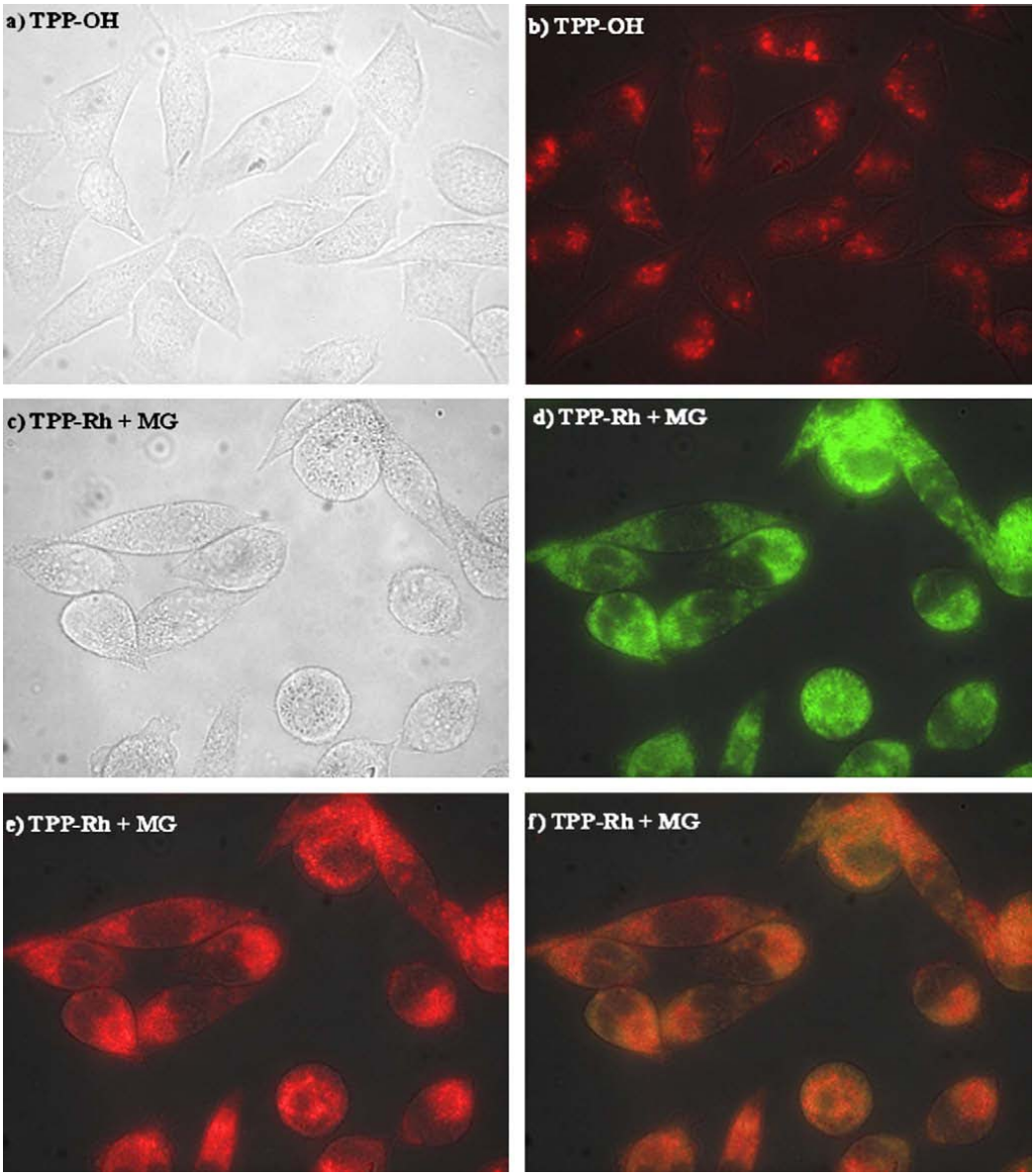

Figure 14. Sub-cellular localization of TPP-OH and TPP-conjugates: Cells

treated with TPP-OH (2 μM) alone: (a) Bright field (50 ms), (b) red filter (5s); TPP–Rh (5 μM) + MG (1 μM): (c) bright field (50 ms), (d) green filter (23 ms), (e) red filter (230 ms), (f) overlap: bright field (c), green filter (d) and red filter. All images were made using R3230A cells after incubated with dye(s) for 8 h (TPP-OH, TPP–Rh, and TPP–AO) or 1 h (MG).

2.6. Summary and conclusions

The biological evaluation of two conjugates, TPP-Rh and TPP-AO, was done. The high photo toxicities of the conjugates could be attributed to both their high intracellular accumulation and their mitochondrial localization. The conjugation of TPP to Rh and AO did improve intracellular uptake and in vitro photodynamic activity. In particular, TPP-Rh seemed to preferentially localize into mitochondria. Our study suggests that Rh moiety might provide two benefits to other photosensitizers: enhanced cellular uptake and mitochondrial localization, which are two important subjects in PDT.

2.7. Further studies

From the above studies Rh shows promising results. Hence preparation of Rh conjugates in conjugation with other second generation photosensitizers will be studied in the next chapter.

Chapter 3. In vitro and in vivo biological evaluation of core-modified porphyrin lipophilic cation conjugated photosensitizers for targeting mitochondria

3. 1. Introduction

Photodynamic therapy (PDT) has gained great popularity as a treatment modality for both neoplastic and non-neoplastic diseases. A beauty of PDT lies in its ability to ablate malignant tissue without systemic toxicity, which is a major drawback of traditional methods like chemotherapy and radiotherapy. PDT involves an energy transformation from photonic energy (light) to chemical energy (reactive singlet oxygen) via a non-toxic photosensitizer. Singlet oxygen ($^1O_2$) is the principle cytotoxic agent in PDT.[2, 190] Due to the short lifetime (<0.04 μs) and small radius of diffusion in biological systems (<0.02 μm),[191] the photosensitizer should be closely located to the target (the site of action) damaged by PDT.

The mitochondrion is a key organelle for cell survival due to its involvement in energy production and apoptotic pathways.[69-75] Hence, by targeting the mitochondria of the cell we may not only achieve apoptotic cell death but also maximize PDT effect. A number of photosensitizers have been designed to target the mitochondria of a cell for improved PDT treatment.[132] A few of them are benzoporphyrin-derivatives,[192] and delocalized lipophilic cations (DLCs) like Rhodamine 123,[168] thiopyrylium AA-1,[193] Rhodacyanin MKT-

077.[194] One popular targeting strategy is to take advantage of DLCs' tendency of preferential accumulation in mitochondria.[126, 141, 195-198] DLCs penetrate the hydrophobic layer of plasma and mitochondria membrane and accumulate inside the mitochondria. According to the Nernst equation, every 60 mV difference in membrane potential could lead to 10-fold increase in the accumulation of compounds bearing positive charge.[197] A maximum of ~ 180 mV of potential difference has been measured in the mitochondrial membrane.[135] Theoretically, up to 1000 fold more mitochondrial accumulation compared to extracellular fluid could be achieved based on the charge on the molecule.

In our previous work, (Chapter 2) we designed TPP-DLC (TPP: tetraphenyl porphyrin & DLC: rhodamine B or acridine orange) conjugates and achieved mitochondrial localization and higher cellular uptake by conjugating porphyrin to rhodamine.[173] We obtained 8 and 14 times higher uptake with the conjugate compared to unconjugated porphyrin and rhodamine, respectively. Core-modified porphyrins (CMPs) have been extensively studied as second-generation photosensitizers due to their multiple advantages.[199-204] Especially, the dithiaporphyrins were prepared in a highly pure and well-characterized form. CMPs can also absorb longer wavelength light (690-710 nm) than Photofrin (a clinically approved photosensitizer, 630 nm) and tetra-pyrrole prophyrins (648 nm)[173] and are highly photostable.[205] In addition,

CMPs showed high singlet oxygen generation quantum yield ($\Phi(^1O_2)$, ~ 0.8) making them very efficient PS for PDT treatment.[202]

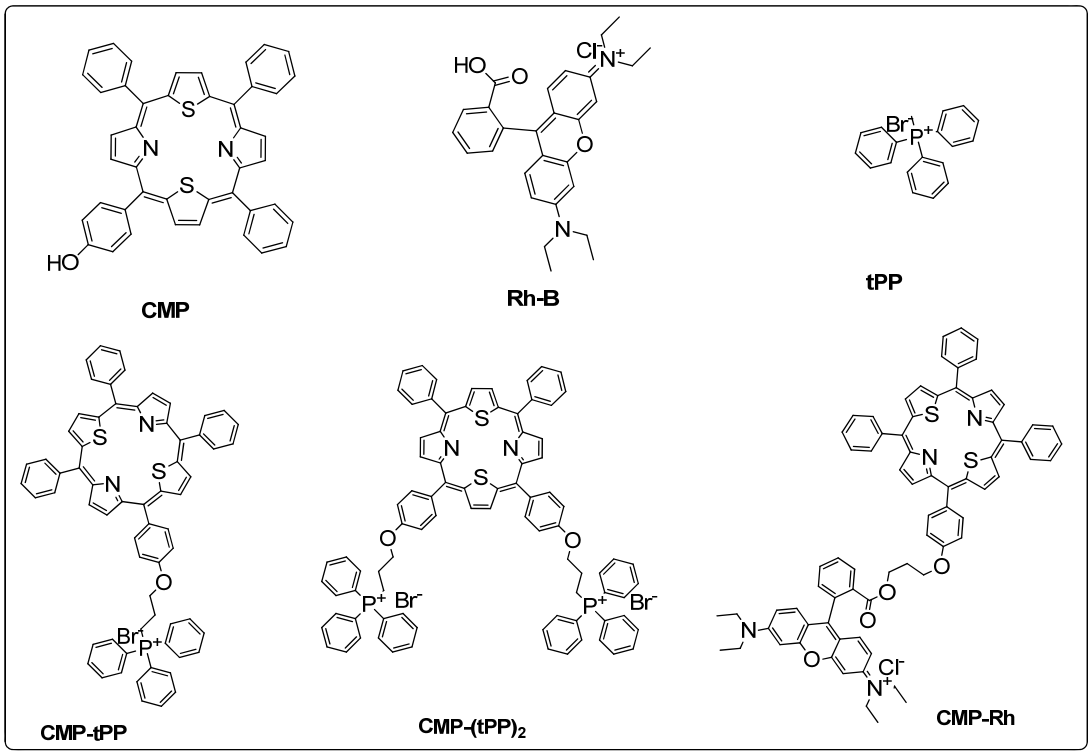

Figure 15. Structures of DLC-conjugated CMPs[206].

In the current work, we attempted to develop mitochondria-specific CMP conjugates by tethering them to DLCs. Three conjugates were designed such as CMP-Rh (a core modified porphyrin-rhodamine B), CMP-tPP (a core modified porphyrin-mono-triphenyl phosphonium), and CMP-$(tPP)_2$ (a core modified porphyrin-di-triphenyl phosphonium cation)(Figure 15). The choice of rhodamine B is mainly due to its effective delivery of photosensitizers (tetraphenyl phorphyrin (TPP) and phthalocyanine (Pc)) into the mitochondria .[173, 207] Triphenyl phosphene (tPP) was chosen since it also improved the

mitochondrial uptake of several bioactive compounds by several hundred fold.[208-211] We prepared both mono- and di-substituted CMP-tPPs to see the effect of a number of cations on mitochondrial localization. We envisioned that these DLCs deliver the conjugates to mitochondria and thus eventually augment the PDT efficiency of CMP.

The compounds used in this project were contributed by Mr. Gregory Nkepang. All the compound were characterized using NMR. I performed the photophysical characterization and biological evaluation of the dyes.

3.2. Experimental section

3.2.1. General methods

3.2.2. Photophysical studies

The photophysical properties of the synthesized conjugates and their corresponding components were determined in either chloroform or dimethyl sulphoxide. Electronic absorption spectra were recorded using either a PerkinElmer UV-Vis spectrophotometer (LAMBDA 25). Steady state fluorescence spectra were recorded with a PerkinElmer fluorescence spectrometer LS45 or a Molecular Device fluorescence plate reader (Gemini EM).

3.2.2.1. Absorption spectra and molar extinction coefficients

Dilute solutions of the respective dyes were prepared at appropriate concentrations, where the Beer-Lambert law holds true (absorbances less than 1 OD). With the exception of rhodamine B (prepared in methanol) all other samples were prepared in chloroform. The molar extinction coefficients of the respective samples were then calculated from the Beer-Lambert equation:

$$A = \varepsilon cl \qquad (10)$$

Where A is the absorbance, is the molar absorption coefficient (M-1 cm-1), c is the concentration of the solution (M) and l is the path length (cm). All experiments were done in triplicates and the results were reported in M-1 cm-1.

3.2.2.2. n-Octanol/pH 7.4 buffer partition coefficients

n-Octanol/water partition coefficients of the dyes were determined by the "shake flask" direct measurement method.[212] Saturated solutions of the dyes were prepared by adding the dyes to a mixture of equal volumes (1 mL) of *n*-octanol and a pH 7.4 phosphate buffered saline (PBS). The saturated solutions were placed in an ultrasound bath for 30 min, then left to settle for 4 h. Then, each layer was diluted with chloroform and the absorbance of the

dyes in the respective solutions was determined. The partition coefficients were then obtained by calculating the ratio of the concentrations of the respective dyes in the two layers ([Dye]n-octanol/[Dye]buffer). Results were reported as log $D_{7.4}$ values.

3.2.2.3. Aggregation tendency of the dyes in a medium

Tendency of the dyes to aggregate in a culture medium was indirectly determined by comparing their fluorescence intensities in the culture medium to that in DMSO.[213] The dyes were dissolved in DMSO (2 mM), diluted to the appropriate concentrations with more DMSO, and 10 µL of the diluted solution added to 190 µL of either complete media or DMSO in 96 well plates to give 10 µM solutions. The plates were then left for an hour after which the fluorescence readings were taken at the appropriate excitation and emission wavelengths (CMPOH, CMP-tPP, CMP-$(tPP)_2$ excitation 410 nm, emission 714 nm, CMP-Rh, Rh B excitation 520 nm, emission 590 nm). The change in the fluorescence intensities of the dyes in a complete medium compared to that in DMSO was then used to estimate the aggregation tendencies of the dyes. The results were expressed in arbitrary units.

$$\text{Aggregation tendency} = \text{Flu}_{\text{Organic solvent}} - \text{Flu}_{\text{Aqueous solvent}} \qquad (11)$$

3.2.2.4. Energy transfer (ET) in the CMP-Rh conjugate

Due to the proximity of the two fluorophores, CMP-Rh was expected to act as a ET pair where Rh B acts as the donor and CMP acts as acceptor. Thus, it was necessary to determine the ET efficiency to estimate the SO generating capability of the conjugate. Decrease in fluorescence intensities of the donor molecule at specific wavelengths, measured in the presence of the acceptor molecule at different distances, was used to demonstrate ET in the conjugate.[214] A solution of the conjugate (molecules in a close proximity) and an equimolar mixture of the conjugate's individual components CMP-OH and Rh B (molecules at a long range) were compared. Stock solutions of the CMP-Rh, CMP and Rh B (2 mM) were prepared in tetra hydro furan(THF). The compound stock solutions were then diluted with THF to give 1 μM solutions. The fluorescence intensities of CMP-Rh and a mixture of CMP-OH and Rh B were measured by exciting at 435 nm and 525 nm and the fluorescence was measured from 535-650 nm to or 500-750 nm. The decrease in fluorescence intensity of the Rh B peak at 580 nm was used to demonstrate ET.

3.2.2.5. Singlet oxygen generation

The generation of singlet oxygen by the respective dyes upon irradiation was determined indirectly, by measuring the rates of oxidation of 1,3-diphenylisobenzofuran (DPBF).[215, 216]

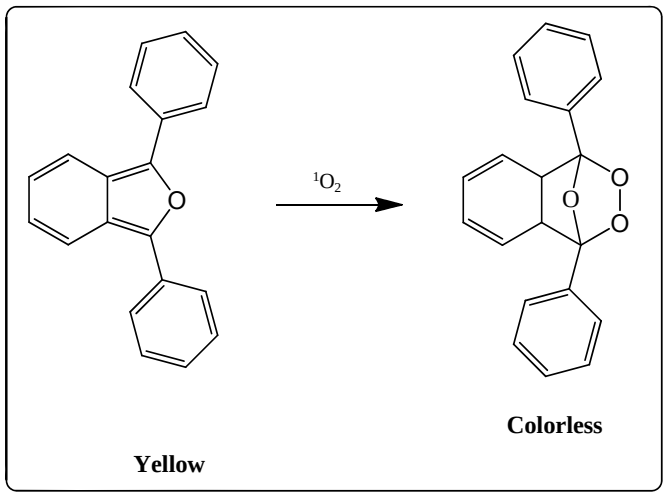

Figure 16. DPBF oxidation by singlet oxygen via [2+4] cycloaddition

Stock solutions of the respective dyes (2 mM) were prepared in DMSO. A solution of the respective photosensitizer (5 μM) and DPBF (100 μM) in THF were then prepared in culture tubes, so that the 2 mL solutions had not more than 2 % (v/v) of DMSO as a cosolvent. The culture tubes were then irradiated using 690 ± 10 nm light (LC122-A, LumaCare) for all the dyes at 1 $mWcm^{-2}$ for 20 min. Every 2 min, the absorption readings at 414 nm were taken. The rates of DPBF oxidation by the different dyes were then compared.

$$\text{Efficiency of } [^1O_2] \text{ generation} = \frac{\Delta [\text{DPBF}]t}{[\text{DPBF}]t_0} \times 100\% \qquad (12)$$

3.2.3. In vitro studies

3.2.3.1. Cells and culture conditions

Mouse colon cancer cells (Colon 26) or human breast cancer cells (MCF-7) were used for all biological experiments. All reagents and culture media were obtained from Invitrogen and Sigma-Aldrich. The cells were maintained in minimum essential medium (α-MEM) supplemented with 10% bovine growth serum, 2mM L-glutamine, 50 units/mL penicillin G, 50 µg/mL streptomycin and 1.0 µg/mL fungizone. The cells were incubated at 37 °C in 5 % CO_2 using a Sanyo MCO-18AIC-UV incubator. Colon 26 cells were sub-cultured biweekly and MCF-7 cells were sub-cultured once a week to maintain the cells at approximately 80 % confluency. The dyes in all studies were initially dissolved in DMSO to make a 2 mM stock solution. A Lab-line Barnstead International orbital shaker was used for all phototoxicity tests to make more homogeneous light exposure. A BioTek® plate reader (Synergy™ 2) was used to read UV/Vis absorbance. A Molecular Device fluorescence plate reader (Gemini EM) was used to read the fluorescence.

3.2.3.2. Intracellular accumulation

Dye concentrations in cells were determined using the fluorescence intensities of the dyes at appropriate excitation and emission wavelengths, following the procedures in our previous reports.[204, 217] Intracellular accumulation at treatment concentrations 10 and 5 μM were determined.

3.2.3.3. Dark toxicity

The cells were treated and cell viability was determined as described in the experimental section for phototoxicity without irradiation at 5μM concentration.[204]

3.2.3.4. Phototoxicity

Colon 26 cells were seeded at 1 - 1.5 $\times$ 10^4 cells/well in 96 well plates then incubated for 24 h in 5 % CO_2 at 37 ^{o}C. The stock solutions of the dyes (2 mM in DMSO) were diluted to appropriate concentrations with the complete medium (see 3.2.3.1) and added to the cells to give final dye concentrations (0.25, 0.5, 1, 2, 5 μM). After incubation for 24 h, the medium was removed and the cell monolayer was rinsed twice with 190 μL of a 0.9 % NaCl solution. The complete medium was then added to the wells and the well plate was placed on the well plate shaker. The well plate lids were removed

and the wells were exposed to 690 nm diode laser (except Rh B with 540 ± 10 nm LumaCare) delivered at 5.6 $mWcm^{-2}$ for 30 min. To achieve more uniform irradiation, the entire well plate was gently orbited on the shaker. After the irradiation, the cells were again incubated for 24 h, after which the cytotoxicity was determined by MTT assay and expressed as a percent of the controls (cells exposed to light in the absence of the dyes).

3.2.3.5. Sub-cellular localization

General procedures for image slide preparation: Cells were seeded at 2 - 3 $\times$ 10^4 cells/well in 24 well plates containing one 12 mm diameter cover slip per well and then incubated for 24 h. The dyes diluted to the appropriate concentrations were then added to the well plates and incubated for 14 h. [For dual imaging with Rh-123, 2 μM of Rh-123 was added to the cells at 12 hr time point and the cells incubated for 2 more hours.] After 14 h the media was removed and the cell monolayer rinsed three times with 1 mL of PBS solution. The cover slip was then mounted on a slide and the images were taken using a Leica DMI4000B fluorescence microscope fitted with a QImaging Fast 1394 camera and spot advance version 4.6 processing software. The images were processed for better visualization with Adobe Photoshop Element 5.0.

Dual staining of each dye with Rh-123 (Rhodamine 123, M-7514 from Sigma Aldrich) was made to determine their mitochondrial localization. Since both CMP-OH and the conjugates (CMP-tPP, CMP-$(tPP)_2$ and CMP-Rh) fluoresce in the red region of the optical spectrum, a red filter (Propidium Iodide filter, exciter: HQ535/50; emitter: HQ645/75; set: 41005 from Chroma Technology Co.) was used to acquire the images. For Rh123, which fluoresces in the green region of the optical spectrum, the images were obtained using a green filter (FTC/Bdipy/Fluo3/DiO filter, exciter: HQ480/40; emitter: HQ535/50; set: 41001 from Chroma Technology Co.). To determine the appropriate exposure times, the minimum time required to take an image of cells individually stained with Rh-123, CMP-Rh, CMP-tPP, or CMP-$(tPP)_2$ were obtained from the independent experiments. For dual staining experiments, the cells were stained with Rh-123 and either CMP-Rh, CMP-tPP or CMP-$(tPP)_2$ and images were obtained using both the green and red filters. The green and red images were then superimposed, and the regions of colocalization appeared as yellow.

3.2.4. In vivo studies

3.2.4.1. Animals

Female BALB⁄c mice were purchased from NCI (Frederick, MD). Mice were housed and handled in the animal facility of College of Pharmacy, University of Oklahoma Health Sciences Center, Oklahoma City, OK. All animal

experiments were approved by IACUC, University of Oklahoma Health science Center, Oklahoma City.

3.2.4.2. In vivo biodistribution

Mice were injected via i.p. with various cations (25 μmol kg^{-1}). At specified time intervals (24, 48 and 72 h post injection), the mice (three mice per each time point) were euthanized by CO_2 inhalation. Tissues were excised from major organs and tumor. Collected tissues were rinsed with PBS and blotted dry. 100 mg of excised tissues were homogenized with DMSO (1 mL). The homogenates were centrifuged at 5160 g for 20 min and then the supernatant was used for fluorescence measurement (excitation at 440 nm and emission at 720 nm). The amount of compound in each sample was determined relative to the standard curve and expressed in ‘‘nmol g^{-1} tissue’’ unit.

3.2.5. Statistical analysis

Statistical analyses were performed using the Student's t-test for pairwise comparisons. A *P* value of < 0.05 was considered significant. The Hill (sigmoid Emax) equation was used to determine IC_{50} values.

3.3. Results and discussion

3.3.1. Photophysical studies

3.3.1.1. Absorption spectra & molar extinction coefficients

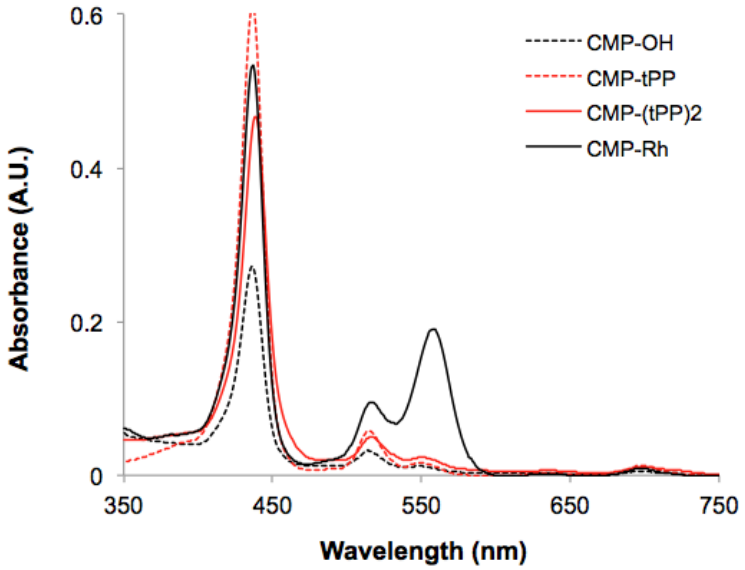

Figure 17. Absorption spectra of CMP-OH, CMP-tPP, CMP-$(tPP)_2$, and CMP-Rh at 2 μM in $CHCl_3$.

Three conjugates showed all the characteristic absorption peaks of its respective components, indicating that no significant electronic interactions might occur at the ground state (Figure 17).[218] While absorption maxima and extinction coefficient of all the conjugates remained practically the same, the extinction coefficients of CMP-OH had much lower molar extinction coefficients than those of the others (Table 1). It might indicate some degree of aggregation in the ground state.[219] There was a slight red shift of Rh B

peak from 550 to 558 nm in CMP-Rh as observed in our previous conjugate TPP-Rh. This might be due to the proximity of the CMP moiety that seemed to change the polarity of the environment of rhodamine moiety, consequently red shifting the maxima of Rh B in the conjugate.[220, 221]

Compds.	Soret Band	Band IV	Band III	Band II	Band I	Log D $_{7.4}$
CMP-OH	436 (146)	517 (17.3)	548 (5.7)	636 (2.6)	699 (2.8)	2.3
CMP-tPP	437 (293)	515 (27.8)	549 (8.3)	634 (1.7)	698 (5.9)	2.04
CMP-(tPP)$_2$	438 (231)	516 (23.7)	551 (11.0)	634 (6.0)	700 (5.4)	1.79
CMP-Rh	437 (280)	517 (50.0)	558 (101.3)	NA	700 (4.4)	2.01
Rh B*			550 (110.6)			2.07

$\lambda_{max,}$ nm (μ x 10^3 $M^{-1}cm^{-1}$). * In Methanol

Table 1. UV- vis - near - IR band maxima and extinction coefficients in chloroform & n-octanol/pH 7.4 buffer partition coefficients of dyes.

3.3.1.2. Aggregation tendency of the dyes

Generally, the aggregation tendency of a dye is greatly dependent on various factors such as lipophilicity, molecular symmetry, flexibility.[219] Aggregation usually leads to a dramatic decrease in both fluorescence emission and

singlet oxygen generation, consequently decreasing the photodynamic activity of photosensitizers.[213] High aggregation tendency in a medium could be translated to that in the cytoplasm. Consequently, it could cause reduced phototoxicity. Although the lipophilicities (Log $D_{7.4}$) of the dyes are pretty close, within 1.79 - 2.04, their aggregation tendencies in the medium showed variations (Figure 18). All three conjugates seemed to aggregate more in aqueous media and less in DMSO. CMP-OH showed the most severe aggregation in the medium, only 2.5% fluorescence emission in the medium compared to that in DMSO. This suggests that the aggregation of the conjugates could be attributed mostly to the highly planar and rigid structure of CMP-OH. However, Rh B and CMP-Rh showed a different aggregation pattern, aggregating almost similarly in both medium and DMSO. This is probably due to the presence of the rotatable pendent phenyl ring of rhodamine moiety, thus reducing the aggregation in the medium.

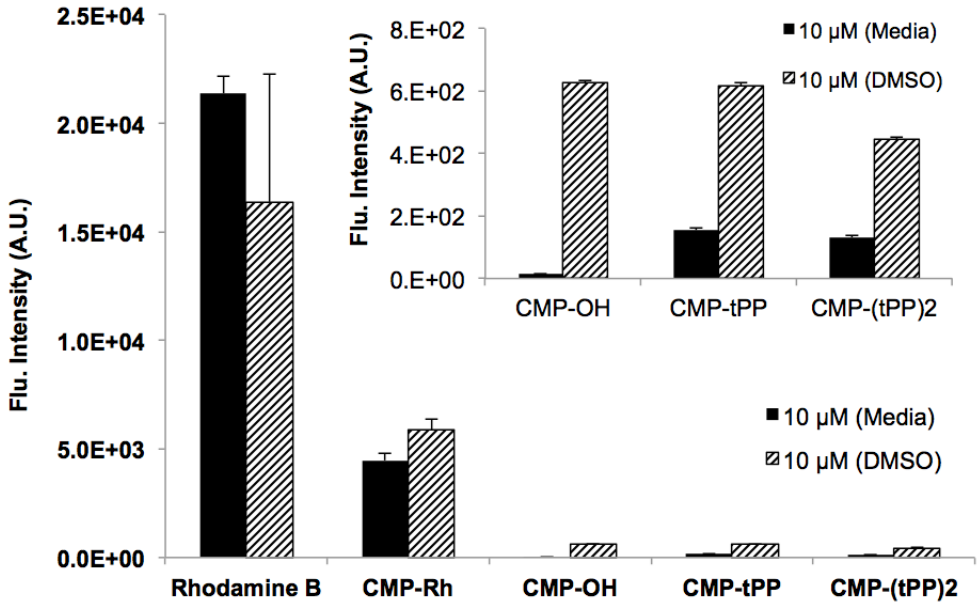

Figure 18. Fluorescence emission from the dyes (10 μM) in both the complete medium and DMSO: CMP-OH, CMP-tPP and CMP-$(tPP)_2$ excitation at 430 nm & emission at 714 nm and CMP-Rh and Rh B excitation at 520 nm and emission at 590 nm. Inset shows an expanded area.

3.3.1.3. Energy transfer in the conjugate CMP-Rh

Energy transfer (ET), a communication between two chromophores, is a possible phenomena when the two chromophores are in proximity. Among the three conjugates, only CMP-Rh has two chromophores with a potential of ET. We also observed ET between TPP and Rh.[173] If there is ET from CMP to Rh, it could reduce singlet oxygen generation capability of CMP of the CMP-Rh. Thus, to estimate ET we measured fluorescence quenching in

three samples: 1) CMP-Rh, 2) CMP-OH (or Rh B), and 3) a mixture of CMP-OH and Rh B at an equimolar concentration (2 μM). If there is ET, fluorescence of excited chromophores should be reduced. Fluorescence emission spectra were recorded after irradiation at 435 or 525 nm to excite CMP or Rh moiety (Figure 19).

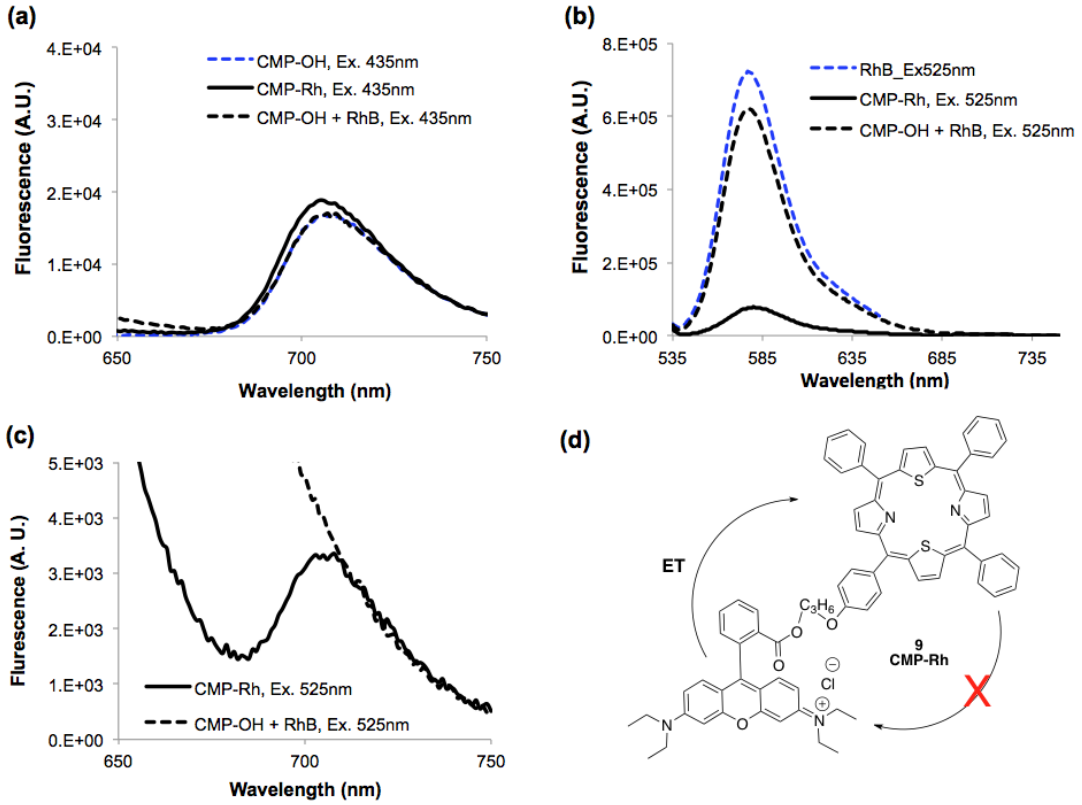

Figure 19. Fluorescence spectra of CMP-Rh, CMP-OH, and Rh B a) excited at 435 nm, b) excited at 525 nm, c) magnified graph of b in the CMP emission peak area, and d) ET directions in CMP-Rh.

Interestingly, when CMP of CMP-Rh was excited at 435 nm, it showed very similar CMP emission (λ_{max}, 705 nm) intensity with those of CMP-OH and a mixture of CMP-OH and Rh B (Figure 19a). There might be no significant

energy loss in CMP-Rh when excited at 435 nm. On the other hand, when Rh of CMP-Rh was excited at 525 nm, there was dramatic decrease (~ 80 %) in fluorescence emission from CMP-Rh compared to those of Rh B and a mixture of CMP-OH and Rh B (Figure 19b). In addition, after excitation of the Rh group at 525 nm, a significant CMP emission was detected from CMP-Rh but not from CMP-OH + Rh B (Figure 19c). There might be a ET from Rh to CMP. Since there may not be effective energy transfer from CMP to Rh, it is unlikely that singlet oxygen generation capability of CMP in CMP-Rh is reduced.

3.3.1.4. Singlet oxygen generation:

Singlet oxygen generation efficiency of the photosensitizers was evaluated using DPBF (1,3-diphenylisobenzofurane), a popular singlet oxygen probe.[2] The rates of DPBF oxidation by all three conjugates were similar to that of CMP-OH (Figure 20). Even CMP-Rh and CMP-$(tPP)_2$ showed faster DPBF oxidation. In our previous studies, CMPs gave highly effective singlet oxygen quantum yields, ~ 0.8.[222-224] This indicates all conjugates were able to generate singlet oxygen at rates comparable to that of CMP-OH with CMP-Rh being the most efficient followed by CMP-$(tPP)_2$. No significant DPBF oxidation was detected by light alone, Rh B, or tPP alone.

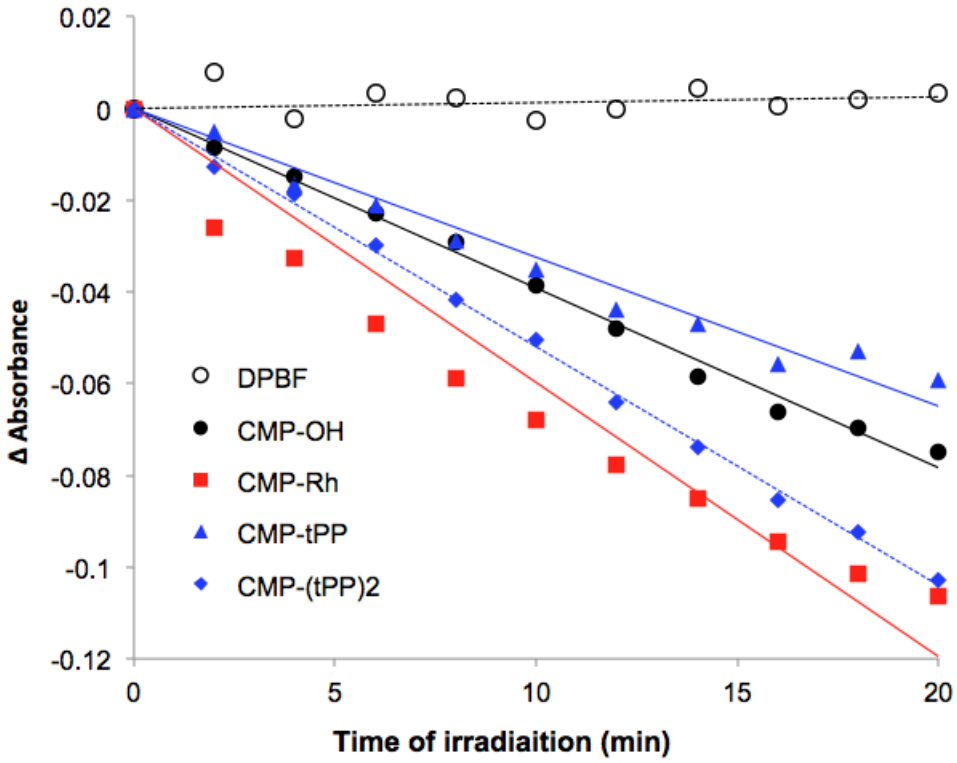

Figure 20. Relative rates of DPBF oxidation by singlet oxygen generated from the respective dyes irradiated with 690 ± 10 nm light (LC122-A, LumaCare) at 1 $mWcm^{-2}$. 5 μM of the respective dyes were mixed with 100 μM of DPBF and the mixture irradiated for 20 min. Absorbance readings at 414 nm were taken every 2 min.

3.3.2 In vitro studies

3.3.2.1. Cellular uptake

Cellular uptake was determined using the fluorescence of the conjugates after colon 26 cells were incubated with each conjugate for 24 hr at 5 or 10

μM. Interestingly, all three cationic conjugates showed greatly enhanced uptake compared to the unconjugated dyes (CMP-OH or Rh B)) (Figure 21). CMP-Rh and CMP-$(tPP)_2$ showed about 7 times and CMP-tPP showed about 14 times higher than CMP-OH at 10 μM. Similarly, the conjugates CMP-Rh, CMP-tPP, CMP-$(tPP)_2$ showed 10.6, 18.9, 8.3 times higher uptake than CMP-OH at 5 μM. The higher accumulation of the conjugates compared to CMP-OH could be attributed to the delocalized positive charge on the molecules and reduced aggregation due to their increased flexibility by the aliphatic linker. The delocalized positive charge on the molecules might facilitate binding to negatively charged proteoglycan on cell membrane and allow diffusion into the cells and the mitochondria against the potential gradient.[177-180] The increased flexibility of the conjugate might contribute to the enhanced uptake at least in part by decreasing the aggregation and increasing the entropy of the conjugates.[181]

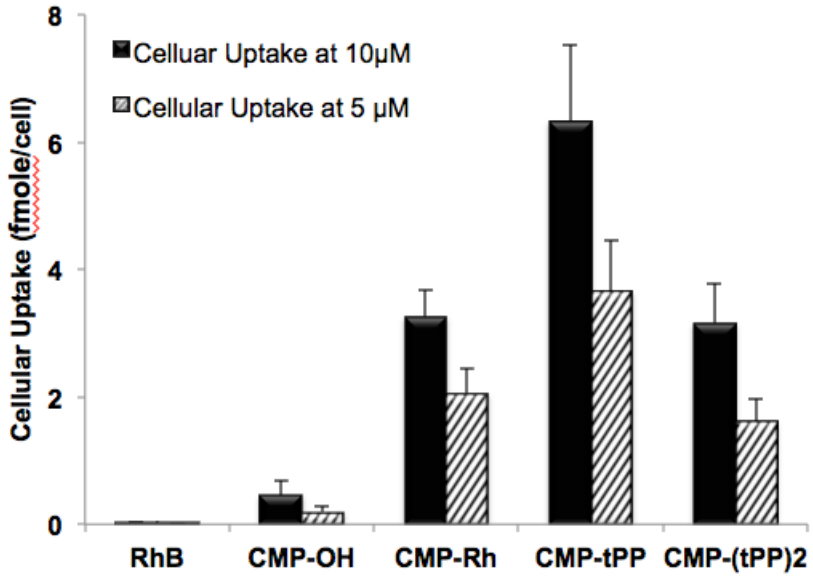

Figure 21. Intracellular accumulation of the dyes in Colon 26 cells. Cells were incubated with the respective dyes (at 5 or 10 μM) for 24 h and the intracellular uptake was determined from a fluorescence standard curve of each dye.

3.2.2.2. Dark toxicity

No significant dark toxicity was observed in cells treated with up to 5 μM of CMP-OH, Rh B, tPP or three conjugates (Figure 22). This may probably be due to their inability to generate singlet oxygen in the dark.

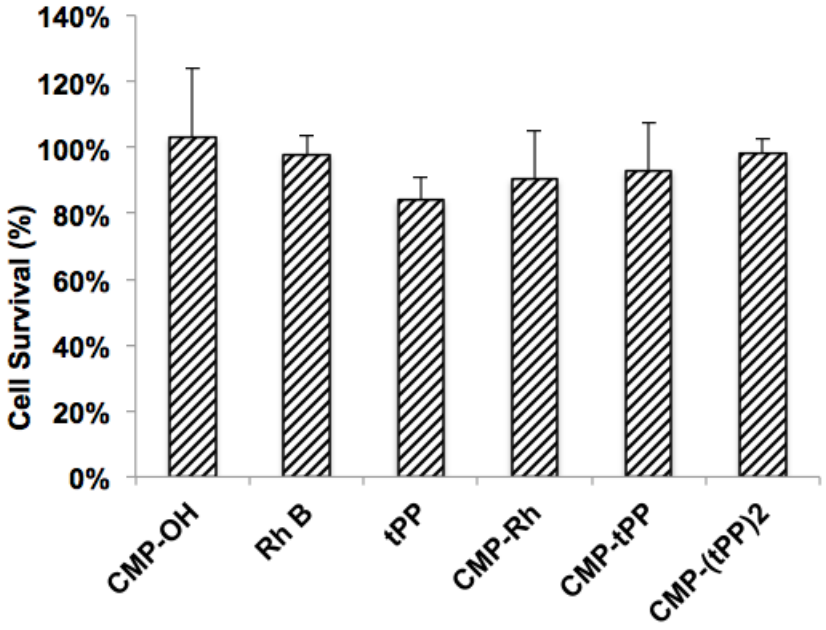

Figure 22. Dark toxicities of the respective dyes incubated in Colon 26 cells for 24 h at 5 μM concentrations.

3.3.2.3. Phototoxicity

The conjugates showed greatly increased phototoxicity compared to the unconjugated photosensitizer (CMP-OH) (Figure 23). No significant phototoxicity was observed in cells treated with up to 5 μM of CMP-OH after irradiation with a 690 nm diode laser at 5.6 $mWcm^{-2}$ for 30 min. On the other hand, cells treated with 5 μM of either CMP-Rh, CMP-tPP or CMP-$(tPP)_2$ and irradiated under the same condition showed > 70% cell killing. CMP-tPP showed the highest phototoxicity under the above irradiation conditions with an IC_{50} of 0.9 μM, followed by CMP-$(tPP)_2$ with an IC_{50} of 1.67 μM and then

CMP-Rh with an IC_{50} of 2.36 μM. The absence of phototoxicity observed in the cells treated with up to 5 μM of CMP-OH could be attributed mainly to their low intracellular accumulation (0.19 fmole/cell). Rh B did not show any toxicity upto 5 μM as expected, due to its inability to generate singlet oxygen. On the other hand, the greater phototoxicity observed with CMP-tPP, CMP-$(tPP)_2$, and CMP-Rh could be attributed to their high intracellular accumulation with effective singlet oxygen generation capability.

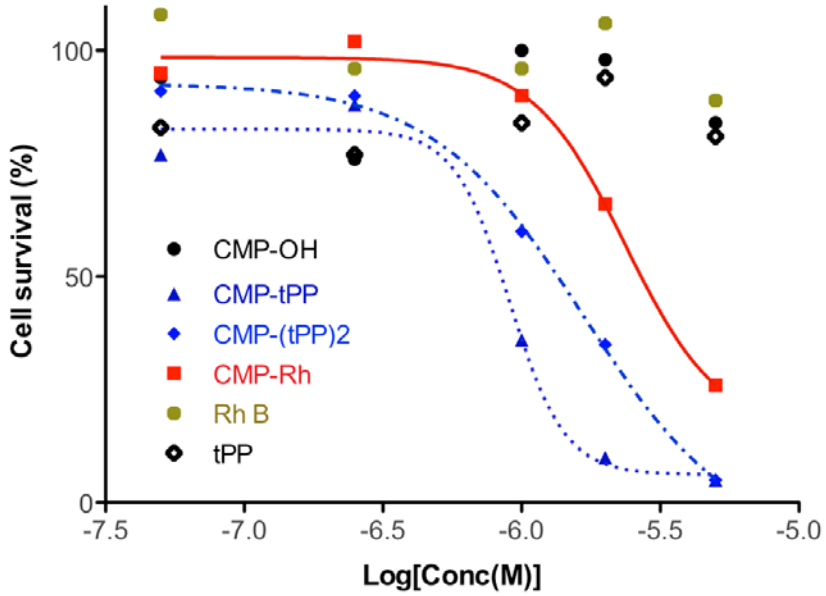

Figure 23. Phototoxicity of Colon 26 cells treated with the respective dyes and irradiated with a 690 nm diode laser for all dyes (except Rh B with 540 ± 10 nm LumaCare) at 5.6 $mWcm^{-2}$ for 30 min. Cells were incubated with the respective dyes at 0.25, 0.5, 1, 2 and 5 μM, respectively for 24 h prior to irradiation. Each data point is the average of two independent experiments with more than 4 data and error bars are not shown for clarity.

3.3.2.4. Sub-cellular localization

Since the conjugates were designed to target mitochondria, mitochondrial localization was estimated using fluorescence dual staining with mitochondrial molecular probe, Rhodamine 123 (Figure 24). Green filter (excitation 480/40 emission 527/30) was used to obtain signal from Rhodamine 123. Red filter (excitation 535/50 emission 645/75) was used to obtain signal from CMP of the CMP conjugates.

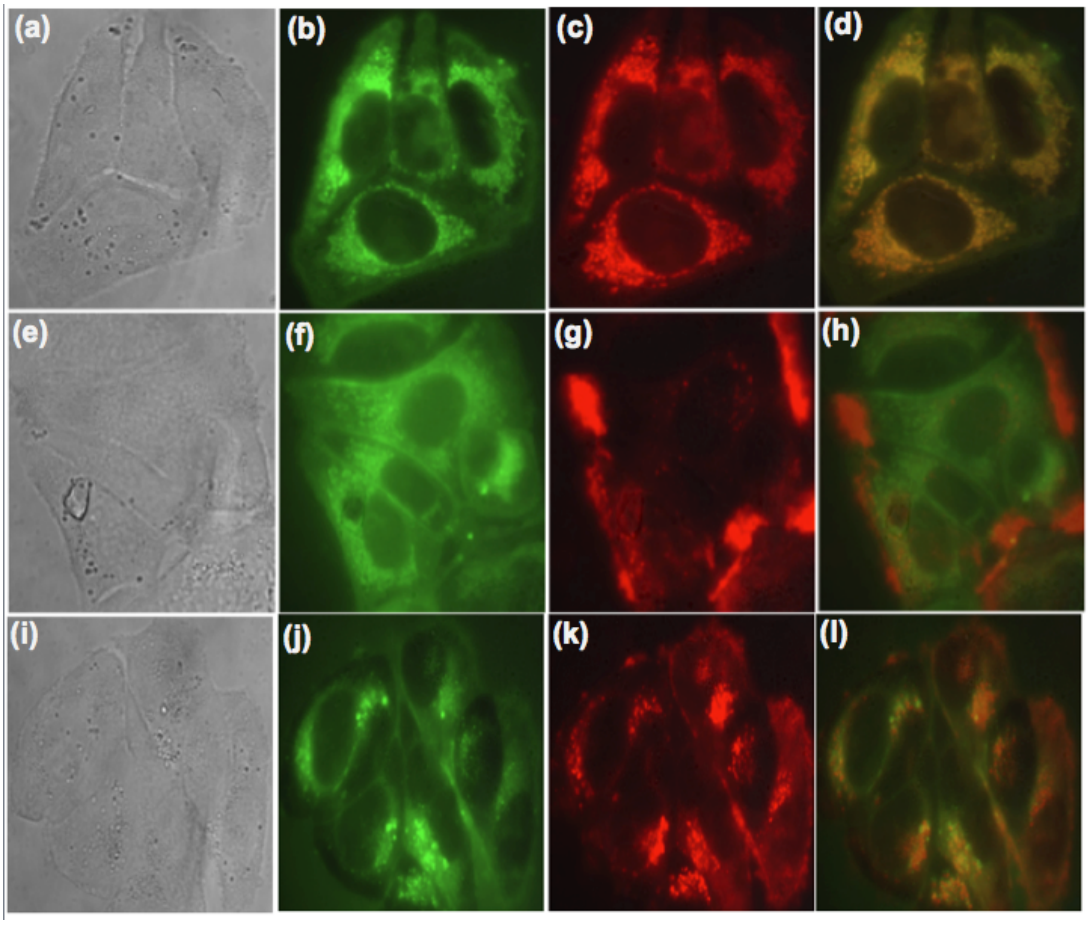

Figure 24. Sub-cellular localization of the conjugates: MCF-7 cells treated with Rh 123 and one of the conjugates. ***CMP-Rh + Rh 123*** (5 μM + 2 μM) (a) Bright field (b) Green filter (c) Red filter, and (d) overlap of (b) and (c); ***CMP-tPP + Rh 123*** (5 μM + 2 μM) (e) Bright field (f) Green filter (g) Red filter, and (h) overlap of (f) and (g); ***CMP-(tPP)2 + Rh 123*** (5 μM + 2 μM) (i) Bright field (j) Green filter (k) Red filter, and (l) overlap of (j) and (k).

CMP-Rh showed a very similar staining pattern to Rh-123 (Figure 24c). CMP-Rh was distributed throughout the cytoplasm like Rh-123 (Figure 24b). In addition, CMP-Rh and Rh-123 showed punctuate staining patterns

consistent with typical mitochondrial probe images. This sub-cellular localization of CMP-Rh was further confirmed by the overlapping of the two images (Figure 24d), where yellow area present co-localization of CMP-Rh and Rh 123. The CMP-Rh might be accumulated in mitochondria due to the presence of the delocalized lipophilic cation that facilitated their accumulation in mitochondria. On the other hand, CMP-tPP did not show any significant staining of mitochondria. Bright CMP fluorescence was detected from edges of cells. Very minimal yellowish area was shown (Figure 24h). CMP-$(tPP)_2$ also showed some degree of mitochondrial localization. More yellowish areas (Figure 24l) were shown than CMP-tPP (Figure 24h). However, it was less than that of CMP-Rh (Figure 24d).

3.3.3. In vivo studies

3.3.3.1. Time-dependent biodistribution of CMP-tPP

In the biodistribution study, liver and spleen exhibited higher accumulation of CMP-tPP (Figure 25). Liver tissue, rich in reticuloendothelial system, had maximum uptake and retention among the tissues (100 nmol g^{-1} of tissue at 24 h post injection). Biodistribution of porphyrins is reported to be associated with the number of LDL receptors in respective tissues.[174] Organs like liver, kidney and lung have elevated number of LDL receptors.[174] The tissue distribution pattern is consistent with this observation. Liver and kidney exhibited higher accumulation of CMP-tPP. This observation was in

accordance with the fact that hydrophobic PDT agents are mostly eliminated from the organism via bile-gut pathway.[174] The sequence of decrease in uptake levels was liver, spleen, lungs, heart, kidney, tumor, skin and muscle. This pattern of biodistribution of photosensitizer was similar to Photofrin.[174] The concentrations of CMP-tPP accumulated in tumor at 24, 48 and 72 h post injection were 5, 19 and 20 nmol g^{-1} of tissue, respectively. Tissue distribution so far showed 20 nmole/gm of CMP-tPP in tumor and was approximately 3 times higher than the unconjugated IY69 (data not shown) which showed 7.61 nmole gm^{-1}.[174]

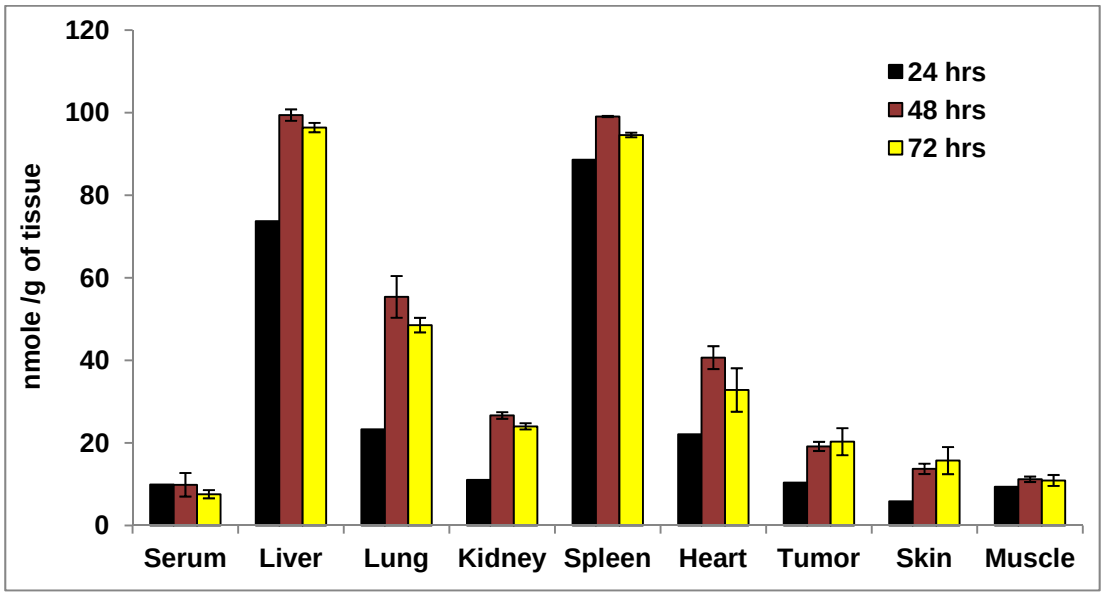

Figure 25. Tissue distribution of CMP-tPP: CMP-tPP (25 μmol kg^{-1}) was injected i.p. to BALB⁄c mice. Mice were euthanized at three time points (24, 48 and 72 h). Tissues were excised and homogenized in DMSO. Fluorescence measurements were made with DMSO fraction to determine the amount of CMP-Monocation. Data are expressed as mean ± SD, n = 2

3. Summary and conclusion

Three conjugates, CMP-Rh, CMP-tPP, and CMP-$(tPP)_2$, were successfully synthesized by linking the hydroxy core modified porphyrins (CMP-OH and CMP-$(OH)_2$) to either rhodamine B (Rh B) or triphenyl phosphonium (tPP) respectively via a saturated hydrocarbon linker in moderate yields. Although ET from Rh to CMP was observed in CMP-Rh, it was able to generate singlet oxygen at a rate comparable to that of CMP-OH. The conjugation of CMP to Rh and tPP did greatly improve intracellular uptake and in vitro photodynamic activity compared to CMP-OH. The high phototoxicity of the conjugates could be attributed to their intracellular accumulation. Our goal was to deliver CMP to mitochondria by conjugating it with DLCs (Rh or tPP). The Rh moiety seemed an excellent delivery vector for CMP to mitochondria. The Di tPP group also delivered it to mitochondria somewhat but mono tPP group was not effective. However, it was not clear from our results if the mitochondrial localization can enhance phototoxicity. Although CMP-Rh showed the most preferential localization into mitochondria among the three, it was less potent than the other two conjugates. The in vivo studies with CMP-tPP showed higher distribution in tumor compared to a previously studied porphyrin IY69.

Chapter 4. Biological evaluation of visible/near IR activatable prodrugs

4.1. Introduction

A most critical setback of chemotherapy is its non-specific action on healthy cells, which creats systemic side effects. New approaches encompassing tumor-targeted drug delivery, site-activated pro-drugs, and combination therapy have been studied to reduce side effects.[225-229] The main goal of any methodology is to keep the concentration of drug at a non-toxic level in the non-specific sites but above effective concentrations at the tumor sites. PDT is a fairly new strategy where otherwise inactive PS can be activated by shining light of near IR wavelength to generate SO to regio-selectively kill the surrounding tumor cells. In PDT, light can be used to activate the compounds for site-specific controlled release of cytotoxic agents. Site-specific release of biological moieties using UV and short-visible light[230, 231] have been studied comprehensively, but of longer wavelengths that can penetrate deep into tissue are not common due to a lack of suitable chemistry. Recent advances put forward a "smart" approach, which utilizes the properties of photosensitization and distinctive chemistry of SO[232-235].

SO in PDT can cleave the unsaturated bond in olefins. Despite this the following points have to be considerd to apply this strategy: 1) very few SO cleavable linkers, 2) facile synthetic approach, 3) regeneration of unaltered parent drug, and 4) translatability into in vivo level. Dr. You et al. have

discovered photo-unclick chemistry of aminoacrylate to address all the above shortcomings.[236]

4.2. Mechanism of release of the anti-cancer drug from prodrug conjugate

The prodrug system contains a PS and anti-cancer drug that are connected via a SO cleavable bond. Once irradiated with light (690 nm diodelaser). The bond is cleaved and anti-cancer drug is released only at the irradiated site (tumor site). The following diagram explains the anti-cancer drug release mechanism.

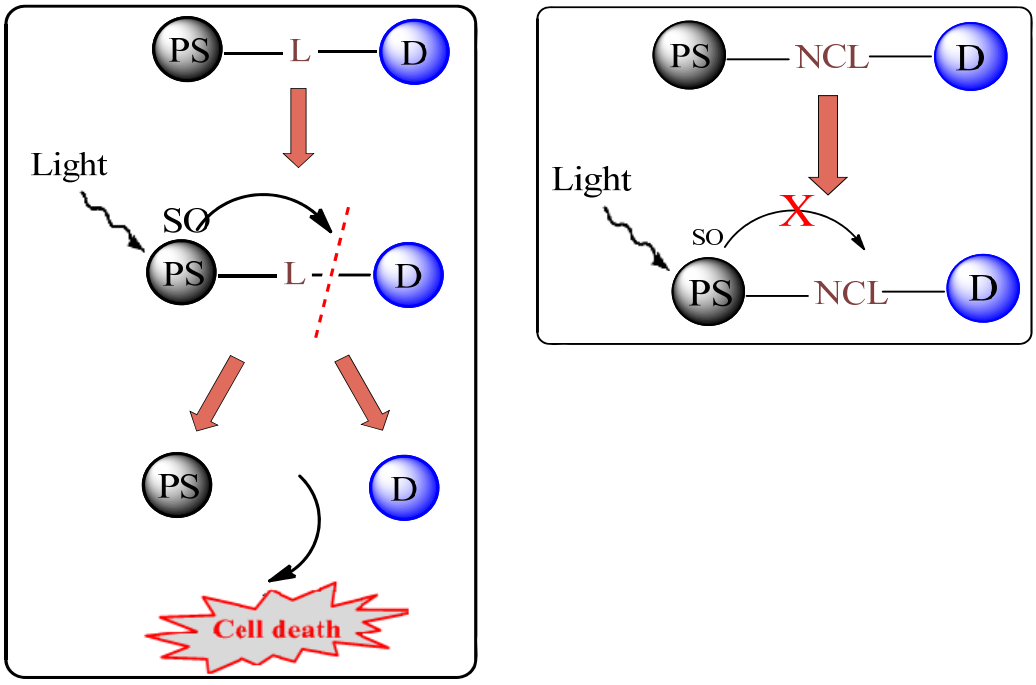

Figure 26. Mechanism of release of anti-cancer drug from the prodrug conjugate. L = Cleavable linker, NCL = Non-cleavable linker

A photosensitizer and anti-cancer drug were linked either via a SO cleavable olifenic bond or a non-cleavable bond. CMP is used as the PS. CA-4 or Taxol were used as anti-cancer drugs. CA-4 interacts with tubulin and prevents its polymerization[237] and hence prevents cell division. The choice of CA-4 is due to its small size and simple structure and presence of OH on the phenolic ring, which helps in forming ester bonds with any molecule. A water-soluble prodrug of CA-4 (CA-4 phosphate, fosbretabulin) is under clinical study for anticancer therapy.

Taxol is a well known anti-cancer drug.[238] Taxol exhibits nanomolar IC50 under in vitro conditions. Taxol stabilizes the microtubule polymer and protects it from dissociation and hence enabls the metaphase chromosomes to attain spindle conformation. This blocks the progression of mitosis. Taxol induces apoptotic cell death due to extended activation of mitosis or a revision of G-phase of cell cycle due to cell division[239, 240].

CMPs were choosen as they have been extensively studied as a second-generation photosensitizer due to their multiple advantages.[204, 222-224, 241, 242] Especially, the dithiaporphyrins were prepared as a highly pure and well-characterized form. CMPs absorb longer wavelength light (690-710 nm) and are highly photostable[205] whereas Photofrin absorbs at 630 nm and tetranitrogenic prophyrins absorbs at 648 nm.[173] In addition, CMPs showed high singlet oxygen generation quantum yield ($\Phi(^1O_2)$, ~ 0.8), which makes them very efficient PS for PDT treatment.[223]

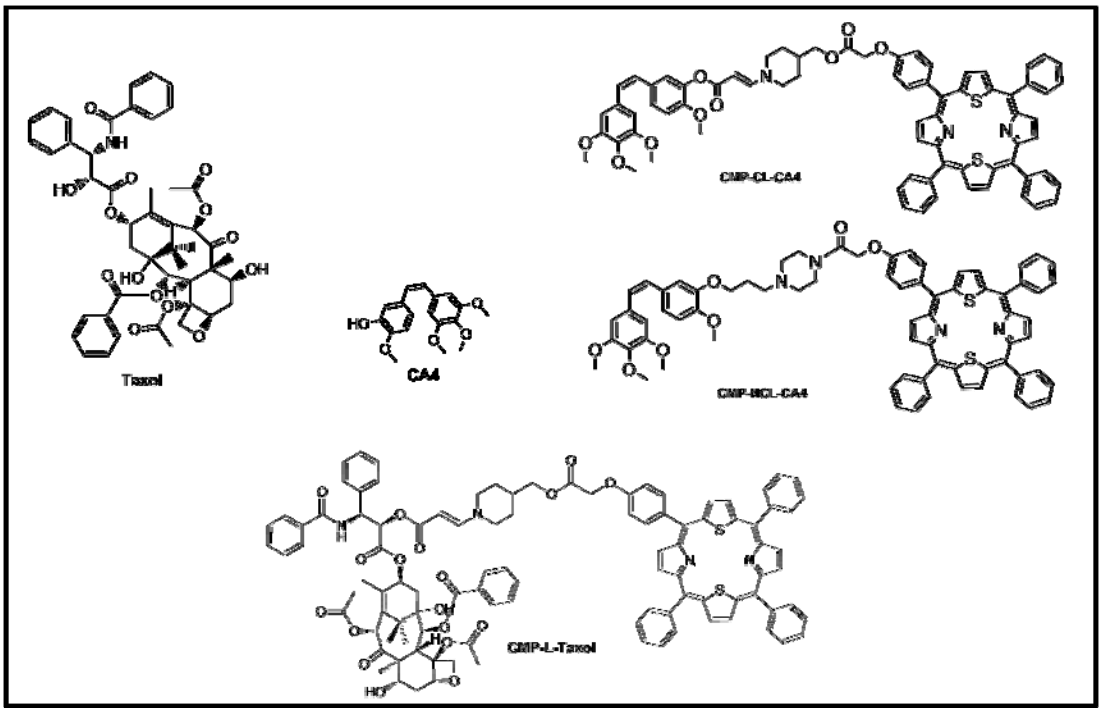

Figure 27. Structures of compounds.[243]

Compounds CMP-L-CA4, CMP-NCL-CA4, and CMP-L-Taxol were synthesized by Dr. Moses Bio. CA4 and Taxol were obtained commercially.

4.3. Experimental procedure

4.3.1. Cells and culture conditions

Mouse colon cancer cells (Colon 26) or human breast cancer cells (MCF-7) were used for all biological experiments. All reagents and culture media were obtained from Invitrogen and Sigma-Aldrich. The cells were maintained in minimum essential medium (α-MEM) supplemented with 10% bovine growth serum, 2mM L-glutamine, 50 units/mL penicillin G, 50 μg/mL streptomycin

and 1.0 µg/mL fungizone. The cells were incubated at 37 °C in 5 % CO_2 using a Sanyo MCO-18AIC-UV incubator. Colon 26 cells were sub-cultured biweekly and MCF-7 cells were sub-cultured once a week to maintain the cells at approximately 80 % confluency. The dyes in in vitro studies were initially dissolved in DMSO to make a 2 mM stock solution. For in vivo studies samples were prepared in a mixture of DMSO, Tween 80 and 5% dextrose solution.

4.3.2. Bystander effect by CMP-L-CA4

Colon 26 cells were seeded at 5,000 cells/ml/well in 24-well plates and then incubated for 24 h. Stock solutions (4 mM in DMSO) were diluted with medium. The diluted solutions (25 µL) were added to wells (1 mL) to get the appropriate final concentrations [CMP-L-CA4 (50 nM) and IY69 (5 µM)]. After 24 h incubation, the plates were irradiated from the bottom with
690 nm diode laser at 11 mW/cm^2 for 15 min. While irradiating, half of each well was blocked with a black masking tape (THORLABS, Cat# T743-1.0) to protect cells on the other half of each well. The irradiated plates were incubated for an additional 48 h. Then a Calcein AM live cell staining assay was performed (from Molecular Probes, Tervigen Cat# 4892-010-K)
according to the manufacturer supplied standard protocol. Briefly, the cells were washed once with the Calcein AM wash buffer (1 mL) and then fresh wash buffer (250 mL) and the working reagent (250 mL) were added to the

wells. The cells were incubated for 30 min. Fluorescent images were obtained with an Olympus IX51 inverted microscope with green fluorescence channel to visualize live cells. All images were taken at 10× magnifications.

4.3.3. Apoptosis assay

On day 0 of the experiment, MCF7 cells (2.0×10^6 cells/well) were seeded in a 24 well plates. On day 1, 2 mM DMSO stocks of respective compounds were diluted in the media and added into each well to achieve final concentrations of 10 uM for all the compounds except IY69. Compound IY69 was used at a final concentration of 500 nM. The compound seeded cells were irradiated on day 1 with 690 nm diode laser for 30 min at 5.6 mW/cm^2 (energy 10.08 J /cm^2) without washing the compound. Post irradiation, the cells were incubated for another 72 hrs. The day of apoptosis assay, the cell monolayer was washed with chilled PBS. The cells were collected by trypsinizing with 100 uL of trypsin/EDTA. Harvested cells were centrifuged at 1200 rpm, 4 ^{o}C, for 5 min to obtain the cell pellet. The supernatant was discarded and the cell pellet was suspended in fresh chilled PBS and recentrifuged at 1200 rpm, 4 ^{o}C, for 5 min. There after, various samples were processed in different ways. Untreated cells were suspended either in 100uL of 1X Annexin V binding buffer, 100uL of 1X Annexin V binding buffer + 5µL of Alexa Fluor® 488 Annexin V or 100 µL of 1X Annexin V binding buffer +

1µL of PI, 100uL of 1X Annexin V binding buffer + 5uL of Alexa Fluor® 488 Annexin V + 1 µL of PI. PDT treated cells were suspended in 100 µL of 1X Annexin V binding buffer + 5 µL of Alexa Fluor® 488 Annexin V + 1 µL of PI. After addition of the respective reagents the cells were incubated at room temperature for 15 min. Just before reading the samples 400 µL of 1X Annexin V binding buffer was added.

Flow cytometric analyses were performed BD Accuri™ C6 Flow Cytometer (BD Biosceinces, CA) equipped with an argon-ion laser. Each sample was analyzed using 10,000 events/sample acquired in list mode by a Macintosh Quadra 650 minicomputer (Apple computer Inc., Cupertino, C). Data analysis was performed via three-step procedure using the BD Accuri™ C6 software (BD, San Jose, CA). Alexa Fluor® 488 Annexin V was analyzed using excitation and emission wavelengths of 488 and 533/30 nm (FL-1 channel); PI, 488 and 585/40 nm (FL-2 channel). Debris and clumps were gated out using forward and orthogonal light scatter. Detection of phosphatidyl serine exposure on the external leaflet of the plasma membrane employing annexin V was assayed. This phenomenon is one of the early events in the cascade of events characterizing apoptosis.

4.3.4. Antitumor efficacy study

Four- to six-week old female BALB⁄ c mice (18–20 g, Charles River Laboratories, Inc.) were used for the murine tumor model. The mice were implanted s.c. with 2×10^6 colon 26 cells in PBS (100 μL) on the lower back-neck region. Tumor growth was monitored with digital caliper. Two dimensions l and w (l: the longest axis of tumor and w: the axis perpendicular to l) were used to calculate tumor volume ($lw^2⁄2$). Mice with a tumor of the diameter 3–5 mm were used for the experiments. Stock solutions in DMSO (4 or 8 mM) and further dilutions in 1% Tween 80 and 5% dextrose solution to achieve final doses were as follows: CMP-L-CA4; 4 mM → 2 or 4 μmole/kg, CMP-NCL-CA4 + CA4; 4 mM → 2 μmole/kg, CMP-L-CA4 + CA4; 8 mM each → 4 μmole/kg. Samples were filtered using 0.2 μm sterile syringe filter. To each mouse, 200 μL of sample was injected via i.p. once a day on day 0, 1, and 2. Then, 90 min later mice were anesthetized with ketamine 80 mg/kg and xylazine 6 mg/kg, i.p. injection. Tumors were irradiated with a 690 nm diode laser at 200 mW/cm^2 for 30 min (360 J/cm^2). Tumor size was measured with the digital caliper every day after the treatment.

4.3.5. Statistical analysis

Statistical analyses were performed using the Student's t-test for pairwise comparisons. A *P* value of < 0.05 was considered significant.

4.4. Results and discussion:

4.4.1. A bystander effect by CMP-L-CA4:

A bystander effect (damage of neighboring cells) was found when CMP-L-CA4 was irradiated. The cytotoxicity caused was due to the released CA4 and not by SO in [CMP-L-CA4 + hv] (Figure 28). The SO generated has a relatively short lifetime of ~ 40 ns and can diffuse approximately 20–200 nm.[21, 244, 245] This means PDT cannot generate a bystander effect and the SO generated in one cell cannot damage neighboring cells. To study the bystander effect of CMP-L-CA4, the left half of each well was irradiated and images of the center of the well were obtained. As anticipated, cells in the non-irradiated portion where also damaged in a similar manner as the irradiated portion due to the bystander effect in CMP-L-CA4 (Figure 28b). However, the compound IY69 damaged only the irradiated portion of the well[217] (Figure 28c). This was because SO generated does not show a bystander effect. This evidently confirmed that CMP-L-CA4 killed the cells primarily by the released CA4.

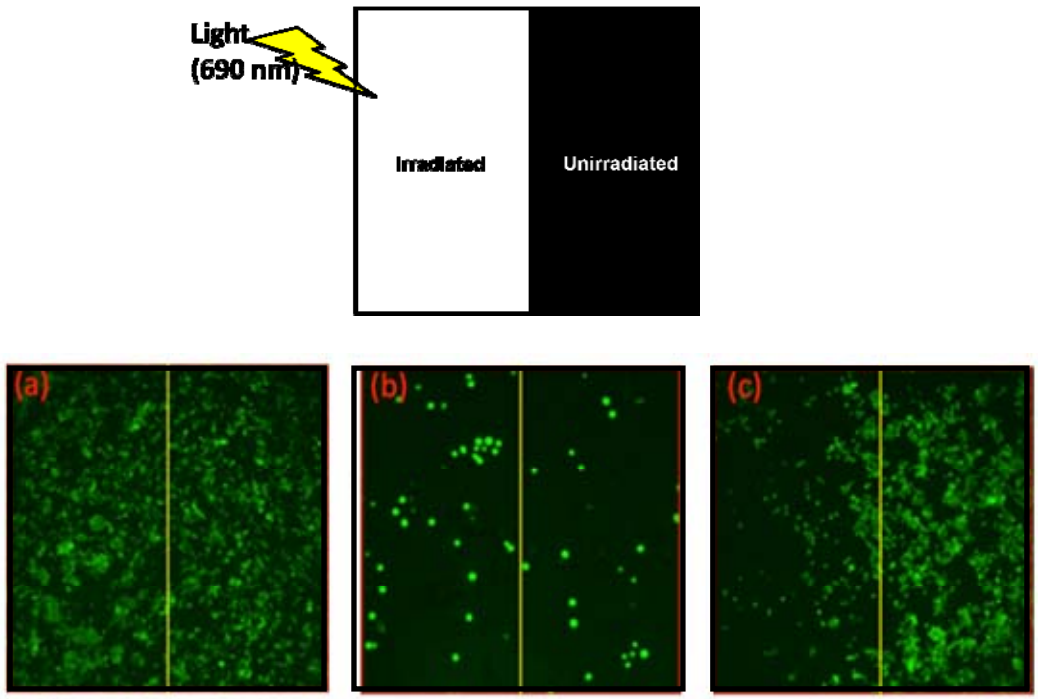

Figure 28. Fluorescence live cell images of the center of each well treated with (a) control, (b) CMP-L-CA4 (50 nM) and (c) **IY69** (5 μM): only the left half of each well was irradiated with 690 nm diode laser (11 mW/cm^2 for 15 min). At these concentrations, CMP-L-CA4 and **IY69** did not produce significant dark toxicity.

4.4.2. Apoptosis assay

The apoptotic effect of these prodrug conjugates was further evaluated by Annexin V FITC/PI (AV/PI) dual staining assay to examine the occurrence of phosphatidylserine externalization and also to understand whether it is due to physiological apoptosis or non-specific necrosis. In this study MCF-7 cells were treated with various compounds for 72 h at 10 nM concentration, except for IY69, which was treated at 500 nM concentration, to examine the

apoptotic effect. It was observed that these compounds showed significant apoptosis against MCF-7 cells as shown in Figure 29. Results indicated that IY69 showed 5.41%, CMP-L-Taxol showed 10.38%, and CMP-L-CA4 showed 7.43% of apoptosis, respectively, whereas the standard Taxol and CA4 showed 9.31% and 12.32% of apoptosis respectively. From this experiment it was suggested that these compounds significantly induce apoptosis in MCF-7 cells.

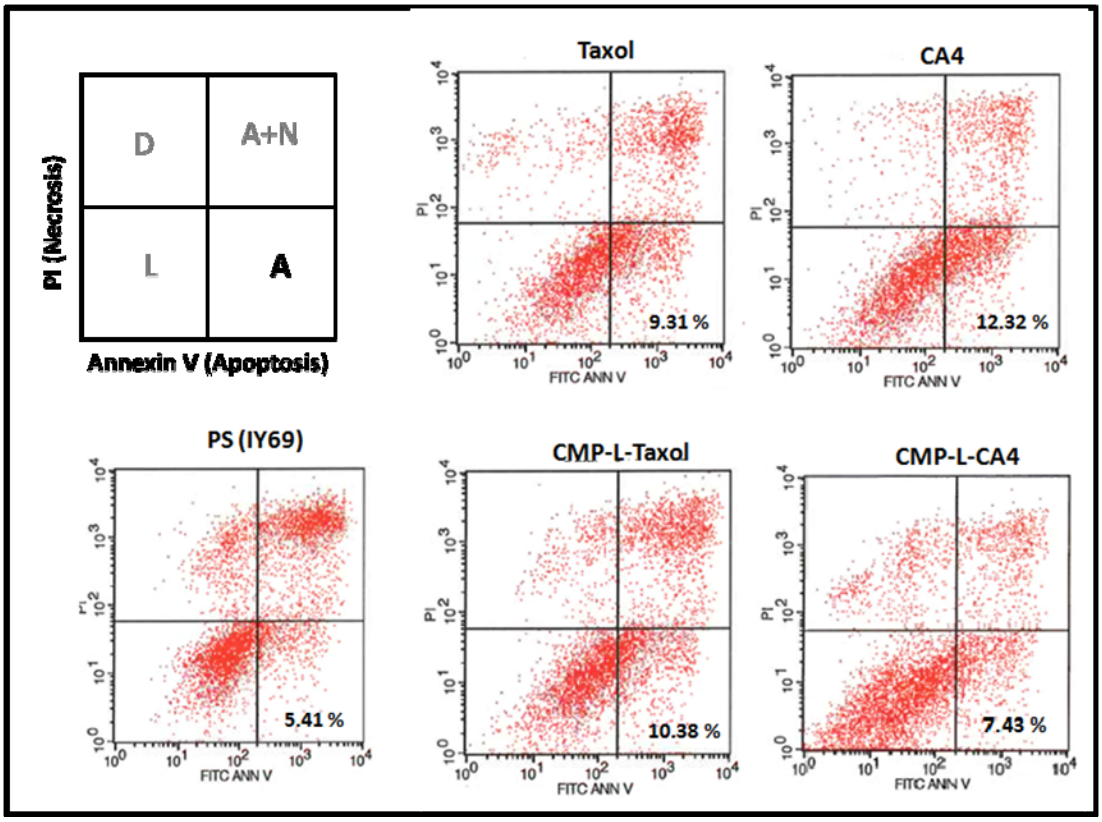

Figure 29. Apoptosis assay. Annexin V-PI staining of MCF-7 cells treated with various compounds and irradiated after 24 hr for 30 min with 690 nm diode laser. Apoptosis assay was performed 72 hr post-irradiation. D=dead cells, L=live cells, A+N=Apoptotic+Necrotic cells, A=Apoptotic cells

4.4.3. Antitumor efficacy

BALB/c mice were subcutaneously inoculated with tumor on the shoulder region with colon 26 cells. After the tumor attained 4-6 mm, diameter, various compounds were injected. After 1.5 h each tumor was irradiated with 690 nm diode laser (360 J/cm^2 = 200 mW/cm^2 for 30 min) on days 0, 1 and 2.

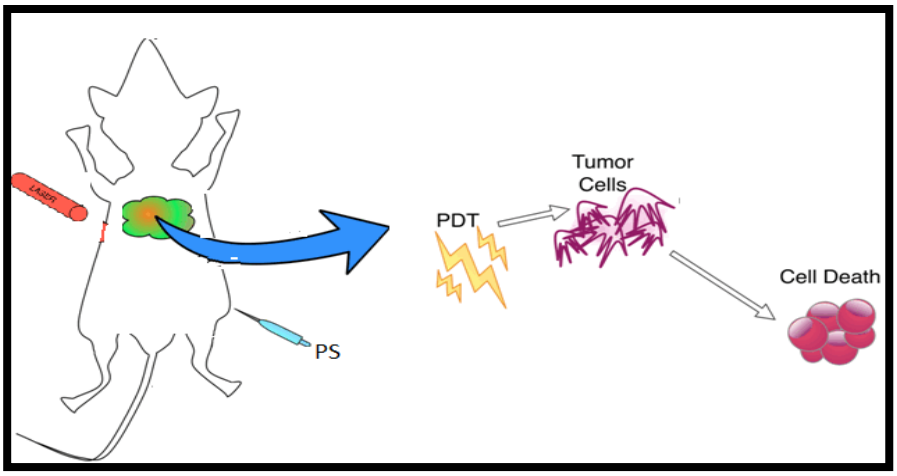

Figure 30. Schematics for in vivo PDT shows a mice bearing tumor was injected with PS and irradiated with laser light. This cause cell death.

Several interesting observations were made. Firstly, the non-irradiated group G4 [CMP-L-CA4 + CA4 (4 μmole/kg each)] did not show much difference in tumor suppression compared to the untreated group G5 ($P > 0.05$). The anti-tumor effects in these groups were negligible in absence of light. Second, after irradiation, the G2 [CMP-L-CA4] group had a much better ($P < 0.05$) anti-tumor effect than the group (G4) that was not irradiated. Irradiation enhanced the anti-tumor efficacy of CMP-L-CA4, possibly due to the release

of CA4 and the PDT effect (CMP moiety + hv). Third, the G3 group [CMP-NCL-CA4 + CA4 + hv] had a significant ($P < 0.05$) impediment in tumor growth when compared to the control group G5. It might be largely due to the result of the PDT effect by CMP-NCL-CA4 + hv because no considerable delay occurred in tumor growth with CA4 itself at the same dose in the pilot studies. This was consistent with previous report of a minimal antitumor effect of CA4 even at a very high dose (506 μmole/kg).[246] In addition, signs of necrosis were seen on the treated tumors, which are characteristic of the PDT effect. The most important group G1[CMP-L-CA4 (2 μmole/kg) + hv] showed a significantly ($p < 0.05$) better antitumor effect than the G3 group that was similar to a combination therapy [PDT with CMP-NCL-CA4 plus a systemic CA4 (2 μmole/kg each) + hv)]. The enhanced antitumor effect in the group G1 may come from the released CA4. Interestingly, no observe any significant acute toxicity in terms of loss in body weight from any group was observed (Figure 33).

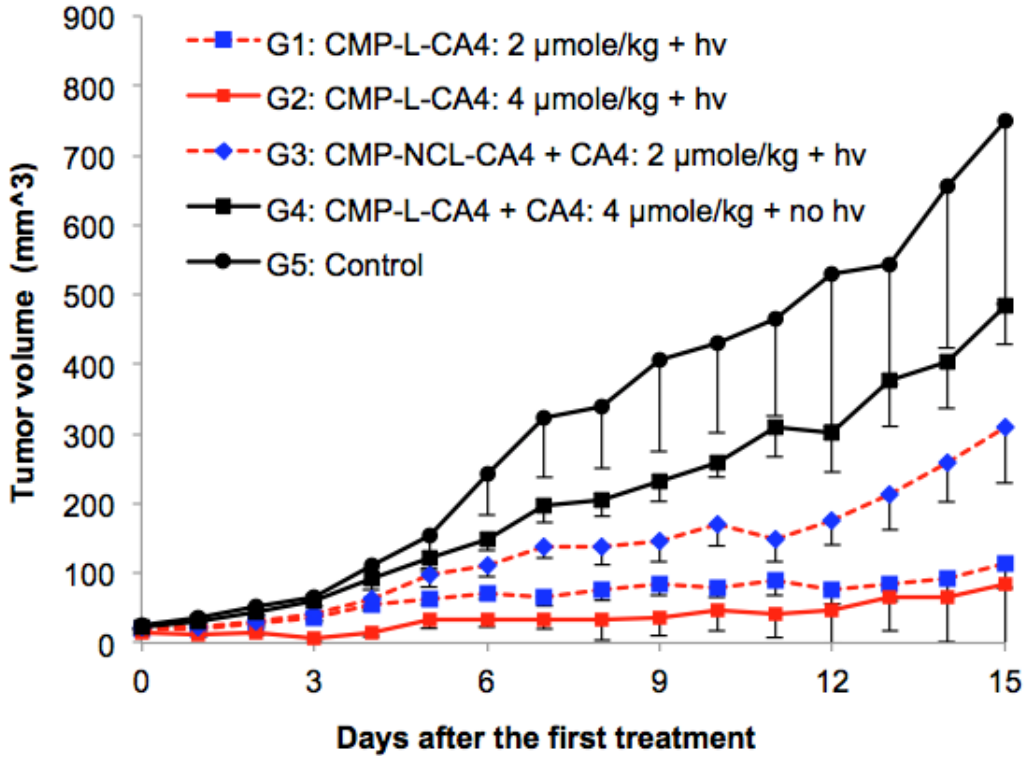

Figure 31. Tumor growth curves. Drug administration: once a day on days 0, 1, and 2; hv = 360 J/cm^2 with 690 nm; 6 mice per group except 3 mice in the control group. Error bars represent SE.

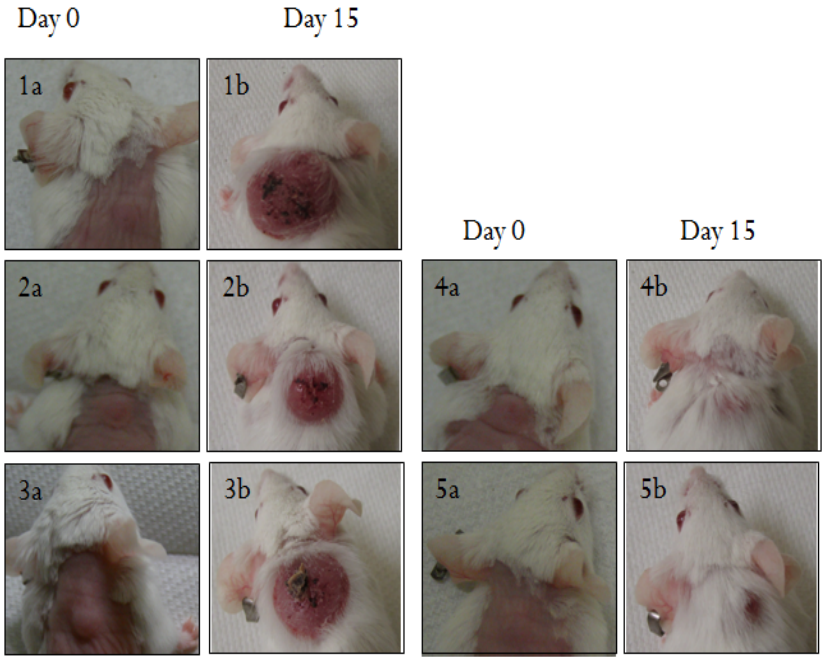

Figure 32. Mice bearing tumors treated with different compounds and the tumor growth pattern comparison on a) day 0 b) day 15. 1) Control, 2) CMP-L-CA4_4umole/kg, no hv 3) CMP-NCL-CA4_2umole/kg, hv 4) CMP-CL-CA4_2umole/kg, hv 5) CMP-CL-CA4_4umole/kg, hv

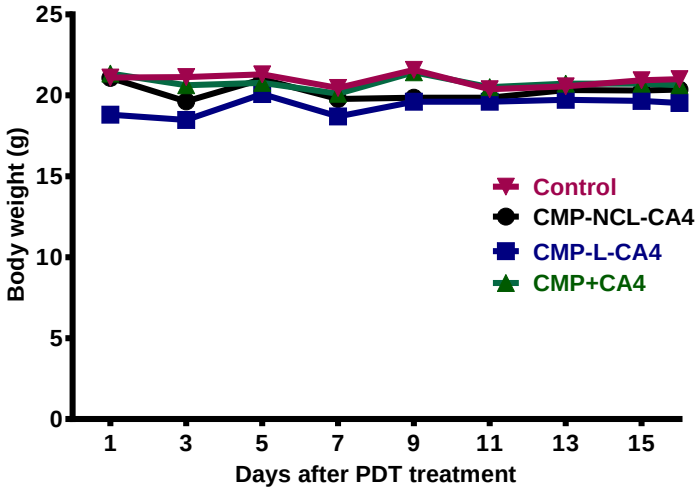

Figure 33. Acute toxicity: Body weight change in mice treated with CMP-NCL-CA4_2umole/kg, hv; CMP-CL-CA4_2umole/kg, hv; CMP+CA4_4umole/kg, hv; Control groups

4.5. Conclusion

This study showed the release of the anti-cancer drug using the principles of PDT in biological conditions for the first time. The released CA4 caused the bystander effect. All the conjugates showed apoptosis comparable to known apoptotic agents. There was no acute toxicity with the conjugated compounds. CMP-L-CA4 was most effective in releasing the CA4.

Chapter 5. Conclusion

Systemic side effects are the main drawback of chemotherapy for cancer treatment. Through this dissertation, I tried to address the problem in two different approaches utilizing the principles of PDT. PDT is a minimally invasive cancer treatment modality with great prospective to selectively destroy tumor cells and thus reduce systemic side effects. Nonetheless, PDT suffers some inadequacies that need to be tackled to be make it more appropriate for clinical use. In developing a good PS one has to consider the following factors: the short lifespan of SO in biological systems which is, ~40 ns and considerably small radius of action, which is ~20 nm. Because of this it is important for the PS to localize in the most crucial organelles involved in the cell death to achieve maximum effect from PS. Mitochondria are the most crucial organelles in the cell due to their involvement of apoptotic cell death. Mitochondria possess a unique property: a higher trans membrane potential in cancerous cells compared to normal cells. Compounds bearing positive charge accumulate specifically in cancerous cells compared to normal cells. In the part-I of mitochondrial delivery a TPP-OH that absorbs around 650 nm was used as a PS and Rh B or acridine orange were used as cations. Conjugation of photosensitizer to cationic dyes improved the uptake into mitochondria with TPP-Rh 8 times higher in cellular uptake compared to unconjugated porphyrin TPP-OH. When irradiated with 400-800 nm broad band light at 3mW/cm^2, TPP-Rh showed IC_{50} of 3.95 μM;

this was much higher when compared to TPP-OH, which was > 20 μM. The higher cellular uptake could be one of the major reasons for the higher phototoxicity. Subcellular localization studies suggested TPP-Rh localized in mitochondria. A colocalization study with a MG, a known mitochondrial probe, and superimposition of signal from both the dyes showed an overlap. The compound TPP-AO showed some dark toxicity at 10 μM and showed mitochondrial and nucleosomal staining.

In the part-II of mitochondrial delivery CMP which absorbs around near IR (690nm) and cations RhB and tPP. All the conjugates showed similar photophysical properties as the unconjugated porphyrin. Studies showed less aggregation of the cations in DMSO. Electron transfer was observed in CMP-Rh from RhB to CMP but this did not affect the SO generating capability. All the conjugates showed comparable SO generation to CMP-OH. In vitro uptake of CMP-tPP was the highest with 14 folds higher than CMP-OH and followed by uptake of CMP-Rh, which was 7 times. No dark toxicity was observed up to 5 μM concentration with any of the dyes. CMP-tPP showed the highest phototoxicity under the above irradiation conditions with an IC50 of 0.9 μM and followed by CMP-$(tPP)_2$ with an IC50 of 1.67 μM and then CMP-Rh with an IC50 of 2.36 μM. Subcellular localization of CMP-Rh was closest to Rh-123 which is a mitochondrial localizing dye. CMP-tPP did not show any mitochondrial localization. CMP-$(tPP)_2$ showed mitochondrial localization to some extent.

In vivo studies with CMP-tPP so far showed 3 times higher uptake in tumor and other tissue in comparison to our earlier studied compound IY69.

In a second approach of targeted delivery, prodrugs of porphyrin and anti-cancer drugs attached via a SO cleavable linker were biologically evaluated. The SO generated in PDT can show its action within a radius of 20 nm and is short lived (40 ns). That means PDT cannot generate a bystander effect. In the case of the CMP-L-CA4 prodrug, once the anti cancer drug was released, it showed a bystander effect. Only half of each well of 24 well plate was irradiated. Up on irradiation, the released CA4 not only killed the cells in the irradiated portion but also caused bystander effect in the unirradiated portion. In vivo tumor efficacy showed interesting results. CMP-L-CA4 + CA4 at 4 μM each in absence of light showed no significant effect. But upon irradiation, CMP-L-CA4 at 2 μM showed the highest tumor suppression of all the groups due to the release of CA4. CMP-NCL-CA4 + CA4 2 μM each in the presence of light showed better anti tumor activity than the untreated group. This effect is assumed to be from PDT as CA4 itself did not show any anti tumor effect at our treatment conditions.

Overall, these studies indicate that by conjugating PS to lipophilic cation Rh B via a short saturated hydrocarbon linker or conjugating a PS with an anti-cancer drug via a SO cleavable linker, compounds can be specifically targeted to tumor site. This also avoids systemic side effect.

References

1. Pushpan, S. K.; Venkatraman, S.; Anand, V. G.; Sankar, J.; Parmeswaran, D.; Ganesan, S.; Chandrashekar, T. K., Porphyrins in photodynamic therapy - a search for ideal photosensitizers. *Curr Med Chem Anticancer Agents* **2002,** *2*, 187-207.

2. Sharman, W. M.; Allen, C. M.; van Lier, J. E., Photodynamic therapeutics: basic principles and clinical applications. *Drug Discov Today* **1999,** *4*, 507-517.

3. Dougherty, T. J.; Gomer, C. J.; Henderson, B. W.; Jori, G.; Kessel, D.; Korbelik, M.; Moan, J.; Peng, Q., Photodynamic therapy. *J Natl Cancer Inst* **1998,** *90*, 889-905.

4. Hudson, R.; Boyle, R. W., Strategies for selective delivery of photodynamic sensitisers to biological targets. *J Porphyr Phthalocya* **2004,** *8*, 954-975.

5. Ochsner, M., Photophysical and photobiological processes in the photodynamic therapy of tumours. *J Photochem Photobiol B* **1997,** *39*, 1-18.

6. Foote, C. S., Definition of type I and type II photosensitized oxidation. *Photochem Photobiol* **1991,** *54*, 659.

7. Turro, N., *Molecular Photochemistry*. New York, 1965.

8. Ethan D. Sternberg, D. D. *Porphyrin-based photosensitizers for use in photodynamic therapy*; Department of Chemistry, University of California at Berkeley, Berkeley, CA., 94720, USA1998; p 51.

9. Brancaleon, L.; Moseley, H., Laser and non-laser light sources for photodynamic therapy. *Lasers Med Sci* **2002,** *17*, 173-86.

10. Fritsch, C.; Stege, H.; Saalmann, G.; Goerz, G.; Ruzicka, T.; Krutmann, J., Green light is effective and less painful than red light in

photodynamic therapy of facial solar keratoses. *Photodermatol Photoimmunol Photomed* **1997,** *13*, 181-5.

11. Wainwright, M., Photodynamic therapy: the development of new photosensitisers. *Anticancer Agents Med Chem* **2008,** *8*, 280-91.

12. Wilson, B. C. P., M. S., Photodynamic Therapy of Neoplastic Disease. Kessel, D., Ed. CRP Press: Boca Raton, 1990; Vol. 1, pp 129-144.

13. Bonnett, R., Photosensitizers of the Porphyrin and Phthalocyanine Series for Photodynamic Therapy. *Chemical Society Reviews* **1995,** *24*, 19-33.

14. Redmond, R. W.; Gamlin, J. N., A compilation of singlet oxygen yields from biologically relevant molecules. *Photochem Photobiol* **1999,** *70*, 391-475.

15. DeRosa, M. C.; Crutchley, R. J., Photosensitized singlet oxygen and its applications. *Coordination Chemistry Reviews* **2002,** *233*, 351-371.

16. *Targets in heterocyclic systems. Chemistry and properties*. 2005; Vol. 9.

17. Moan, J.; Berg, K., The photodegradation of porphyrins in cells can be used to estimate the lifetime of singlet oxygen. *Photochem Photobiol* **1991,** *53*, 549-53.

18. Peng, Q.; Moan, J.; Nesland, J. M., Correlation of subcellular and intratumoral photosensitizer localization with ultrastructural features after photodynamic therapy. *Ultrastruct Pathol* **1996,** *20*, 109-129.

19. Redmond, R. W.; Kochevar, I. E., Spatially resolved cellular responses to singlet oxygen. *Photochem Photobiol* **2006,** *82*, 1178-86.

20. Juzeniene, A.; Moan, J., The history of PDT in Norway Part one: Identification of basic mechanisms of general PDT. *Photodiagnosis and Photodynamic Therapy* **2007,** *4*, 3-11.

21. Niedre, M.; Patterson, M. S.; Wilson, B. C., Direct near-infrared luminescence detection of singlet oxygen generated by photodynamic therapy in cells in vitro and tissues in vivo. *Photochem Photobiol* **2002,** *75*, 382-91.

22. Barr, H. e. a., Comparison of Lasers for Photodynamic Therapy with a Phthalocyanine Photosensitizer. *Lasers Med. Sci* **1989,** *4*, 7-12.

23. Roeder, B.; Naether, D.; Lewald, T.; Braune, M.; Nowak, C.; Freyer, W., Photophysical properties and photodynamic activity in vivo of some tetrapyrroles. *Biophys Chem* **1990,** *35*, 303-12.

24. Lang, K.; Mosinger, J.; Wagnerova, D. M., Photophysical properties of porphyrinoid sensitizers non-covalently bound to host molecules; models for photodynamic therapy. *Coordination Chemistry Reviews* **2004,** *248*, 321-350.

25. *Advances in Photodynamic Therapy. Basic, Translational, and Clinical*. Artech House, 685 Canton Street, Norwood, MA 020622008.

26. Freitas, I., Lipid accumulation: the common feature to photosensitizer-retaining normal and malignant tissues. *J Photochem Photobiol B* **1990,** *7*, 359-61.

27. Nowis, D.; Makowski, M.; Stoklosa, T.; Legat, M.; Issat, T.; Golab, J., Direct tumor damage mechanisms of photodynamic therapy. *Acta Biochim Pol* **2005,** *52*, 339-52.

28. Moser, J. G., *Definitions and general properties of 2nd & 3rd generation photosensitizers.*; arwood Academic Publishers: London, 1997.

29. Lipson RL, G. M., Baldes EJ In *Hematoporphyrin derivative for detection and management of cancer*, Proceedings of the 9th International Cancer Congress, Tokyo, Japan1966: Tokyo, Japan; p 393.

30. Nseyo, U. O.; Shumaker, B.; Klein, E. A.; Sutherland, K., Photodynamic therapy using porfimer sodium as an alternative to cystectomy in patients with refractory transitional cell carcinoma in situ of the bladder. Bladder Photofrin Study Group. *J Urol* **1998,** *160*, 39-44.

31. Orenstein, A.; Kostenich, G.; Roitman, L.; Shechtman, Y.; Kopolovic, Y.; Ehrenberg, B.; Malik, Z., A comparative study of tissue distribution and photodynamic therapy selectivity of chlorin e6, Photofrin II and ALA-induced protoporphyrin IX in a colon carcinoma model. *Br J Cancer* **1996,** *73*, 937-44.

32. Allison, R. R.; Downie, G. H.; Cuenca, R.; Hu, X. H.; Childs, C. J. H.; Sibata, C. H., Photosensitizers in clinical PDT. *Photodiagnosis and Photodynamic Therapy* **2004,** *1*, 27-42.

33. Sternberg, E. D.; Dolphin, D.; Bruckner, C., Porphyrin-based photosensitizers for use in photodynamic therapy. *Tetrahedron* **1998,** *54*, 4151-4202.

34. Pantos, G. Studies of Polyaza Pyrrole-containing Systems and Linear and Macrocyclic Polypyrrolic Architectures. Dissertation, The University of Texas at Austin2005.

35. Stapleton, M.; Rhodes, L. E., Photosensitizers for photodynamic therapy of cutaneous disease. *J Dermatolog Treat* **2003,** *14*, 107-12.

36. Moser, J. G., *Photodynamic tumour therapy 2nd and 3rd generation photosensitizers.*; Harwood academic publishers: New Delhi, India, 1998.

37. Sharman, W. M.; van Lier, J. E.; Allen, C. M., Targeted photodynamic therapy via receptor mediated delivery systems. *Adv Drug Deliv Rev* **2004,** *56*, 53-76.

38. Verma, S.; Watt, G. M.; Mai, Z.; Hasan, T., Strategies for enhanced photodynamic therapy effects. *Photochem Photobiol* **2007,** *83*, 996-1005.

39. Madar-Balakirski, N.; Tempel-Brami, C.; Kalchenko, V.; Brenner, O.; Varon, D.; Scherz, A.; Salomon, Y., Permanent occlusion of feeding arteries and draining veins in solid mouse tumors by vascular targeted photodynamic therapy (VTP) with Tookad. *PLoS One* **2010,** *5*, e10282.

40. Chen, B.; Pogue, B. W.; Luna, J. M.; Hardman, R. L.; Hoopes, P. J.; Hasan, T., Tumor vascular permeabilization by vascular-targeting photosensitization: effects, mechanism, and therapeutic implications. *Clin Cancer Res* **2006,** *12*, 917-23.

41. Tozer, G. M.; Bicknell, R., Therapeutic targeting of the tumor vasculature. *Semin Radiat Oncol* **2004,** *14*, 222-32.

42. Tozer, G. M.; Kanthou, C.; Baguley, B. C., Disrupting tumour blood vessels. *Nat Rev Cancer* **2005,** *5*, 423-35.

43. Chen, B.; Pogue, B. W.; Hoopes, P. J.; Hasan, T., Vascular and cellular targeting for photodynamic therapy. *Crit Rev Eukaryot Gene Expr* **2006,** *16*, 279-305.

44. Savellano, M. D.; Hasan, T., Targeting cells that overexpress the epidermal growth factor receptor with polyethylene glycolated BPD verteporfin photosensitizer immunoconjugates. *Photochem Photobiol* **2003,** *77*, 431-9.

45. Stevens, T.; Garcia, J. G.; Shasby, D. M.; Bhattacharya, J.; Malik, A. B., Mechanisms regulating endothelial cell barrier function. *Am J Physiol Lung Cell Mol Physiol* **2000,** *279*, L419-22.

46. Fingar, V. H., Vascular effects of photodynamic therapy. *J Clin Laser Med Surg* **1996,** *14*, 323-8.

47. Henderson, B. W.; Dougherty, T. J., How does photodynamic therapy work? *Photochem Photobiol* **1992,** *55*, 145-57.

48. Michels, S.; Schmidt-Erfurth, U., Sequence of early vascular events after photodynamic therapy. *Invest Ophthalmol Vis Sci* **2003,** *44*, 2147-54.

49. Konan, Y. N.; Gurny, R.; Allemann, E., State of the art in the delivery of photosensitizers for photodynamic therapy. *J Photochem Photobiol B* **2002,** *66*, 89-106.

50. Hudson, R.; Carcenac, M.; Smith, K.; Madden, L.; Clarke, O. J.; Pelegrin, A.; Greenman, J.; Boyle, R. W., The development and characterisation of porphyrin isothiocyanate-monoclonal antibody conjugates for photoimmunotherapy. *Br J Cancer* **2005,** *92*, 1442-9.

51. Staneloudi, C.; Smith, K. A.; Hudson, R.; Malatesti, N.; Savoie, H.; Boyle, R. W.; Greenman, J., Development and characterization of novel photosensitizer : scFv conjugates for use in photodynamic therapy of cancer. *Immunology* **2007,** *120*, 512-7.

52. Moser, J. G., Photodynamic tumor therapy: 2nd and 3rd generation photosensitizers. **1998**, 242.

53. Zheng, G.; Chen, J.; Stefflova, K.; Jarvi, M.; Li, H.; Wilson, B. C., Photodynamic molecular beacon as an activatable photosensitizer based on protease-controlled singlet oxygen quenching and activation. *Proc Natl Acad Sci U S A* **2007,** *104*, 8989-94.

54. Dolmans, D. E.; Fukumura, D.; Jain, R. K., Photodynamic therapy for cancer. *Nat Rev Cancer* **2003,** *3*, 380-7.

55. Oleinick, N. L.; Morris, R. L.; Belichenko, I., The role of apoptosis in response to photodynamic therapy: what, where, why, and how. *Photochem Photobiol Sci* **2002,** *1*, 1-21.

56. Almeida, R. D.; Manadas, B. J.; Carvalho, A. P.; Duarte, C. B., Intracellular signaling mechanisms in photodynamic therapy. *Biochim Biophys Acta* **2004,** *1704*, 59-86.

57. Abels, C., Targeting of the vascular system of solid tumours by photodynamic therapy (PDT). *Photochem Photobiol Sci* **2004,** *3*, 765-71.

58. Castano, A. P.; Mroz, P.; Hamblin, M. R., Photodynamic therapy and anti-tumour immunity. *Nat Rev Cancer* **2006,** *6*, 535-45.

59. Fingar, V. H.; Wieman, T. J.; Wiehle, S. A.; Cerrito, P. B., The role of microvascular damage in photodynamic therapy: the effect of treatment on vessel constriction, permeability, and leukocyte adhesion. *Cancer Res* **1992,** *52*, 4914-21.

60. van Duijnhoven, F. H.; Aalbers, R. I.; Rovers, J. P.; Terpstra, O. T.; Kuppen, P. J., The immunological consequences of photodynamic treatment of cancer, a literature review. *Immunobiology* **2003,** *207*, 105-13.

61. Christensen, T.; Feren, K.; Moan, J.; Pettersen, E., Photodynamic effects of haematoporphyrin derivative on synchronized and asynchronous cells of different origin. *Br J Cancer* **1981,** *44*, 717-24.

62. Herman, S.; Kalechman, Y.; Gafter, U.; Sredni, B.; Malik, Z., Photofrin II induces cytokine secretion by mouse spleen cells and human peripheral mononuclear cells. *Immunopharmacology* **1996,** *31*, 195-204.

63. Granville, D. J.; McManus, B. M.; Hunt, D. W., Photodynamic therapy: shedding light on the biochemical pathways regulating porphyrin-mediated cell death. *Histol Histopathol* **2001,** *16*, 309-17.

64. Robertson, J. D.; Orrenius, S., Molecular mechanisms of apoptosis induced by cytotoxic chemicals. *Crit Rev Toxicol* **2000,** *30*, 609-27.

65. Solary, E.; Droin, N.; Bettaieb, A.; Corcos, L.; Dimanche-Boitrel, M. T.; Garrido, C., Positive and negative regulation of apoptotic pathways by cytotoxic agents in hematological malignancies. *Leukemia* **2000,** *14*, 1833-49.

66. Verheij, M.; Bartelink, H., Radiation-induced apoptosis. *Cell Tissue Res* **2000,** *301*, 133-42.

67. Ashkenazi, A.; Dixit, V. M., Death receptors: signaling and modulation. *Science* **1998,** *281*, 1305-8.

68. Deschesnes, R. G.; Huot, J.; Valerie, K.; Landry, J., Involvement of p38 in apoptosis-associated membrane blebbing and nuclear condensation. *Mol Biol Cell* **2001,** *12*, 1569-82.

69. Kroemer, G.; Reed, J. C., Mitochondrial control of cell death. *Nat Med* **2000,** *6*, 513-9.

70. Reed, J. C., Mechanisms of apoptosis. *Am J Pathol* **2000,** *157*, 1415-30.

71. Kroemer, G.; Dallaporta, B.; Resche-Rigon, M., The mitochondrial death/life regulator in apoptosis and necrosis. *Annu Rev Physiol* **1998,** *60*, 619-42.

72. Costantini, P.; Jacotot, E.; Decaudin, D.; Kroemer, G., Mitochondrion as a novel target of anticancer chemotherapy. *J Natl Cancer I* **2000,** *92*, 1042-1053.

73. Gottlieb, R. A., Mitochondria: execution central. *FEBS Lett* **2000,** *482*, 6-12.

74. Green, D. R., Apoptotic pathways: paper wraps stone blunts scissors. *Cell* **2000,** *102*, 1-4.

75. Qin, Z. H.; Wang, Y.; Kikly, K. K.; Sapp, E.; Kegel, K. B.; Aronin, N.; DiFiglia, M., Pro-caspase-8 is predominantly localized in mitochondria and released into cytoplasm upon apoptotic stimulation. *J Biol Chem* **2001,** *276*, 8079-86.

76. Hamblin M. R; Mroz, P., *Advances in Photodynamic Therapy: Basic, Translational and Clinical* Artech House Publishers: Boston, 2008.

77. Agarwal, M. L.; Clay, M. E.; Harvey, E. J.; Evans, H. H.; Antunez, A. R.; Oleinick, N. L., Photodynamic therapy induces rapid cell death by apoptosis in L5178Y mouse lymphoma cells. *Cancer Res* **1991,** *51*, 5993-6.

78. Separovic, D.; He, J.; Oleinick, N. L., Ceramide generation in response to photodynamic treatment of L5178Y mouse lymphoma cells. *Cancer Res* **1997,** *57*, 1717-21.

79. Xue, L. Y.; He, J.; Oleinick, N. L., Rapid tyrosine phosphorylation of HS1 in the response of mouse lymphoma L5178Y-R cells to photodynamic treatment sensitized by the phthalocyanine Pc 4. *Photochem Photobiol* **1997,** *66*, 105-13.

80. Kessel, D.; Luo, Y., Cells in cryptophycin-induced cell-cycle arrest are susceptible to apoptosis. *Cancer Lett* **2000,** *151*, 25-9.

81. Hamblin, M. R. M., P.;, *Advances in Photodynamic Therapy. Basic, Translational, and Clinical*. Artech House: Norwood, MA, 2008.

82. Carthy, C. M.; Granville, D. J.; Jiang, H.; Levy, J. G.; Rudin, C. M.; Thompson, C. B.; McManus, B. M.; Hunt, D. W., Early release of mitochondrial cytochrome c and expression of mitochondrial epitope 7A6 with a porphyrin-derived photosensitizer: Bcl-2 and Bcl-xL overexpression do not prevent early mitochondrial events but still depress caspase activity. *Lab Invest* **1999,** *79*, 953-65.

83. Buytaert, E.; Dewaele, M.; Agostinis, P., Molecular effectors of multiple cell death pathways initiated by photodynamic therapy. *Biochim Biophys Acta* **2007,** *1776*, 86-107.

84. Kessel, D.; Reiners, J. J., Jr., Apoptosis and autophagy after mitochondrial or endoplasmic reticulum photodamage. *Photochem Photobiol* **2007,** *83*, 1024-8.

85. Patel, A. S.; Lin, L.; Geyer, A.; Haspel, J. A.; An, C. H.; Cao, J.; Rosas, I. O.; Morse, D., Autophagy in idiopathic pulmonary fibrosis. *PLoS One* **2012,** *7*, e41394.

86. Eskelinen, E. L., Doctor Jekyll and Mister Hyde: autophagy can promote both cell survival and cell death. *Cell Death Differ* **2005,** *12 Suppl 2*, 1468-72.

87. Kessel, D.; Vicente, M. G.; Reiners, J. J., Jr., Initiation of apoptosis and autophagy by photodynamic therapy. *Lasers Surg Med* **2006,** *38*, 482-8.

88. Xue, L. Y.; Chiu, S. M.; Azizuddin, K.; Joseph, S.; Oleinick, N. L., The death of human cancer cells following photodynamic therapy: apoptosis competence is necessary for Bcl-2 protection but not for induction of autophagy. *Photochem Photobiol* **2007,** *83*, 1016-23.

89. Luo, S.; Rubinsztein, D. C., Atg5 and Bcl-2 provide novel insights into the interplay between apoptosis and autophagy. *Cell Death Differ* **2007,** *14*, 1247-50.

90. Proskuryakov, S. Y.; Konoplyannikov, A. G.; Gabai, V. L., Necrosis: a specific form of programmed cell death? *Exp Cell Res* **2003,** *283*, 1-16.

91. Kessel, D.; Oleinick, N. L., Photodynamic therapy and cell death pathways. *Methods Mol Biol* **2010,** *635*, 35-46.

92. Noodt, B. B.; Berg, K.; Stokke, T.; Peng, Q.; Nesland, J. M., Different apoptotic pathways are induced from various intracellular sites by tetraphenylporphyrins and light. *Br J Cancer* **1999,** *79*, 72-81.

93. Vantieghem, A.; Assefa, Z.; Vandenabeele, P.; Declercq, W.; Courtois, S.; Vandenheede, J. R.; Merlevede, W.; de Witte, P.; Agostinis, P., Hypericin-induced photosensitization of HeLa cells leads to apoptosis or necrosis. Involvement of cytochrome c and procaspase-3 activation in the mechanism of apoptosis. *FEBS Lett* **1998,** *440*, 19-24.

94. Kim, H. R.; Luo, Y.; Li, G.; Kessel, D., Enhanced apoptotic response to photodynamic therapy after bcl-2 transfection. *Cancer Res* **1999,** *59*, 3429-32.

95. Noodt, B. B.; Rodal, G. H.; Wainwright, M.; Peng, Q.; Horobin, R.; Nesland, J. M.; Berg, K., Apoptosis induction by different pathways with methylene blue derivative and light from mitochondrial sites in V79 cells. *Int J Cancer* **1998,** *75*, 941-8.

96. Dellinger, M., Apoptosis or necrosis following Photofrin photosensitization: influence of the incubation protocol. *Photochem Photobiol* **1996,** *64*, 182-7.

97. Kessel, D.; Poretz, R. D., Sites of photodamage induced by photodynamic therapy with a chlorin e6 triacetoxymethyl ester (CAME). *Photochem Photobiol* **2000,** *71*, 94-6.

98. Kochevar, I. E.; Lynch, M. C.; Zhuang, S.; Lambert, C. R., Singlet oxygen, but not oxidizing radicals, induces apoptosis in HL-60 cells. *Photochem Photobiol* **2000,** *72*, 548-53.

99. Lin, C. P.; Lynch, M. C.; Kochevar, I. E., Reactive oxidizing species produced near the plasma membrane induce apoptosis in bovine aorta endothelial cells. *Exp Cell Res* **2000,** *259*, 351-9.

100. Rosenkranz, A. A.; Jans, D. A.; Sobolev, A. S., Targeted intracellular delivery of photosensitizers to enhance photodynamic efficiency. *Immunol Cell Biol* **2000,** *78*, 452-64.

101. Gomer, C. J.; Rucker, N.; Banerjee, A.; Benedict, W. F., Comparison of mutagenicity and induction of sister chromatid exchange in Chinese hamster cells exposed to hematoporphyrin derivative photoradiation, ionizing radiation, or ultraviolet radiation. *Cancer Res* **1983,** *43*, 2622-7.

102. Gomer, C. J.; Rucker, N.; Murphree, A. L., Transformation and mutagenic potential of porphyrin photodynamic therapy in mammalian cells. *Int J Radiat Biol Relat Stud Phys Chem Med* **1988,** *53*, 651-9.

103. Ahmad, N.; Kalka, K.; Mukhtar, H., In vitro and in vivo inhibition of epidermal growth factor receptor-tyrosine kinase pathway by photodynamic therapy. *Oncogene* **2001,** *20*, 2314-7.

104. Wong, T. W.; Tracy, E.; Oseroff, A. R.; Baumann, H., Photodynamic therapy mediates immediate loss of cellular responsiveness to cytokines and growth factors. *Cancer Res* **2003,** *63*, 3812-8.

105. Volden, G.; Christensen, T.; Moan, J., Photodynamic Membrane Damage of Hematoporphyrin Derivative-Treated Nhik-3025 Cells-Invitro. *Photobiochemistry and Photobiophysics* **1981,** *3*, 105-111.

106. Moan, J.; McGhie, J.; Jacobsen, P. B., Photodynamic effects on cells in vitro exposed to hematoporphyrin derivative and light. *Photochem Photobiol* **1983,** *37*, 599-604.

107. Moan, J.; Pettersen, E. O.; Christensen, T., The mechanism of photodynamic inactivation of human cells in vitro in the presence of haematoporphyrin. *Br J Cancer* **1979,** *39*, 398-407.

108. Leung, W. N.; Sun, X.; Mak, N. K.; Yow, C. M., Photodynamic effects of mTHPC on human colon adenocarcinoma cells: photocytotoxicity, subcellular localization and apoptosis. *Photochem Photobiol* **2002,** *75*, 406-11.

109. Ichinose, S.; Usuda, J.; Hirata, T.; Inoue, T.; Ohtani, K.; Maehara, S.; Kubota, M.; Imai, K.; Tsunoda, Y.; Kuroiwa, Y.; Yamada, K.; Tsutsui, H.; Furukawa, K.; Okunaka, T.; Oleinick, N. L.; Kato, H., Lysosomal cathepsin initiates apoptosis, which is regulated by photodamage to Bcl-2 at mitochondria in photodynamic therapy using a novel photosensitizer, ATX-s10 (Na). *Int J Oncol* **2006,** *29*, 349-55.

110. Kessel, D.; Luo, Y.; Mathieu, P.; Reiners, J. J., Jr., Determinants of the apoptotic response to lysosomal photodamage. *Photochem Photobiol* **2000,** *71*, 196-200.

111. Kessel, D.; Luo, Y., Intracellular sites of photodamage as a factor in apoptotic cell death. *J Porphyr Phthalocya* **2001,** *5*, 181-184.

112. Reiners, J. J., Jr.; Caruso, J. A.; Mathieu, P.; Chelladurai, B.; Yin, X. M.; Kessel, D., Release of cytochrome c and activation of pro-

caspase-9 following lysosomal photodamage involves Bid cleavage. *Cell Death Differ* **2002,** *9*, 934-44.

113. Caruso, J. A.; Mathieu, P. A.; Joiakim, A.; Leeson, B.; Kessel, D.; Sloane, B. F.; Reiners, J. J., Jr., Differential susceptibilities of murine hepatoma 1c1c7 and Tao cells to the lysosomal photosensitizer NPe6: influence of aryl hydrocarbon receptor on lysosomal fragility and protease contents. *Mol Pharmacol* **2004,** *65*, 1016-28.

114. Berg, K.; Dietze, A.; Kaalhus, O.; Hogset, A., Site-specific drug delivery by photochemical internalization enhances the antitumor effect of bleomycin. *Clin Cancer Res* **2005,** *11*, 8476-85.

115. Berg, K.; Prasmickaite, L.; Selbo, P. K.; Hellum, M.; Bonsted, A.; Hogset, A., Photochemical internalization (PCI)--a novel technology for release of macromolecules from endocytic vesicles. *Oftalmologia* **2003,** *56*, 67-71.

116. Berg, K.; Selbo, P. K.; Prasmickaite, L.; Tjelle, T. E.; Sandvig, K.; Moan, J.; Gaudernack, G.; Fodstad, O.; Kjolsrud, S.; Anholt, H.; Rodal, G. H.; Rodal, S. K.; Hogset, A., Photochemical internalization: a novel technology for delivery of macromolecules into cytosol. *Cancer Res* **1999,** *59*, 1180-3.

117. Selbo, P. K.; Kaalhus, O.; Sivam, G.; Berg, K., 5-Aminolevulinic acid-based photochemical internalization of the immunotoxin MOC31-gelonin generates synergistic cytotoxic effects in vitro. *Photochem Photobiol* **2001,** *74*, 303-10.

118. Selbo, P. K.; Sivam, G.; Fodstad, O.; Sandvig, K.; Berg, K., In vivo documentation of photochemical internalization, a novel approach to site specific cancer therapy. *Int J Cancer* **2001,** *92*, 761-6.

119. Berg, K.; Madslien, K.; Bommer, J. C.; Oftebro, R.; Winkelman, J. W.; Moan, J., Light induced relocalization of sulfonated meso-tetraphenylporphines in NHIK 3025 cells and effects of dose fractionation. *Photochem Photobiol* **1991,** *53*, 203-10.

120. Jordan, M. A.; Wilson, L., Microtubules as a target for anticancer drugs. *Nat Rev Cancer* **2004,** *4*, 253-65.

121. Sporn, L. A.; Foster, T. H., Photofrin and light induces microtubule depolymerization in cultured human endothelial cells. *Cancer Res* **1992,** *52*, 3443-8.

122. Berg, K.; Moan, J., Lysosomes and microtubules as targets for photochemotherapy of cancer. *Photochem Photobiol* **1997,** *65*, 403-9.

123. Berg, K.; Moan, J.; Bommer, J. C.; Winkelman, J. W., Cellular inhibition of microtubule assembly by photoactivated sulphonated meso-tetraphenylporphines. *Int J Radiat Biol* **1990,** *58*, 475-87.

124. Juarranz, A.; Espada, J.; Stockert, J. C.; Villanueva, A.; Polo, S.; Dominguez, V.; Canete, M., Photodamage induced by Zinc(II)-phthalocyanine to microtubules, actin, alpha-actinin and keratin of HeLa cells. *Photochem Photobiol* **2001,** *73*, 283-9.

125. Costantini, P.; Jacotot, E.; Decaudin, D.; Kroemer, G., Mitochondrion as a novel target of anticancer chemotherapy. *J Natl Cancer Inst* **2000,** *92*, 1042-53.

126. Rodriguez, M. E.; Azizuddin, K.; Zhang, P.; Chiu, S. M.; Lam, M.; Kenney, M. E.; Burda, C.; Oleinick, N. L., Targeting of mitochondria by 10-N-alkyl acridine orange analogues: role of alkyl chain length in determining cellular uptake and localization. *Mitochondrion* **2008,** *8*, 237-46.

127. Moor, A. C., Signaling pathways in cell death and survival after photodynamic therapy. *J Photochem Photobiol B* **2000,** *57*, 1-13.

128. Gross, A.; McDonnell, J. M.; Korsmeyer, S. J., BCL-2 family members and the mitochondria in apoptosis. *Genes Dev* **1999,** *13*, 1899-911.

129. Crompton, M., Mitochondrial intermembrane junctional complexes and their role in cell death. *J Physiol* **2000,** *529 Pt 1*, 11-21.

130. Halestrap, A. P.; Doran, E.; Gillespie, J. P.; O'Toole, A., Mitochondria and cell death. *Biochem Soc Trans* **2000,** *28*, 170-7.

131. Hilf, R., Mitochondria are targets of photodynamic therapy. *J Bioenerg Biomembr* **2007,** *39*, 85-9.

132. Morgan, J.; Oseroff, A. R., Mitochondria-based photodynamic anti-cancer therapy. *Adv Drug Deliv Rev* **2001,** *49*, 71-86.

133. Chen, L. B., Mitochondrial membrane potential in living cells. *Annu Rev Cell Biol* **1988,** *4*, 155-81.

134. Chen, L. B., Fluorescent Labeling of Mitochondria. *Methods in Cell Biology* **1989,** *29*, 103-123.

135. Davis, S.; Weiss, M. J.; Wong, J. R.; Lampidis, T. J.; Chen, L. B., Mitochondrial and plasma membrane potentials cause unusual accumulation and retention of rhodamine 123 by human breast adenocarcinoma-derived MCF-7 cells. *J Biol Chem* **1985,** *260*, 13844-50.

136. Belostotsky, I.; da Silva, S. M.; Paez, M. G.; Indig, G. L., Mitochondrial targeting for photochemotherapy. Can selective tumor cell killing be predicted based on n-octanol/water distribution coefficients? *Biotech Histochem* **2011,** *86*, 302-14.

137. Bernal, S. D., T.J. Lampidis, R.M. McIsaac, L.B. Chen., Anticarcinoma activity in vivo of rhodamine 123, a mitochondrial-specific dye. *Science* **1993,** *222*, 169–172.

138. Kandela, I. K.; Bartlett, J. A.; Indig, G. L., Effect of molecular structure on the selective phototoxicity of triarylmethane dyes towards tumor cells. *Photochemical & Photobiological Sciences* **2002,** *1*, 309-314.

139. Ross, M. F.; Kelso, G. F.; Blaikie, F. H.; James, A. M.; Cocheme, H. M.; Filipovska, A.; Da Ros, T.; Hurd, T. R.; Smith, R. A.; Murphy, M. P., Lipophilic triphenylphosphonium cations as tools in mitochondrial

bioenergetics and free radical biology. *Biochemistry (Mosc)* **2005,** *70*, 222-30.

140. Jensen, T. J.; Vicente, M. G.; Luguya, R.; Norton, J.; Fronczek, F. R.; Smith, K. M., Effect of overall charge and charge distribution on cellular uptake, distribution and phototoxicity of cationic porphyrins in HEp2 cells. *J Photochem Photobiol B* **2010,** *100*, 100-11.

141. Sibrian-Vazquez, M.; Nesterova, I. V.; Jensen, T. J.; Vicente, M. G., Mitochondria targeting by guanidine- and biguanidine-porphyrin photosensitizers. *Bioconjug Chem* **2008,** *19*, 705-13.

142. Gregory Gregoriadis, Y. P., *Liposomes in nanomedicin*. John Wiley & sons, Ltd: Chichester, 2010.

143. Waterhouse, D. N.; Madden, T. D.; Cullis, P. R.; Bally, M. B.; Mayer, L. D.; Webb, M. S., Preparation, characterization, and biological analysis of liposomal formulations of vincristine. *Methods Enzymol* **2005,** *391*, 40-57.

144. Haran, G.; Cohen, R.; Bar, L. K.; Barenholz, Y., Transmembrane ammonium sulfate gradients in liposomes produce efficient and stable entrapment of amphipathic weak bases. *Biochim Biophys Acta* **1993,** *1151*, 201-15.

145. Goren, D.; Horowitz, A. T.; Tzemach, D.; Tarshish, M.; Zalipsky, S.; Gabizon, A., Nuclear delivery of doxorubicin via folate-targeted liposomes with bypass of multidrug-resistance efflux pump. *Clin Cancer Res* **2000,** *6*, 1949-57.

146. Allen, T. M.; Cullis, P. R., Drug delivery systems: entering the mainstream. *Science* **2004,** *303*, 1818-22.

147. Liechty, W. B.; Kryscio, D. R.; Slaughter, B. V.; Peppas, N. A., Polymers for drug delivery systems. *Annu Rev Chem Biomol Eng* **2010,** *1*, 149-73.

148. Shive, M. S.; Anderson, J. M., Biodegradation and biocompatibility of PLA and PLGA microspheres. *Adv Drug Deliv Rev* **1997,** *28*, 5-24.

149. Langer, R., Drug delivery and targeting. *Nature* **1998,** *392*, 5-10.

150. Brouwers, J. R., Advanced and controlled drug delivery systems in clinical disease management. *Pharm World Sci* **1996,** *18*, 153-62.

151. Gemma Vilara, J. T.-P., and Fernando Albericio, Polymers and Drug Delivery Systems. *Current Drug Delivery* **2012,** *9*.

152. Wiener, E. C.; Brechbiel, M. W.; Brothers, H.; Magin, R. L.; Gansow, O. A.; Tomalia, D. A.; Lauterbur, P. C., Dendrimer-based metal chelates: a new class of magnetic resonance imaging contrast agents. *Magn Reson Med* **1994,** *31*, 1-8.

153. Jansen, J. F. G. A.; Debrabandervandenberg, E. M. M.; Meijer, E. W., Encapsulation of Guest Molecules into a Dendritic Box. *Science* **1994,** *266*, 1226-1229.

154. D'Emanuele, A.; Attwood, D., Dendrimer-drug interactions. *Advanced Drug Delivery Reviews* **2005,** *57*, 2147-2162.

155. Jansen, J. F. G. A.; Meijer, E. W.; Debrabandervandenberg, E. M. M., The Dendritic Box - Shape-Selective Liberation of Encapsulated Guests. *Journal of the American Chemical Society* **1995,** *117*, 4417-4418.

156. Pan, D.; Turner, J. L.; Wooley, K. L., Folic acid-conjugated nanostructured materials designed for cancer cell targeting. *Chem Commun (Camb)* **2003**, 2400-1.

157. Daly, T.; Royal, R. E.; Kershaw, M. H.; Treisman, J.; Wang, G.; Li, W.; Herlyn, D.; Eshhar, Z.; Hwu, P., Recognition of human colon cancer by T cells transduced with a chimeric receptor gene. *Cancer Gene Ther* **2000,** *7*, 284-91.

158. Sakharov, D. V.; Jie, A. F.; Filippov, D. V.; Bekkers, M. E.; van Boom, J. H.; Rijken, D. C., Binding and retention of polycationic peptides and dendrimers in the vascular wall. *FEBS Lett* **2003,** *537*, 6-10.

159. Wiwattanapatapee, R.; Lomlim, L.; Saramunee, K., Dendrimers conjugates for colonic delivery of 5-aminosalicylic acid. *J Control Release* **2003,** *88*, 1-9.

160. Trivedi, V. P., U.; Bhimani, B.; Daslaniya, D.; Patel, G.; Vyas, B.;, Dendrimer: Polymer of 21st centrury. *International Journal of Pharmaceutical Research and Bio-science* **2012,** *1(2)*, 1-21.

161. Emaus, R. K.; Grunwald, R.; Lemasters, J. J., Rhodamine 123 as a probe of transmembrane potential in isolated rat-liver mitochondria: spectral and metabolic properties. *Biochim Biophys Acta* **1986,** *850*, 436-48.

162. Indig, G. L., G.S. Anderson, M.G. Nichols, J.A. Bartlett, W.S. Mellon, F. Sieber, Assessment of crystal violet and other triarylmethane dyes as photosensitizers for purging of autologous bone marrow grafts from residual tumor cells. *J. Pharm. Sci* **2000,** *89*, 88-99.

163. Kandela, I. K.; Lee, W.; Indig, G. L., Effect of the lipophilic/hydrophilic character of cationic triarylmethane dyes on their selective phototoxicity toward tumor cells. *Biotech Histochem* **2003,** *78*, 157-69.

164. Lacerda, S. H. D., B. Abraham, T. C. Stringfellow, G. L. Indig, Photophisical, photochemical, and tumor-selectivity properties of bromine derivatives of Rhodamine 123. *Photochem. Photobiol* **2005,** *81*, 1430-1438.

165. Indig, G., Mechanisms of action of cationic dyes in photodynamic therapy of tumors. *Recent Res. Devel. Pure & Applied Chem* **1999,** *3*, 9-19.

166. Duxbury, D. F., The Photochemistry and Photophysics of Triphenylmethane Dyes in Solid and Liquid-Media. *Chemical Reviews* **1993,** *93*, 381-433.

167. Bartlett, J. Chemical aspects of mitochondrial targeting in photodynamic therapy. University of Wisconsin-Madison2002.

168. Modica-Napolitano, J. S.; Aprille, J. R., Basis for the selective cytotoxicity of rhodamine 123. *Cancer Res* **1987,** *47*, 4361-5.

169. Summerhayes, I. C.; Lampidis, T. J.; Bernal, S. D.; Nadakavukaren, J. J.; Nadakavukaren, K. K.; Shepherd, E. L.; Chen, L. B., Unusual Retention of Rhodamine-123 by Mitochondria in Muscle and Carcinoma-Cells. *Proceedings of the National Academy of Sciences of the United States of America-Biological Sciences* **1982,** *79*, 5292-5296.

170. Johnson, L. V.; Walsh, M. L.; Bockus, B. J.; Chen, L. B., Monitoring of relative mitochondrial membrane potential in living cells by fluorescence microscopy. *J Cell Biol* **1981,** *88*, 526-35.

171. Detty, M. R.; Gibson, S. L.; Wagner, S. J., Current clinical and preclinical photosensitizers for use in photodynamic therapy. *J Med Chem* **2004,** *47*, 3897-915.

172. Wainwright, M., Non-porphyrin photosensitizers in biomedicine. *Chemical Society Reviews* **1996,** *25*, 351-+.

173. Ngen, E. J.; Rajaputra, P.; You, Y., Evaluation of delocalized lipophilic cationic dyes as delivery vehicles for photosensitizers to mitochondria. *Bioorg Med Chem* **2009,** *17*, 6631-40.

174. Paul, B.; Rajaputra, P.; You, Y., In vitro and in vivo photodynamic activity of core-modified porphyrin IY69 using 690 nm diode laser. *Photochem Photobiol* **2011,** *87*, 1468-73.

175. Ngen, E. J.; Daniels, T. S.; Murthy, R. S.; Detty, M. R.; You, Y., Core-modified porphyrins. Part 6: Effects of lipophilicity and core structures on physicochemical and biological properties in vitro. *Bioorganic & Medicinal Chemistry* **2008,** *16*, 3171-3183.

176. You, Y.; Gibson, S. L.; Detty, M. R., Phototoxicity of a core-modified porphyrin and induction of apoptosis. *Journal of Photochemistry and Photobiology B: Biology* **2006,** *85*, 155-162.

177. Modica-Napolitano, J. S.; Aprille, J. R., Delocalized lipophilic cations selectively target the mitochondria of carcinoma cells. *Advanced Drug Delivery Reviews* **2001,** *49*, 63-70.

178. Mislick, K. A.; Baldeschwieler, J. D., Evidence for the role of proteoglycans in cation-mediated gene transfer. *Proc. Natl. Acad. Sci.* **1996,** *93*, 12349-12354.

179. Dias, N.; Bailly, C., Drugs targeting mitochondrial functions to control tumor cell growth *Biochem. Pharmacol.* **2005,** *70*, 1-12.

180. Morgan, J.; Oseroff, A. R., Mitochondria-based photodynamic anti-cancer therapy. *Advanced Drug Delivery Reviews* **2001,** *49*, 71-86.

181. Navia, M. A.; Chaturvedi, P. R., Design principles for orally bioavailable drugs. *Drug Disc. Today* **1996,** *1*, 179-189.

182. Harre, K.; Wegner, G., Solution properties and kinetics of aggregation of an alkyl-substituted poly(p-phenylene). *Polymer* **2006,** *47*, 7312-7317.

183. Satonaka, H.; Kusuzaki, K.; Matsubara, T.; Shintani, K.; Wakabayashi, T.; Nakamura, T.; Matsumine, A.; A., U., Flash wave light strongly enhanced the cytocidal effect of photodynamic therapy with acridine orange on mouse osteosarcoma cell line. *Anticancer Res.* **2007,** *27*, 3339-3344.

184. Kusuzaki, K.; Murata, H.; Matsubara, T.; Miyazaki, S.; Okamura, A.; Seto, M.; Matsumine, A.; Hosoi, H.; Sugimoto, T.; Uchida, A., Clinical trial of photodynamic therapy using acridine orange with/without low dose radiation as new limb salvage modality in musculoskeletal sarcomas. *Anticancer Res.* **2005,** *25*, 1225 -1236.

185. Kusuzaki, K.; Takeshita, H.; Murata, H.; Gebhardt, M.; Springfield, D. S.; Mankin, H. J.; Ashihara, T.; Hirasawa, Y., Polyploidization induced by acridine orange in mouse osteosarcoma cells. *Anticancer Res.* **2000,** *20*, 965-970.

186. Matsubara, T.; Kusuzaki, K.; Matsumine, A.; Shintani, K.; H., S.; A., U., Acridine orange used for photodynamic therapy accumulates in malignant musculoskeletal tumors depending on pH gradient. *Anticancer Res.* **2006,** *26*, 187 - 194.

187. Johnson, I. M.; Kumar, S. G.; Malathi, R., De-intercalation of ethidium bromide and acridine orange by xanthine derivatives and their modulatory effect on anticancer agents: a study of DNA-directed toxicity enlightened by time correlated single photon counting. *J. Biomol. Struct. Dyn.* **2003,** *20*, 677-86.

188. Lyles, M. B.; Cameron, I. L., Interactions of the DNA intercalator acridine orange, with itself, with caffeine, and with double stranded DNA. *Biophys. Chem.* **2002,** *96*, 53-76.

189. Musser, D. A.; Wagner, J. M.; Weber, F. J.; Datta-Gupta, N., The binding of tumor localizing porphyrins to a fibrin matrix and their effects following photoirradiation. *Res Commun Chem Pathol Pharmacol* **1980,** *28*, 505-25.

190. Detty, M. R., Photosensitisers for the photodynamic therapy of cancer and other diseases. *Expert Opin Ther Pat* **2001,** *11*, 1849-1860.

191. Moan, J.; Berg, K., The Photodegradation of Porphyrins in Cells Can Be Used to Estimate the Lifetime of Singlet Oxygen. *Photochem Photobiol* **1991,** *53*, 549-553.

192. Peng, T. I.; Chang, C. J.; Guo, M. J.; Wang, Y. H.; Yu, J. S.; Wu, H. Y.; Jou, M. J., Mitochondrion-targeted photosensitizer enhances the photodynamic effect-induced mitochondrial dysfunction and apoptosis. *Ann N Y Acad Sci* **2005,** *1042*, 419-28.

193. Sun, X.; Wong, J. R.; Song, K.; Hu, J.; Garlid, K. D.; Chen, L. B., AA1, a newly synthesized monovalent lipophilic cation, expresses potent in vivo antitumor activity. *Cancer Res* **1994,** *54*, 1465-71.

194. Modica-Napolitano, J. S.; Koya, K.; Weisberg, E.; Brunelli, B. T.; Li, Y.; Chen, L. B., Selective damage to carcinoma mitochondria by the rhodacyanine MKT-077. *Cancer Res* **1996,** *56*, 544-50.

195. Dias, N.; Bailly, C., Drugs targeting mitochondrial functions to control tumor cell growth. *Biochem Pharmacol* **2005,** *70*, 1-12.

196. Dummin, H.; Cernay, T.; Zimmermann, H. W., Selective photosensitization of mitochondria in HeLa cells by cationic Zn (II) phthalocyanines with lipophilic side-chains. *J Photochem Photobiol B* **1997,** *37*, 219-29.

197. Modica-Napolitano, J. S.; Aprille, J. R., Delocalized lipophilic cations selectively target the mitochondria of carcinoma cells. *Adv Drug Deliv Rev* **2001,** *49*, 63-70.

198. Wang, F.; Ogasawara, M. A.; Huang, P., Small mitochondria-targeting molecules as anti-cancer agents. *Mol Aspects Med* **2010,** *31*, 75-92.

199. Stilts, C. E.; Nelen, M. I.; Hilmey, D. G.; Davies, S. R.; Gollnick, S. O.; Oseroff, A. R.; Gibson, S. L.; Hilf, R.; Detty, M. R., Water-soluble, core-modified porphyrins as novel, longer-wavelength-absorbing sensitizers for photodynamic therapy. *Journal of Medicinal Chemistry* **2000,** *43*, 2403-2410.

200. Hilmey, D. G.; Abe, M.; Nelen, M. I.; Stilts, C. E.; Baker, G. A.; Baker, S. N.; Bright, F. V.; Davies, S. R.; Gollnick, S. O.; Oseroff, A. R.; Gibson, S. L.; Hilf, R.; Detty, M. R., Water-soluble, core-modified porphyrins as novel, longer-wavelength-absorbing sensitizers for photodynamic therapy. II. Effects of core heteroatoms and meso-substituents on biological activity. *Journal of Medicinal Chemistry* **2002,** *45*, 449-461.

201. You, Y. J.; Gibson, S. L.; Hilf, R.; Davies, S. R.; Oseroff, A. R.; Roy, I.; Ohulchanskyy, T. Y.; Bergey, E. J.; Detty, M. R., Water soluble, core-modified porphyrins. 3. Synthesis, photophysical properties, and in vitro studies of photosensitization, uptake, and localization with carboxylic acid-substituted derivatives. *Journal of Medicinal Chemistry* **2003,** *46*, 3734-3747.

202. You, Y. J.; Gibson, S. L.; Hilf, R.; Ohulchanskyy, T. Y.; Detty, M. R., Core-modified porphyrins. Part 4: Steric effects on photophysical and biological properties in vitro. *Bioorgan Med Chem* **2005,** *13*, 2235-2251.

203. You, Y. J.; Gibson, S. L.; Detty, M. R., Core-modified porphyrins. Part 5: Electronic effects on photophysical and biological properties in vitro. *Bioorgan Med Chem* **2005,** *13*, 5968-5980.

204. Ngen, E. J.; Daniels, T. S.; Murthy, R. S.; Detty, M. R.; You, Y., Core-modified porphyrins. Part 6: Effects of lipophilicity and core structures on physicochemical and biological properties in vitro. *Bioorg Med Chem* **2008,** *16*, 3171-83.

205. Bellnier, D. A.; Dougherty, T. J., A preliminary pharmacokinetic study of intravenous Photofrin in patients. *J Clin Laser Med Surg* **1996,** *14*, 311-4.

206. Rajaputra, P.; Nkepang, G.; Watley, R.; You, Y., Synthesis and in vitro biological evaluation of lipophilic cation conjugated photosensitizers for targeting mitochondria. *Bioorg Med Chem* **2013,** *21*, 379-87.

207. Castano, A. P.; Demidova, T. N.; Hamblin, M. R., Mechanisms in photodynamic therapy: part one-photosensitizers, photochemistry and cellular localization. *Photodiagnosis and Photodynamic Therapy* **2004,** *1*, 279-293.

208. Murphy, M. P., Selective targeting of bioactive compounds to mitochondria. *Trends Biotechnol* **1997,** *15*, 326-30.

209. Muratovska, A.; Lightowlers, R. N.; Taylor, R. W.; Wilce, J. A.; Murphy, M. P., Targeting large molecules to mitochondria. *Adv Drug Deliv Rev* **2001,** *49*, 189-98.

210. Filipovska, A.; Eccles, M. R.; Smith, R. A.; Murphy, M. P., Delivery of antisense peptide nucleic acids (PNAs) to the cytosol by disulphide conjugation to a lipophilic cation. *FEBS Lett* **2004,** *556*, 180-6.

211. James, A. M.; Sharpley, M. S.; Manas, A. R.; Frerman, F. E.; Hirst, J.; Smith, R. A.; Murphy, M. P., Interaction of the mitochondria-targeted antioxidant MitoQ with phospholipid bilayers and ubiquinone oxidoreductases. *J Biol Chem* **2007,** *282*, 14708-18.

212. Leo, A.; Hansch, C.; Elkins, D., Partition coefficients and their uses. *Chem. Rev.* **1971,** *71*, 525-616.

213. Moser, J. G., Photodynamic tumour therapy 2nd and 3rd generation photosensitizers. **1998**.

214. Lakowitcz, J. R., Principles of Fluorescence Spectroscopy, 3rd ed. *Springer Publishing Company* **2006,** *Chicago*.

215. Wolfgang Spiller, H. K. D. W. S. H. B. R. G. S., Singlet oxygen quantum yields of different photosensitizers in polar solvents and micellar solutions. *Journal of Porphyrins and Phthalocyanines* **1998,** *2*, 145-158.

216. Yogo, T.; Urano, Y.; Ishitsuka, Y.; Maniwa, F.; Nagano, T., Highly efficient and photostable photosensitizer based on BODIPY chromophore. *J. Am. Chem. Soc.* **2005,** *127*, 12162-12163.

217. You, Y.; Gibson, S. L.; Detty, M. R., Phototoxicity of a core-modified porphyrin and induction of apoptosis. *J Photochem Photobiol B* **2006,** *85*, 155-62.

218. Xu, W.; Chen, H.; Wang, Y.; Zhao, C.; Li, X.; Wang, S.; Weng, Y., Photoinduced electron and energy transfer in dyads of porphyrin

dimer and perylene tetracarboxylic diimide. *Chemphyschem* **2008,** *9*, 1409-15.

219. Wu, J. J.; Li, N.; Li, K. A.; Liu, F., J-aggregates of diprotonated tetrakis(4-sulfonatophenyl)porphyrin induced by ionic liquid 1-butyl-3-methylimidazolium tetrafluoroborate. *J Phys Chem B* **2008,** *112*, 8134-8.

220. Chen, Y.; Gryshuk, A.; Achilefu, S.; Ohulchansky, T.; Potter, W.; Zhong, T.; Morgan, J.; Chance, B.; Prasad, P. N.; Henderson, B. W.; Oseroff, A.; Pandey, R. K., A novel approach to a bifunctional photosensitizer for tumor imaging and phototherapy. *Bioconjug Chem* **2005,** *16*, 1264-74.

221. Mohanty, J.; Nau, W. M., Ultrastable rhodamine with cucurbituril. *Angew Chem Int Ed Engl* **2005,** *44*, 3750-4.

222. You, Y.; Gibson, S. L.; Hilf, R.; Davies, S. R.; Oseroff, A. R.; Roy, I.; Ohulchanskyy, T. Y.; Bergey, E. J.; Detty, M. R., Water soluble, core-modified porphyrins. 3. Synthesis, photophysical properties, and in vitro studies of photosensitization, uptake, and localization with carboxylic acid-substituted derivatives. *J Med Chem* **2003,** *46*, 3734-47.

223. You, Y.; Gibson, S. L.; Hilf, R.; Ohulchanskyy, T. Y.; Detty, M. R., Core-modified porphyrins. Part 4: Steric effects on photophysical and biological properties in vitro. *Bioorg Med Chem* **2005,** *13*, 2235-51.

224. You, Y.; Gibson, S. L.; Detty, M. R., Core-modified porphyrins. Part 5: Electronic effects on photophysical and biological properties in vitro. *Bioorg Med Chem* **2005,** *13*, 5968-80.

225. Bao, C.; Jin, M.; Li, B.; Xu, Y.; Jin, J.; Zhu, L., Long conjugated 2-nitrobenzyl derivative caged anticancer prodrugs with visible light regulated release: preparation and functionalizations. *Org Biomol Chem* **2012,** *10*, 5238-44.

226. Kratz, F.; Warnecke, A.; Scheuermann, K.; Stockmar, C.; Schwab, J.; Lazar, P.; Druckes, P.; Esser, N.; Drevs, J.; Rognan, D.; Bissantz, C.; Hinderling, C.; Folkers, G.; Fichtner, I.; Unger, C., Probing the cysteine-34 position of endogenous serum albumin with thiol-binding doxorubicin derivatives. Improved efficacy of an acid-sensitive doxorubicin derivative with specific albumin-binding properties compared to that of the parent compound. *J Med Chem* **2002,** *45*, 5523-33.

227. Snyder, J. W.; Greco, W. R.; Bellnier, D. A.; Vaughan, L.; Henderson, B. W., Photodynamic therapy: a means to enhanced drug delivery to tumors. *Cancer Res* **2003,** *63*, 8126-31.

228. Ellis, G. A.; McGrath, N. A.; Palte, M. J.; Raines, R. T., Ribonuclease-Activated Cancer Prodrug. *ACS Med Chem Lett* **2012,** *3*, 268-272.

229. Rooseboom, M.; Commandeur, J. N.; Vermeulen, N. P., Enzyme-catalyzed activation of anticancer prodrugs. *Pharmacol Rev* **2004,** *56*, 53-102.

230. Yu, H.; Li, J.; Wu, D.; Qiu, Z.; Zhang, Y., Chemistry and biological applications of photo-labile organic molecules. *Chem Soc Rev* **2010,** *39*, 464-73.

231. Mayer, G.; Heckel, A., Biologically active molecules with a "light switch". *Angew Chem Int Ed Engl* **2006,** *45*, 4900-21.

232. Jiang, M. Y.; Dolphin, D., Site-specific prodrug release using visible light. *J Am Chem Soc* **2008,** *130*, 4236-7.

233. Zamadar, M.; Ghosh, G.; Mahendran, A.; Minnis, M.; Kruft, B. I.; Ghogare, A.; Aebisher, D.; Greer, A., Photosensitizer drug delivery via an optical fiber. *J Am Chem Soc* **2011,** *133*, 7882-91.

234. Ruebner, A.; Yang, Z.; Leung, D.; Breslow, R., A cyclodextrin dimer with a photocleavable linker as a possible carrier for the photosensitizer in photodynamic tumor therapy. *Proc Natl Acad Sci U S A* **1999,** *96*, 14692-3.

235. Murthy, R. S.; Bio, M.; You, Y. J., Low energy light-triggered oxidative cleavage of olefins. *Tetrahedron Letters* **2009,** *50*, 1041-1044.

236. Bio, M.; Nkepang, G.; You, Y., Click and photo-unclick chemistry of aminoacrylate for visible light-triggered drug release. *Chem Commun (Camb)* **2012,** *48*, 6517-9.

237. Dark, G. G.; Hill, S. A.; Prise, V. E.; Tozer, G. M.; Pettit, G. R.; Chaplin, D. J., Combretastatin A-4, an agent that displays potent and selective toxicity toward tumor vasculature. *Cancer Res* **1997,** *57*, 1829-34.

238. Muhamad, S. P., A.H.L.; Latif, J.; Rha, C.; Sambandan, T.G., Induction of apoptosis in MCF-7 via the Caspase pathway by longilactone from Eurycoma longifolia Jack. *Research in Pharmaceutical Biotechnology* **2011,** *3*, 1-10.

239. Bharadwaj, R.; Yu, H., The spindle checkpoint, aneuploidy, and cancer. *Oncogene* **2004,** *23*, 2016-27.

240. Brito, D. A.; Yang, Z.; Rieder, C. L., Microtubules do not promote mitotic slippage when the spindle assembly checkpoint cannot be satisfied. *J Cell Biol* **2008,** *182*, 623-9.

241. Stilts, C. E.; Nelen, M. I.; Hilmey, D. G.; Davies, S. R.; Gollnick, S. O.; Oseroff, A. R.; Gibson, S. L.; Hilf, R.; Detty, M. R., Water-soluble, core-modified porphyrins as novel, longer-wavelength-absorbing sensitizers for photodynamic therapy. *J Med Chem* **2000,** *43*, 2403-10.

242. Hilmey, D. G.; Abe, M.; Nelen, M. I.; Stilts, C. E.; Baker, G. A.; Baker, S. N.; Bright, F. V.; Davies, S. R.; Gollnick, S. O.; Oseroff, A. R.; Gibson, S. L.; Hilf, R.; Detty, M. R., Water-soluble, core-modified porphyrins as novel, longer-wavelength-absorbing sensitizers for photodynamic therapy. II. Effects of core heteroatoms and meso-substituents on biological activity. *J Med Chem* **2002,** *45*, 449-61.

243. Bio, M.; Rajaputra, P.; Nkepang, G.; Awuah, S. G.; Hossion, A. M.; You, Y., Site-specific and far-red-light-activatable prodrug of

combretastatin A-4 using photo-unclick chemistry. *J Med Chem* **2013,** *56*, 3936-42.

244. Skovsen, E.; Snyder, J. W.; Lambert, J. D.; Ogilby, P. R., Lifetime and diffusion of singlet oxygen in a cell. *The journal of physical chemistry. B* **2005,** *109*, 8570-3.

245. Moan, J., On the diffusion length of singlet oxygen in cells and tissues. *Journal of Photochemistry and Photobiology B: Biology* **1990,** *6*, 343-344.

246. Ohsumi, K.; Nakagawa, R.; Fukuda, Y.; Hatanaka, T.; Morinaga, Y.; Nihei, Y.; Ohishi, K.; Suga, Y.; Akiyama, Y.; Tsuji, T., Novel combretastatin analogues effective against murine solid tumors: design and structure-activity relationships. *J Med Chem* **1998,** *41*, 3022-32.